Chem



### Review

# Conjugated ladder polymers: Advances from syntheses to applications

James Shao-Jiun Yang<sup>1</sup> and Lei Fang<sup>1,2,\*</sup>

#### **SUMMARY**

Conjugated ladder polymers (CLPs) represent a fascinating class of macromolecules characterized by their multi-stranded,  $\pi$ -conjugated structures with uninterrupted fused rings forming the backbone. Their unique constitution presents synthetic challenges that extend beyond those associated with conventional conjugated polymers. The synthesis of CLPs is typically achieved through one-pot annulative ladder polymerization or a two-step process involving polymerization followed by post-polymerization cyclization. Over the past decade, numerous innovative synthetic techniques and novel CLP structures have emerged. The distinctive architectures of these CLPs endow them with exceptional properties and robustness that are often unmatched by conventional non-ladder polymers. Significant progress has been made in the application of CLPs in various domains, such as organic semiconductors, active materials in organic electrochemical transistors, and organic thermoelectric devices. Despite these advances, the field continues to face a series of chemical and engineering challenges that must be overcome to fully harness the potential of CLPs as a highly promising class of functional organic materials.

#### **INTRODUCTION**

Ladder polymers represent a unique class of multi-stranded macromolecules with uninterrupted sequences of rings and constitutional units joined to each other through at least four atoms, two or more on one side and two or more on the other side of each constitutional unit. The conceptualized synthesis of ladder polymers was first proposed by Staudinger in 1926 through repeated cycloaddition of cyclopentadiene, even before Diels and Alder jointly reported the well-known Diels-Alder cycloaddition in 1928. Specifically, these macromolecules are classified as conjugated ladder polymers (CLPs) (Figure 1) if the ladder backbones are uninterruptedly  $\pi$ -conjugated. Despite the fact that the seminal concept of ladder polymers was introduced in the early 1900s, it was not until the 1960s that the well-characterized synthetic ladder polymer poly(benzobisimidazobenzophenanthroline) (BBL), also a CLP, was synthesized and reported by Van Deusen (Scheme 1A). To date, BBL represents one of the most widely used and durable organic electronic materials.

CLPs can also be viewed as a class of macromolecules that bridges the gap between conventional single-stranded conjugated polymers and conjugated 2D polymers. They exhibit unique variations in charge delocalization, optical properties, and band structures compared with single-stranded polymers and 2D polymers like graphene. The inherent advantage of many CLPs lies in their structural resemblance to graphene for enhanced charge delocalization, while maintaining essential

#### THE BIGGER PICTURE

Over the past century, the vast majority of polymers synthesized and studied by humanity were single stranded. Research on multi-stranded polymers, such as ladder polymers, presents a compelling challenge for chemists. Although ladder polymer chemistry is nascent compared with that of traditional polymers, it has seen significant advancements in recent decades. Among these multi-stranded polymers, conjugated ladder polymers (CLPs) are particularly noteworthy, thanks to their distinct electronic structures that contribute to unique electronic, optical, and magnetic properties. These properties, along with CLPs' extraordinary stability, could address challenges in various cutting-edge application fields; e.g., bioelectronic devices, wearable electronics, and sustainable energy storage. Future research should focus on developing new sustainable synthetic methods, applying large-area processing techniques, and enhancing the integrated functions of these polymers.





properties for diverse applications, including solubility, dispersity, and processability. Therefore, CLPs stand at the intersection of conventional single-stranded polymers, which can be dissolved as individual polymer chains, and 2D polymeric materials like graphene (Figure 1).

With the extra strands of covalent bonds, the stabilities of CLPs are often enhanced significantly, as the extra strands serve as additional linkages to prevent the polymers from fast degradation. Compared with non-ladder conjugated polymers, the structure of CLPs and their sp<sup>2</sup>-hybridized carbon atoms more closely mimic the thermodynamically stable graphene. Kinetically, the degradation of CLPs to oligomers requires a low chance of scissoring two strands of bonds within the same constitutional unit. Greater intrachain electron delocalization is also promoted by the enhanced local backbone coplanarity brought by the extra strands of bonds. With all these advantages, CLPs have recently found their applications in many durable organic electronics. Many examples of CLP syntheses have been summarized in several previous review articles,<sup>5-9</sup> yet the field continues to evolve rapidly. Over the past few years, significant advances have been made to address the multifaceted challenges associated with CLPs, including synthetic difficulties, structural defects, solubility, processability, and application implementation. This review outlines the progress made in the last decade. Discussions begin with the introduction of novel synthesis methods and new structures of CLPs, focusing primarily on developments achieved in solution-phase and scalable solid-state syntheses. Subsequent sections delve into the properties of CLPs related to photophysics and polymer physics, as well as their notable stability and robustness under harsh conditions. The final section examines recent advanced applications of CLPs, with emphasis on durable organic electrochemical transistors (OECTs) and organic thermoelectrics (OTEs).

It is noteworthy that this review cannot cover every aspect of the thriving field of CLPs. Several important topics related to CLPs have been summarized or reviewed elsewhere and are NOT the focus of this review, as pointed out next. On-surface synthesis of graphene nanoribbons (GNRs) and similar CLPs represents an emerging strategy and has been already described in several reviews. 10-14 Similarly, the syntheses and applications of conjugated porous ladder-type polymer networks<sup>15</sup> and non-conjugated ladder polymers, such as polymers of intrinsic microporosity (PIMs), <sup>16,17</sup> have also been summarized in other sources. Pseudo-ladder polymers, which share certain structural features and similar properties of ladder polymers but are not real ladder polymers by strict definition, are not included in this review either. These pseudo-ladder polymers include step-ladder polymers<sup>18–20</sup> and conjugated polymers featuring a second strand of intramolecular non-covalent interactions (e.g., hydrogen bonds<sup>21–23</sup> and chalcogen bonds<sup>24–28</sup>) that enforce a rigid backbone. Last but not least, the processing of CLPs for device applications poses a significant challenge. Recent progress in this area includes methods such as dissolution in strong protic acids, incorporation of solubilizing side groups, processing in nanoparticle form, and in situ solid-state synthesis on substrates. These developments have been extensively discussed in a recently published book chapter.<sup>29</sup>

### **SYNTHESES**

#### **General synthetic strategies**

The synthesis of ladder macromolecules can be analogized to the assembly of a macroscopic ladder, which traditionally comprises two longitudinal supports, or rails, and several transverse components, or rungs. The construction of a ladder can be approached using one of the following methods: (1) modular extension—this method

<sup>&</sup>lt;sup>1</sup>Department of Chemistry, Texas A&M University, College Station, TX 77843-3255, USA

<sup>&</sup>lt;sup>2</sup>Department of Materials Science & Engineering, Texas A&M University, College Station, TX 77843-3003, USA

<sup>\*</sup>Correspondence: fang@chem.tamu.edu https://doi.org/10.1016/j.chempr.2024.04.002



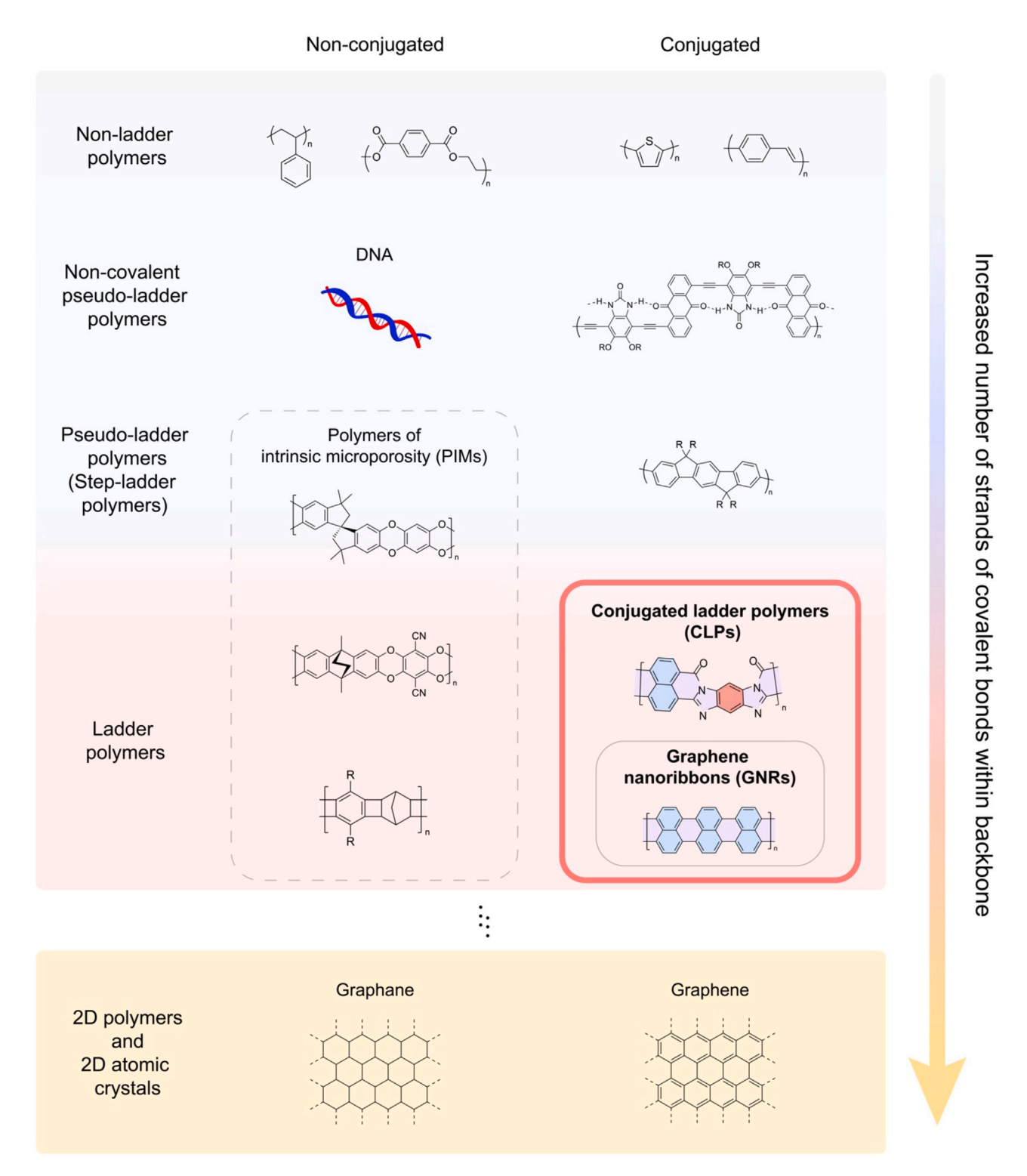
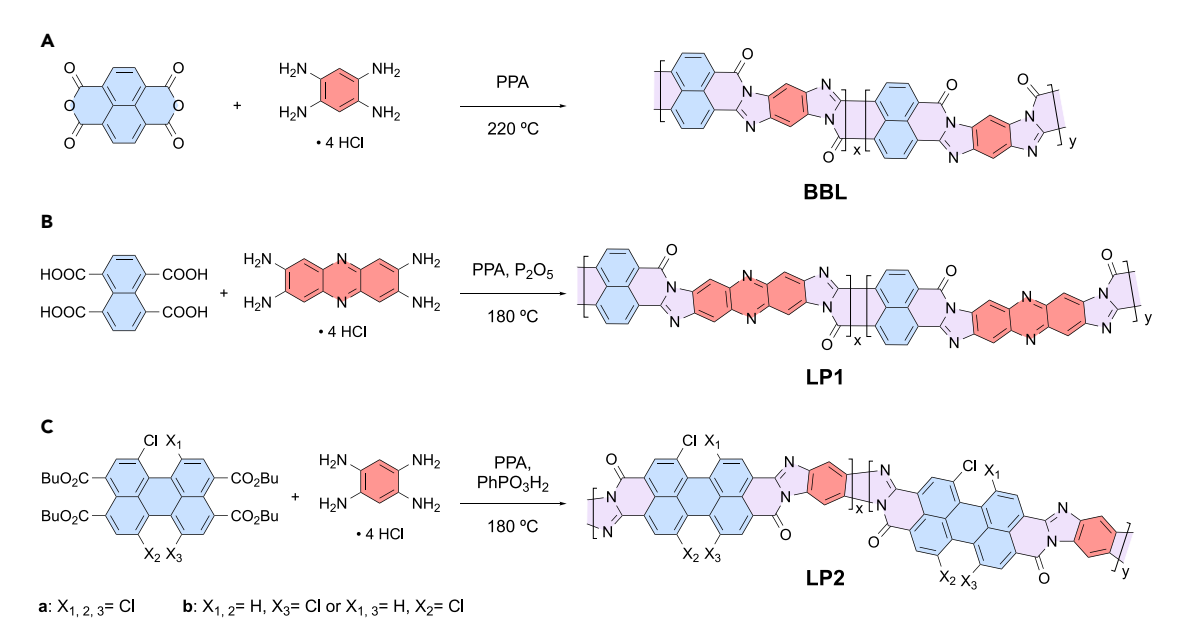


Figure 1. Representative examples of CLPs and other classes of polymers categorized by  $\pi$ -conjugation and the number of strands of covalent bonds within their backbones

The red box represents the scope of this review.







Scheme 1. Syntheses of CLPs through acid-mediated annulative ladder polymerization (A) BBL. (B) LP1. (C) LP2.

begins with the creation of short ladder sections, each comprising two rails connected by several rungs. These sections are then successively joined at the ends of the rails to form a longer, continuous ladder structure (Figure 2A); (2) single-rail progression—in this approach, a single rail is pre-fabricated with all the rungs attached to it. A complementary rail is subsequently generated by connecting the pre-installed rungs to form a complete ladder structure (Figure 2B); and (3) parallel construction—this strategy requires setting up two rails in parallel alignment at the desired distance apart. Rungs are then inserted and affixed between these rails to create the final ladder (Figure 2C). In the context of chemical synthesis of ladder polymers,

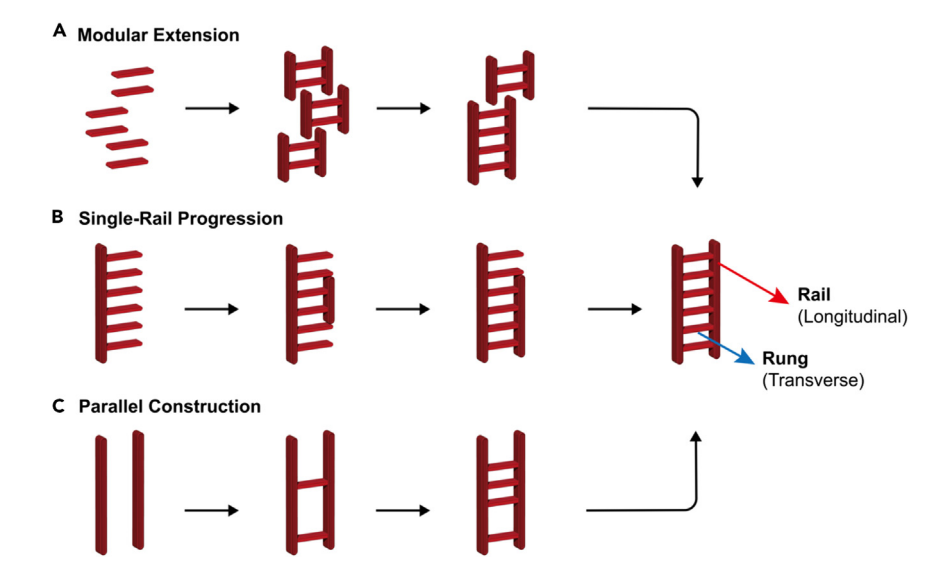


Figure 2. Methods to assemble a ladder

(A) Modular extension by attaching the rails of several ladder segments, (B) single-rail progression through connecting all pre-installed rungs on the first rail to generate the second rail, and

(C) parallel construction through inserting rungs between two parallel pre-positioned rails.

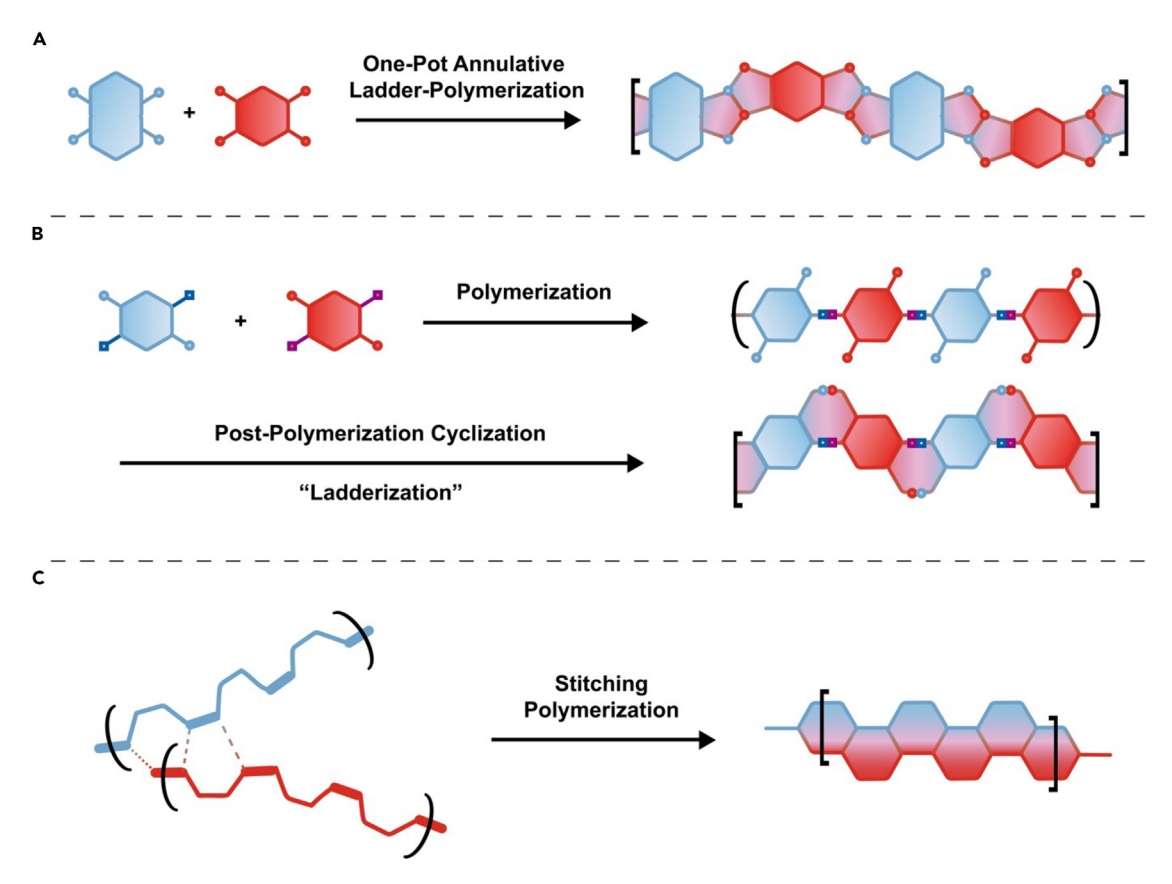


Figure 3. Synthetic strategies for ladder polymers

(A) One-pot annulative ladder polymerization with the two strands of bonds generated through repetitive annulation reactions, (B) post-polymerization cyclization (ladderization) from a single-stranded precursor polymer with pendant functional groups for cyclization, and (C) stitching polymerization from two single-stranded oligomers or polymers.

the rails are analogs to the two strands of bonds along the polymer backbone, while the rungs represent the bonds connecting these rails. These three macroscopic construction approaches correspond to the following strategies of chemical synthesis, respectively: (1) one-pot annulative ladder polymerization—this strategy entails the one-pot formation of the two strands of covalent bonds that are analogous to the "rails" of a ladder, where the starting monomer molecules already contain the pre-formed "rung" bonds (Figure 3A); (2) post-polymerization cyclization—in this approach, a precursor polymer with a single strand of backbone chain is first synthesized. The second strand of bonds is then formed in a post-polymerization cyclization step, in other words, the "ladderization" step, thereby achieving the desired ladder constitution (Figure 3B); and (3) stitching polymerization<sup>30–32</sup>—this method utilizes two pre-formed single-stranded oligomer or polymer chains. These chains are then "stitched" together through covalent bonds to form the rungs, connecting the two strands to create the ladder polymer (Figure 3C).

It is noteworthy that the stitching strategy presents significant challenges for chemical synthesis because of the high probability of uncontrolled cross-linking during the stitching process and the demand of precise length matching of the two single-stranded precursor chains. Therefore, over the past half century, most ladder polymer syntheses were accomplished by using either the one-pot annulative ladder polymerization or the post-polymerization cyclization strategy.





#### One-pot annulative ladder polymerization

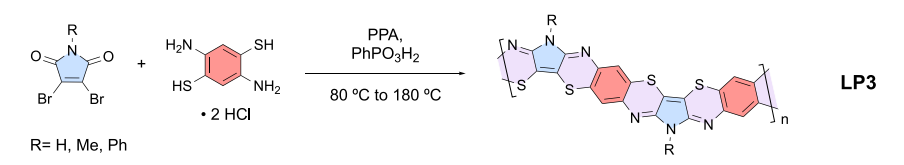
One-pot annulative ladder polymerization facilitates the direct formation of two strands of bonds between monomeric repeating units to produce a ladder-type polymeric structure within a single reaction environment. This process is characterized as annulation, distinct from cyclization, because two strands of bonds are formed either simultaneously in a single step or in consecutive steps without the isolation of intermediates. The primary advantage of this strategy is the minimized synthetic operations by eliminating the need to isolate an intermediate. Compared with post-polymerization cyclization, however, the scope of reactions that permit such direct annulation is somewhat limited. Additionally, achieving a high molar mass via this method can be challenging because of the often-limited solubility of the directly synthesized ladder polymer. Owing to the strong thermodynamic driving force for many of these reactions, these CLPs are expected to possess low levels of defects. Nonetheless, if the reaction intermediates become insoluble and hence are no longer able to participate in the reaction before the completion of ladderization, the CLP products can still contain defects.

One of the most prevalent methods for one-pot ladder polymerization is an acid-mediated annulative condensation reaction, which typically utilizes imide or imine condensation as the principal annulation mechanism. The thermodynamically driven nature of these reactions tends to inhibit the formation of branched or cross-linked by-products, thereby favoring intramolecular cyclization to afford the desired CLP products, which are usually the thermodynamically favored products. Many of these condensation reactions are mediated by strong acids, such as H<sub>2</sub>SO<sub>4</sub>, methanesulfonic acid (MSA), H<sub>3</sub>PO<sub>4</sub>, or polyphosphoric acid (PPA). However, it is critical to recognize that the application of strong acids may restrict the scope of suitable monomers and the tolerance of certain functional groups. Solubilizing side chains are often unnecessary for CLPs synthesized via this method owing to the significant solubilizing effect of strong acids. As a result, these side-chain-free CLPs, which exhibit very low solubility in common organic solvents, can be solution processed from the acid solution into functional thin films, and they demonstrate high charge carrier mobility or electrical conductivity. 33–35

Since the 1960s, when the synthesis of BBL (Scheme 1A) via acid-mediated annulative condensation polymerization was first reported, themists have drawn inspiration from this simple yet highly efficient chemistry to construct fully fused backbones of CLPs. Recently, Jenekhe and coworkers reported the synthesis of phenazine-embedded LP1 (Scheme 1B) in PPA and  $P_2O_5$  and demonstrated its enhanced mechanical properties compared with BBL. Tam, Meng, Huang, Xu, and coworkers extended the  $\pi$ -core of BBL-like CLPs by replacing the naphthalene diimide building block with a multi-chlorinated perylene diimide moiety to afford LP2 (Scheme 1C). The polymerization was optimized and performed in a mixture of PPA and phenylphosphonic acid at 180°C. The use of phenylphosphonic acid and the chlorine substituent-induced backbone twisting of the perylene diimide monomer were necessary to maintain the solubility of the reaction intermediates to achieve reasonably high molar masses of the product.

Tam, Xu, and coworkers also reported the synthesis of a side-chain-free CLP LP3 (Scheme 2) through a one-pot/two-step acid-mediated annulative condensation approach. These two steps—namely, Michael addition polymerization and the subsequent imine condensation—were again mediated in a mixed solvent of PPA and phenylphosphonic acid.<sup>35</sup> The polymerization was initially carried out at a relatively low temperature (80°C) in order to prevent side reactions such as the thermal



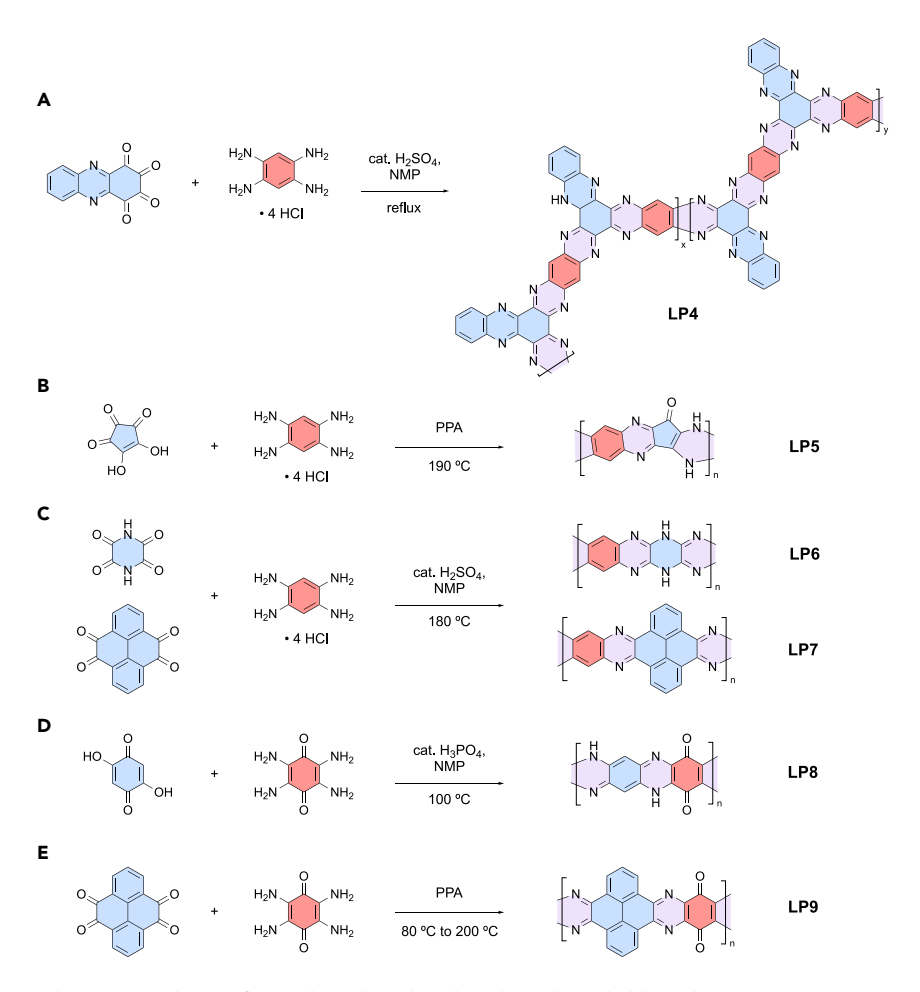


Scheme 2. Synthesis of LP3 through acid-mediated Michael addition and imine condensation

decomposition of monomers, and then the temperature was raised to 180°C for the subsequent thermodynamically driven cyclization. Additionally, LP3 with *N*-methyl and *N*-phenyl substituents (LP3-Me and LP3-Ph) was synthesized by similar methods. <sup>39,40</sup> The properties and applications of these CLPs are discussed in sections "solution-phase conformation and chain rigidity" and "applications for electronic devices."

Most of the CLPs in the aforementioned cases are expected to exhibit high electrical conductivity or charge carrier mobility in the solid state, attributable to the conjugated ladder-type backbone and absence of insulating side chains. Despite challenges in solution processing of these CLPs due to their poor solubility in common organic solvents, many of these polymers can be dispersed and processed using strong acids as solvents, or they can be directly used as materials without solution processing. As a result, the desired high performances of CLPs have been demonstrated in various applications, such as electrode materials for capacitors or as alkaline-ion batteries. Motivated by this prospect, a number of such side-chain-free CLPs were synthesized via acid-mediated annulative condensation ladder polymerization. For instance, Kapaev and coworkers demonstrated the synthesis of LP4 (Scheme 3A), consisting of hexaazatriphenylene backbone through imine condensation of phenazine-1,2,3,4-tetraone dihydrate and 1,2,4,5-benzenetatraamine tetrahydrochloride (TAB·4HCl) in reflux N-methyl pyrrolidone (NMP) in the presence of H<sub>2</sub>SO<sub>4</sub>. <sup>41</sup> Yan, Zhang, and coworkers reported the synthesis of LP5 (Scheme 3B) through the condensation of TAB·4HCl and croconic acid in PPA at 190°C. 42 Wang, Wu, Xu, and coworkers reported the syntheses of LP6 and LP7 (Scheme 3C) through the condensation of TAB·4HCl with piperazine-2,3,5,6-tetraone or pyrene-4,5,9,10-tetraone in NMP at 180°C catalyzed by H<sub>2</sub>SO<sub>4</sub>. <sup>43</sup> Chen and coworkers showed the synthesis of LP8 (Scheme 3D) through condensation of 2,3,5,6-tetramino-1,4-benzoquinone and 2,5-dihydroxy-1,4-benzoquinone in NMP at 100°C catalyzed by H<sub>3</sub>PO<sub>4</sub>. 44 Wang, Wang, Wang, Hu, and coworkers reported the synthesis of LP9 (Scheme 3E) by imine condensation of pyrene-4,5,9,10-tetraone and 2,3,5,6-tetramino-1,4-benzoquinone in heated PPA. 45 In the case of LP5 and LP9, electrically conductive additives such as carbon nanotube and reduced graphene oxide (rGO) were added into the reaction mixture to enhance the overall conductivity of the resulting composite. Zhang and coworkers demonstrated the synthesis of LP10 (Scheme 4) from 2,3,5,6-tetramercapto-1,4-benzoquinone and 2,3,5,6-tetrafluoro-1,4-benzoguinone through nucleophilic substitution in reflux dimethylformamide (DMF).<sup>46</sup> In general, these reactions are often carried out in hot and/or acidic conditions, so that the scope of monomer selection is limited to those robust in such harsh conditions. Furthermore, precise characterization of the constitutional structures, molar masses, and regioregularity of these CLPs still pose challenges due to the poor solubility of these materials in common organic solvents.

In a unique case reported by Zhang and coworkers, LP11 (Scheme 5) was synthesized through imine condensation of phenylene diamine and a hexaphenylbenzene monomer functionalized with 12 aldehyde groups.<sup>47</sup> Interestingly, only four of the

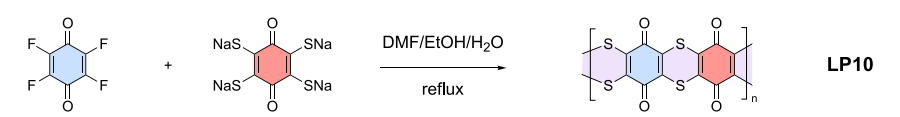


Scheme 3. Syntheses of CLPs through acid-mediated annulative ladder polymerization via imine condensation

(A) LP4. (B) LP5. (C) LP6 and LP7. (D) LP8. (E) LP9.

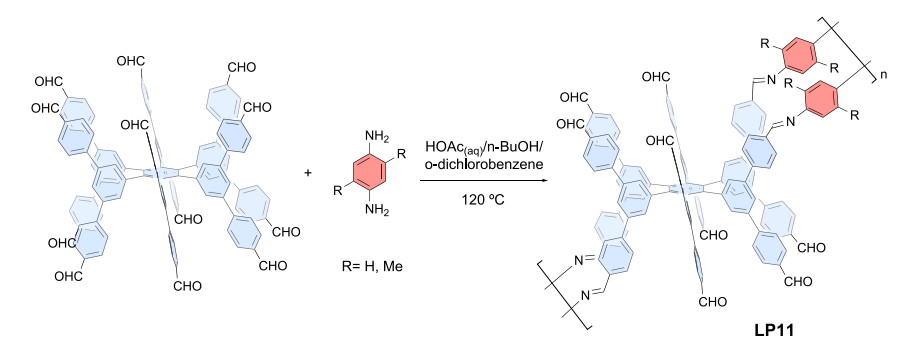
aldehyde groups on each monomer underwent imine condensation, giving rise to the formation of a crystalline one-dimensional CLP instead of a polymer network. The linear structure of the as-synthesized crystalline LP11 was characterized by electron diffraction, revealing a funnel-shaped molecular stack in a woven, interlaced manner. It is believed that this specific molecular arrangement, involving interchain  $\pi$ - $\pi$  interactions and hydrogen bond interactions from the unreacted aldehyde and aryl C–H, contributes to the selectivity of certain aldehyde groups for the one-dimensional growth of LP11. Additionally, LP11 was demonstrated as a material for efficient separation of  $C_2H_2$  and  $CO_2$  gases owing to its microporosity.

The reaction scope of one-pot annulative ladder polymerization can be expanded to other step-growth and chain-growth polymerization methods. The formation of the second strands is typically driven by thermodynamics without the need of additional operation or addition of reagents so that the reaction remains one-pot. For instance,



Scheme 4. Synthesis of LP10 through annulative nucleophilic substitution

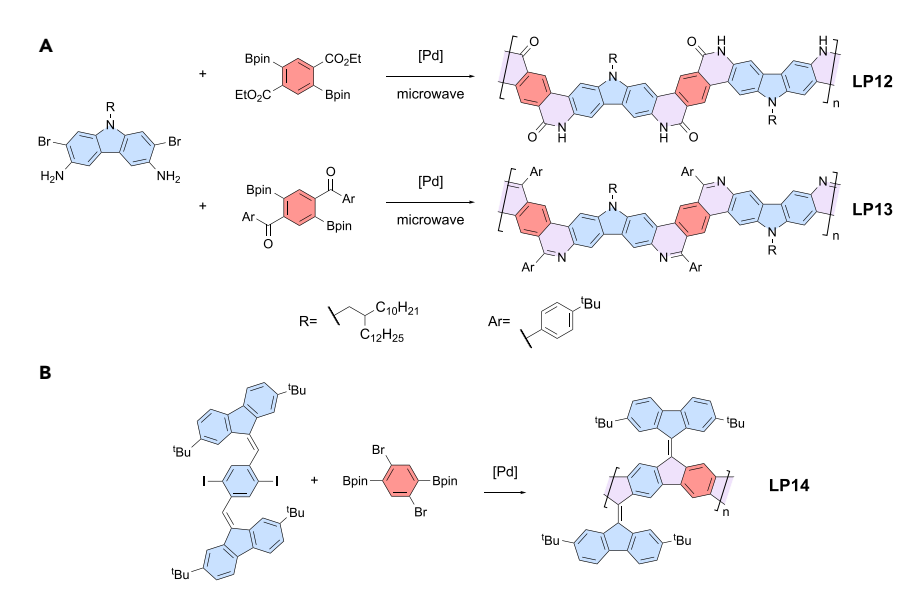




Scheme 5. Synthesis of linear CLP LP11 through annulative imine condensation

Zhang, Zhao, Wu, and coworkers reported the syntheses of LP12 and LP13 (Scheme 6A) through Suzuki polymerization and one-pot cyclization via imine or amide bond formations promoted by heat. 48 In another example, Liu, Wu, and coworkers demonstrated the synthesis of 9,9′-bifluorenylidene-based LP14 (Scheme 6B) through tandem Suzuki polymerization and Heck coupling cyclization in one-pot. 49 The sequential Suzuki and Heck coupling was facilitated by using aryliodide for the former and aryl bromide for the latter, resulting in the desired chemo-selectivity for the precise construction of the ladder structure. By contrast, when aryl bromide was employed as a reaction functional group in the bifluorenyl monomer, a notable amount of competitive side reactions was observed due to the lack of chemo-selectivity between the Suzuki and Heck reactions. With this one-pot tandem polymerization and cyclization, LP14 was synthesized in high conversion accordingly. A low-defect level is assumed, based on the high isolated yield (>90%) of the small-molecule models.

The synthesis of "red carbon" LP15 (Scheme 7), a pyrone-based CLP, from carbon suboxide ( $C_3O_2$ ) represents another intriguing example for one-pot annulative ladder polymerization. Although the synthesis of  $C_3O_2$  and its spontaneous



Scheme 6. Syntheses of CLPs through one-pot Suzuki coupling followed by ladderization

(A) Syntheses of LP12 and LP13 through one-pot Suzuki coupling and amide/imine condensation. (B) Synthesis of LP14 through one-pot Suzuki coupling and Heck coupling.





Scheme 7. Synthesis of red carbon LP15 through a one-pot polymerization and ketene sigmatropic rearrangement

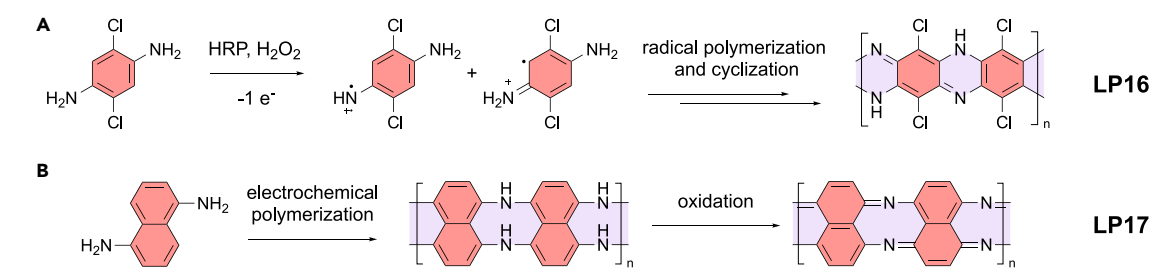
polymerization to a red solid was reported as early as 1874,  $^{50}$  its gaseous state under ambient conditions renders it challenging to store and handle. Recently, Odziomek, López-Salas, and coworkers revisited the synthesis of red carbon and developed a liquid-phase polymerization method. First,  $C_3O_2$  was generated *in situ* from malonic acid in acetic anhydride at  $140^{\circ}$ C. Subsequently, it polymerized into a ketene-functionalized precursor polymer through a chain-growth mechanism, and meanwhile, the ketene groups underwent signatropic rearrangement to afford the pyrone-based CLP at room temperature. The optimized yield of this one-pot reaction was reported to be 20%, and the polymer exhibited low molar mass  $(M_n < 1,000 \text{ g/mol})$ , presumably due to the undesired thermal decomposition of malonic acid to acetic acid and  $CO_2$ , as well as the escape of gaseous  $C_3O_2$  during the reaction.

One-pot formation of two strands of C–C bonds through direct C–H activation represents another promising strategy to synthesize CLPs, as it bypasses the potentially tedious steps of installing multiple functional groups for cyclization. Kaya and Kolcu reported an enzyme-catalyzed, oxidative radical ladder polymerization of LP16 (Scheme 8A) enabled by H<sub>2</sub>O<sub>2</sub> and horseradish peroxidase (HRP).<sup>53</sup> However, it is unclear whether the resulting CLP consists of undesired non-ladder defects generated from uncontrolled radical coupling. Lu and coworkers reported the electrochemical polymerization of LP17 (Scheme 8B), with Fourier transform infrared (FTIR) spectrum showing the disappearance of C–NH<sub>2</sub> stretching and the broadened bands of N–H and C–C stretching, as compared with that of monomer.<sup>54</sup> However, this method can potentially yield chain branching and cross-linking due to the challenge of non-regioselective reaction among multiple aryl C–H bonds.

Although achieving site-selective C-H activation in polymerizations is challenging owing to the difficulty in controlling the regioselectivity of the C-C bond formation, several methods have been reported to promote linear polymer growth without forming branched, cross-linked, or defected structures. For instance, site-selective solid-state polymerizations can be achieved within the nanochannels of metalorganic frameworks (MOFs). Uemura and coworkers reported the scalable synthesis of perylene-derived CLP LP18 (Scheme 9A) assisted by a ZrO-based MOF (MIL-140C),<sup>55</sup> representing a highly promising method for precise CLP synthesis.<sup>56</sup> First, the perylene monomer was incorporated into the nanochannels of the MOF by vapor adsorption. Accommodated in these channels with a specific pore size, the perylene monomers were sterically confined so that the C-C bond formation was possible only at the 3-, 4-, 9-, and 10-position at a high temperature (400°C) (Figure 4), giving rise to the linearly extended perylene-derived CLP. The pure CLP product can be simply retrieved by digesting the MOF template. More recently, the same research team demonstrated the use of 2,6-bis(bromomethyl)naphthalene and 2,6-bis(bromomethyl)anthracene as monomers for the synthesis of LP19a (Scheme 9B) in the



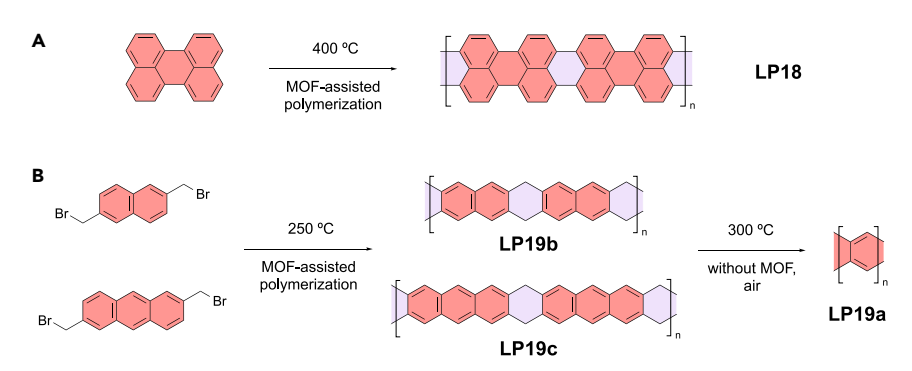




Scheme 8. Syntheses of CLPs through direct C-H activation under oxidation conditions (A) LP16. (B) LP17.

presence of the same MOF template. <sup>57</sup> In this case, the cyclization only took place at the 3- and 7-position of naphthalene or anthracene and the methylene carbons due to the spatial constraints in the MOF channels (Figure 4), affording linear ladder polymers LP19b and LP19c, respectively. After releasing the intermediate LP19b and LP19c from the MOF, dehydro-aromatization was conducted in air at a higher temperature to afford the insoluble CLP LP19a, which represents a rare case of high polyacene. Most polyacenes are known for their structural instability in solution due to their singlet biradical character that often leads to oxidation and dimerization. Interestingly, according to solid-state <sup>13</sup>C NMR, LP19a does not show observable signs of such degradation processes (e.g., carbonyl or bridgehead sp³-carbon signals), presumably because it is insoluble in organic solvents and remains as a solid in ambient conditions.

Topochemical polymerization represents another viable approach of one-pot annulative ladder polymerization to directly access CLPs in the solid state. Topochemical polymerization often occurs in the crystalline state of a monomer, in which regioselective bond formation can be achieved. If the molecules pack in a preferential manner, the polymerization can be confined in 1D or 2D with specific orientation while avoiding defects such as uncontrolled branching or cross-linking. S8-60 Notably, high pressure-induced solid-state polymerizations with slow compression or decompression rates can afford 1D non-conjugated ladder polymer nanothreads with well-defined structures from crystals of benzene,  $^{61-63}$  pyridine,  $^{64}$  and furan. Conjugated  $\pi$ -systems can also be topochemically synthesized in the crystalline solid state. For example, Rubin and coworkers reported the syntheses of CLPs LP20 (Scheme 10A) and LP21 (Scheme 10B) from variable diyne monomers.  $^{66,67}$  The polymerization readily proceeded in the crystalline state of monomers under ambient conditions, and this process could be accelerated by heat and light.



Scheme 9. Syntheses of CLPs through site-selective annulative ladder polymerization within MOF channels

(A) LP18. (B) LP19.



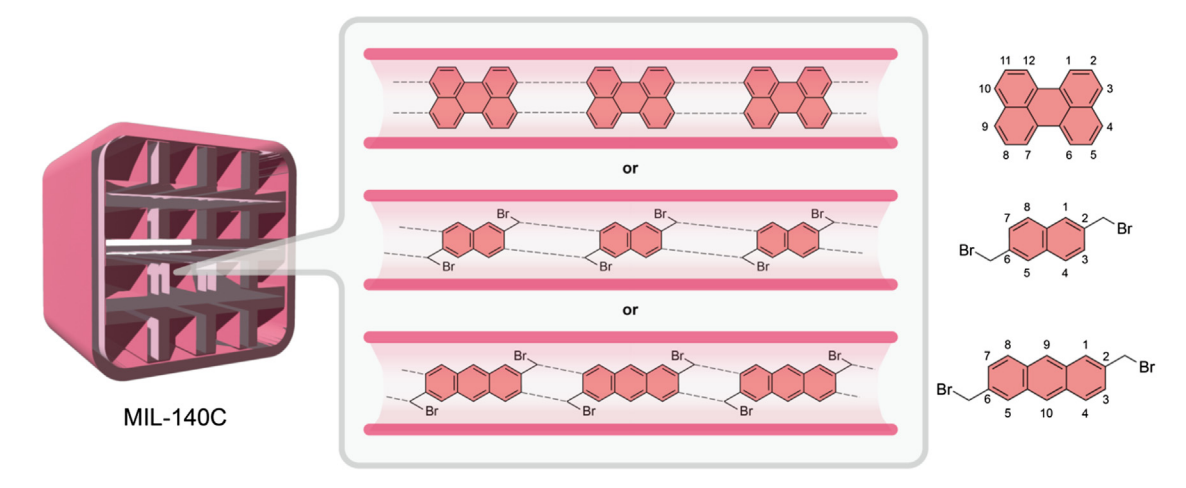


Figure 4. Illustration of site-selective annulative ladder polymerizations for LP18 and LP19a within the MOF channels

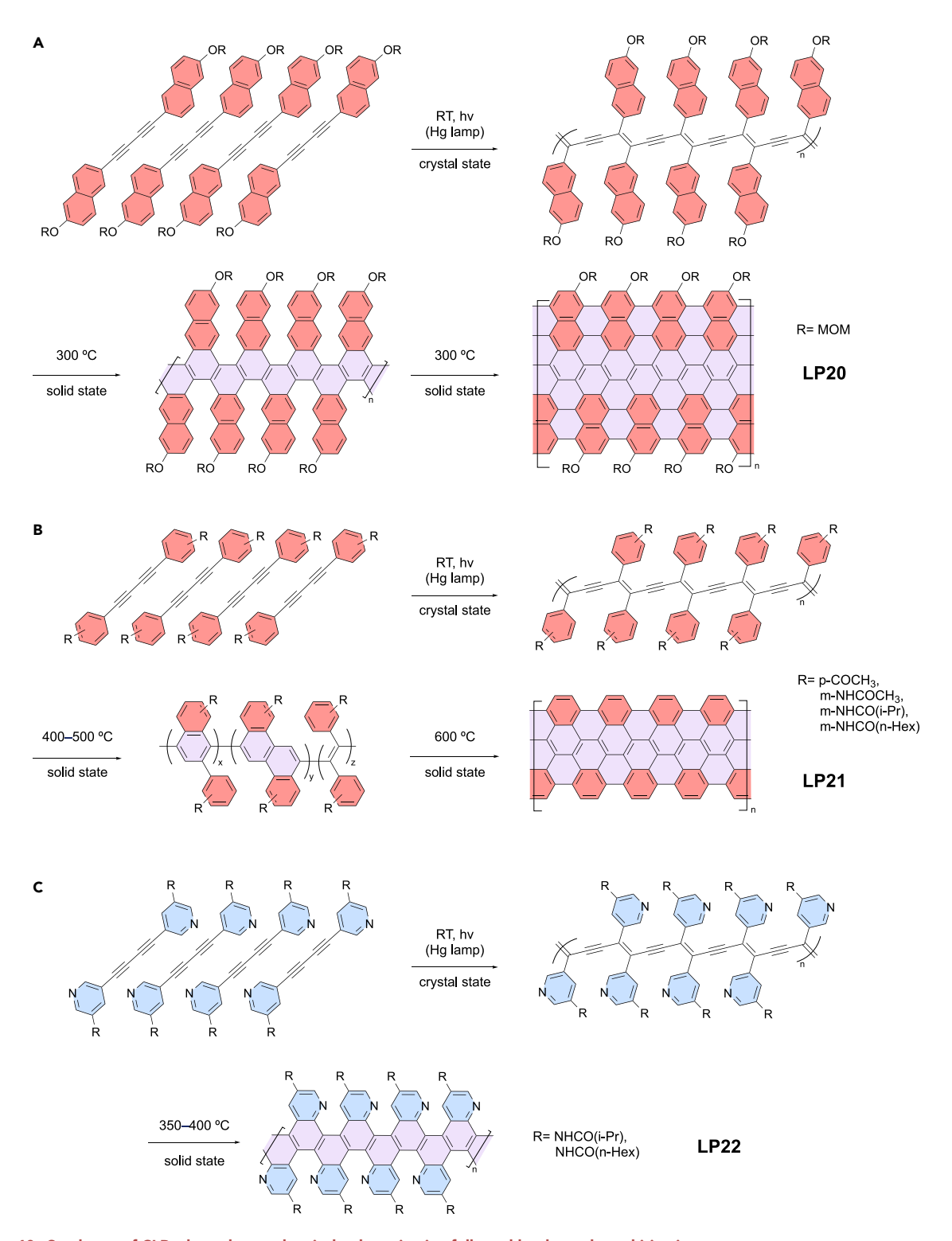
Following polymerization, LP20 was then synthesized through a series of cyclization in solid state at 300°C under inert atmosphere. As for LP21, several major chemical transformations occurring at 400°C-600°C were identified to account for the reaction. First, heating the polymer at 400°C-500°C resulted in the complete loss of alkyne as supported by solid-state <sup>13</sup>C NMR, FTIR, and Raman spectroscopy. Raising the temperature to 600°C further induced cyclodehydrogenation and side-chain cleavage to yield LP21. Defects such as sp<sup>3</sup> carbons were found in LP20, but these were absent in LP21 after thermal graphitization. A nitrogen-embedded analog, LP22 (Scheme 10C), was also synthesized via this method. 68 Similarly, Li, Ju, and coworkers demonstrated the synthesis of LP23 (Scheme 11) by topochemical dehydro-Diels-Alder polymerization. <sup>69</sup> The reaction was performed at room temperature under high pressure (10 GPa), but defects arising from sp<sup>3</sup> carbons were still observed in the product. Generally, although topochemical syntheses driven by pressure, light, or heat appear straightforward, success of these reactions is highly sensitive to the specific packing mode of monomers and the relative distance and orientation of reactive functional groups in the solid state. Even a minor change in these parameters can potentially affect the topochemical reactivity. Furthermore, it is possible that the same monomer shows varying topochemical reactivity across different crystal polymorphs. Given these complexities, devising a versatile approach for the topochemical synthesis of a broad scope of CLPs remains a significant challenge.

### Polymerization followed by post-polymerization cyclization

Besides the one-pot annulative ladder-polymerization strategy, a two-step strategy, involving initial polymerization followed by cyclization, has also been employed extensively to synthesize ladder polymers. The primary advantage of this two-step approach is a broader selection of reactions and monomers potentially suitable for ladder polymer syntheses. Moreover, conducting polymerization and cyclization in two distinct steps often allows for the access of polymers with higher molar masses, thanks to the higher solubility of non-ladder precursor polymers compared with that of the final CLP products.

When selecting suitable reactions for the critical post-polymerization cyclization, it is essential to ensure a high cyclization conversion and low possibility of potential side reactions. Incomplete conversion or side reactions during ladderization can impart defects onto the polymer backbones. Such defected chains are usually challenging to separate from defect-free CLP chains. In addition, uncontrollable side reactions





Scheme 10. Syntheses of CLPs through topochemical polymerization followed by thermal graphitization (A) LP20. (B) LP21. (C) LP22.







Scheme 11. Synthesis of LP23 through topochemical dehydro-Diels-Alder polymerization

may lead to the formation of undesired branching or cross-linking. For example, the pyrolytic synthesis of carbon fiber from polyacrylonitrile technically involves the process of transforming a non-ladder polymer precursor into a ladder-type structure through cyclization (Scheme 12).  $^{70,71}$  However, the formation of C–C or C–N bonds at carbonization temperatures is uncontrollable and takes place intermolecularly to cross-link the material into carbon fibers,  $^{72}$  and therefore, a well-defined CLP intermediate cannot be isolated. In this context, to synthesize a well-defined CLP, the reaction conditions and the reactant concentrations for the post-polymerization cyclization should be controlled. Some common reactions used for such cyclization include oxidative dehydrogenation, electrophilic aromatic substitution (S<sub>E</sub>Ar), photochemical cyclization, boron–oxygen (B–O)/boron–nitrogen (B–N) bond formation, imine condensation, ring-closing metathesis, etc.

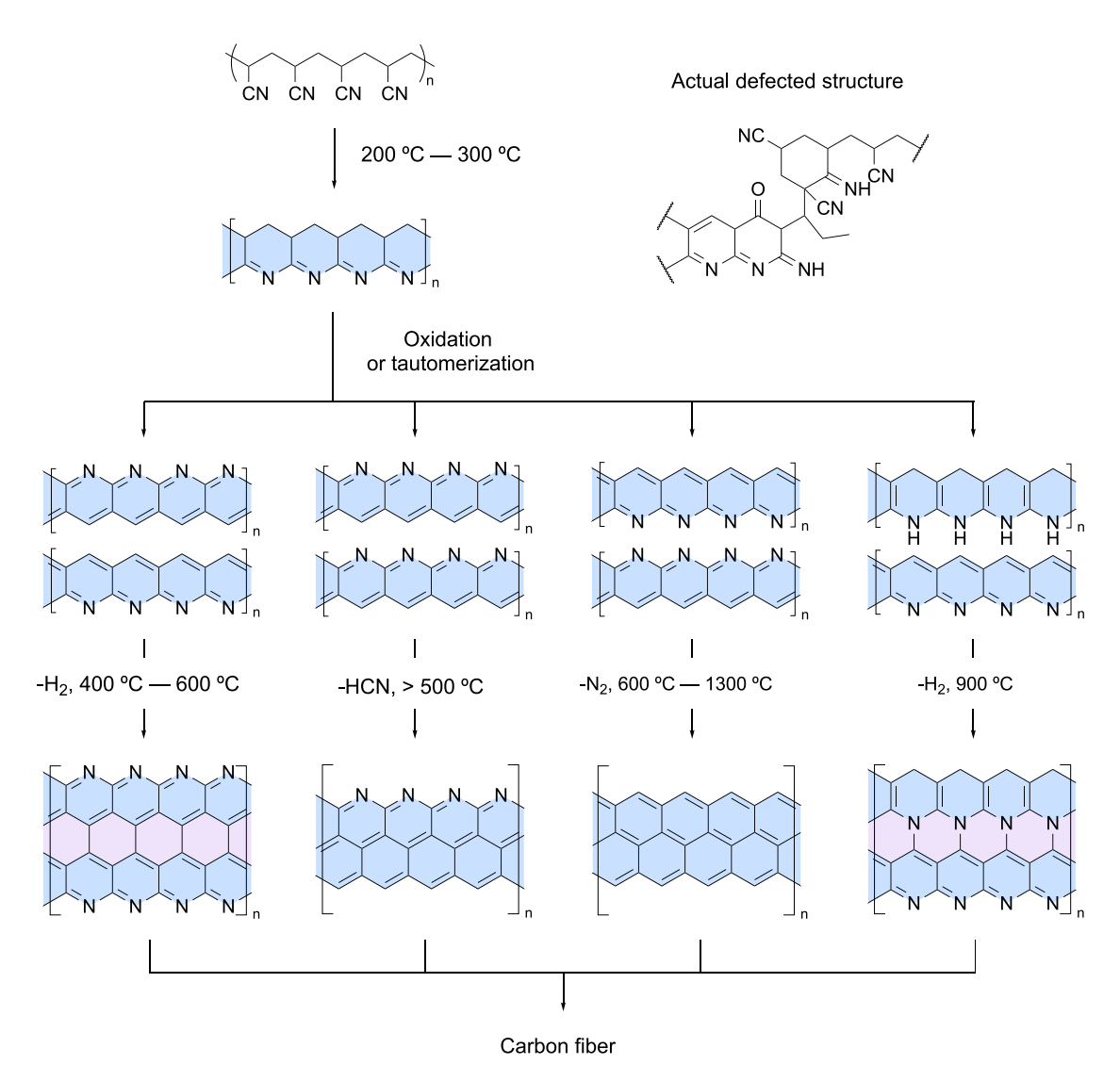
#### Oxidative dehydrogenation

Many reported examples of CLPs are ladderized through the formation of C–C bonds via oxidative dehydrogenation of C–H bonds in a precursor. These methods diminish the need for pre-installed functional groups for cyclization, thereby simplifying the design and synthesis of monomers. Additionally, the structure of monomers can be easily varied, facilitating the synthesis of a broad range of complex polycyclic aromatic hydrocarbons and CLPs. During this oxidation process, carbon atoms with higher electron density typically exhibit increased reactivity, which can lead to a degree of regioselectivity. However, achieving precise control of regioselectivity for many complex precursors still remains a significant challenge for low-defect synthesis.

The most commonly used reaction for dehydrogenation is Scholl oxidation, typically performed in the presence of FeCl<sub>3</sub>. For example, Mikami and coworkers demonstrated the synthesis of LP24 (Scheme 13) by Scholl oxidation of a precursor polymer with thienothiophene and phenylene units.<sup>73</sup> Sharing the feature of most oxidative dehydrogenation reactions, Scholl oxidation is generally suitable for electron-rich precursors and often affords high conversion and regioselectivity in such cases. However, CLPs obtained from Scholl oxidation may contain structural defects due to potential incomplete conversion, over-oxidation, rearrangement, or unintended chlorination, 74-76 and thus special characterization techniques are sometimes needed to rigorously confirm their constitutional structures. For instance, Plunkett and coworkers reported the syntheses of LP25 and LP26 (Scheme 14) by palladium-catalyzed cyclopentannulation polymerization followed by FeCl<sub>3</sub>-promoted Scholl oxidation in a high conversion. Nonetheless, <sup>13</sup>C NMR analysis of such polymer samples with <sup>13</sup>C-enriched ethylene groups<sup>77</sup> revealed the presence of multiple isomeric repeating unit structures in these CLPs, arising from the various regiochemical outcomes possible during the cyclopentannulation step.

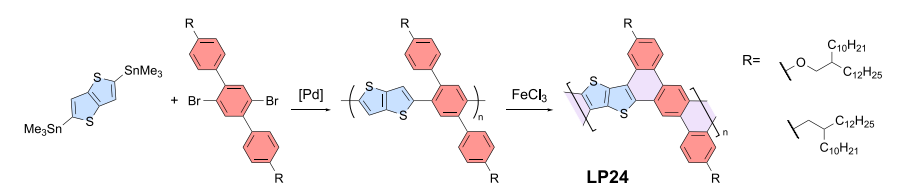
While  $FeCl_3$  is widely used as the oxidant in Scholl reactions, there are cases where it fails to afford the dehydrogenative products in a satisfactory yield, so that alternative oxidants are needed. Wu, Bai, and coworkers synthesized LP27 (Scheme 15A) by tandem alkyne benzannulation and Scholl oxidation. With the use of  $FeCl_3$  for oxidation, the isolated yields of the small-molecule models were found to be less





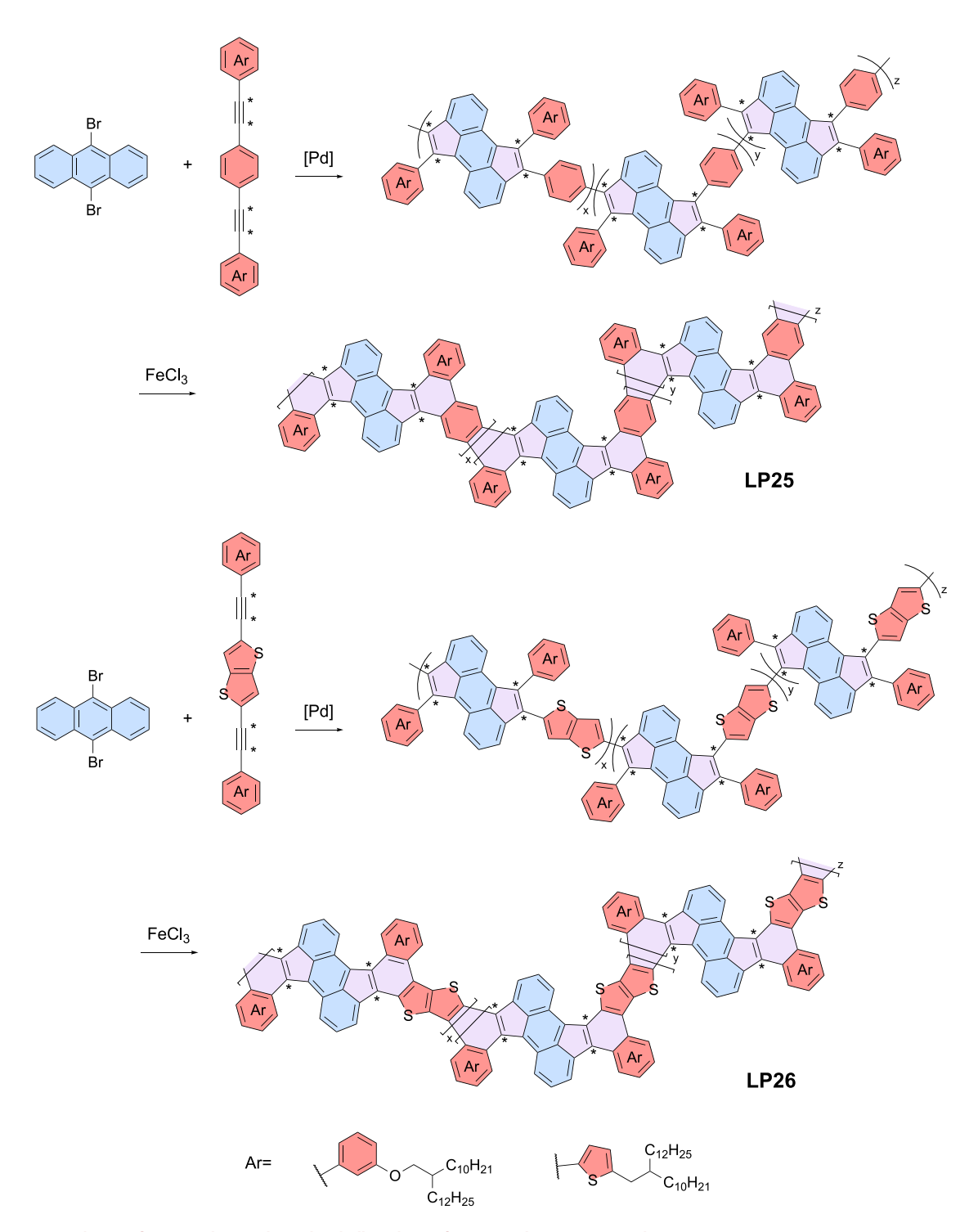
Scheme 12. Pyrolytic synthesis of carbon fiber from polyacrylonitrile, involving uncontrolled post-polymerization cyclization, results in structurally undefined, cross-linked carbon fibers with no isolatable CLP intermediates

than 50%. By contrast, the dehydrogenative products were obtained in 95% yield when the reactions were carried out with  $MoCl_5$  oxidant. The employment of organic oxidants (e.g., 2,3-dichloro-5,6-dicyano-1,4-benzoquinone [DDQ]) with Brønsted acids (e.g., triflic acid) offers an alternative method to address some drawbacks such as metal contamination and chlorination of the product during Scholl oxidation. Recent examples include the synthesis of LP28 (Scheme 15B) from a fluorene-functionalized poly(p-phenylene vinylene) derivative, reported by Takagi and Yamada. <sup>79</sup>



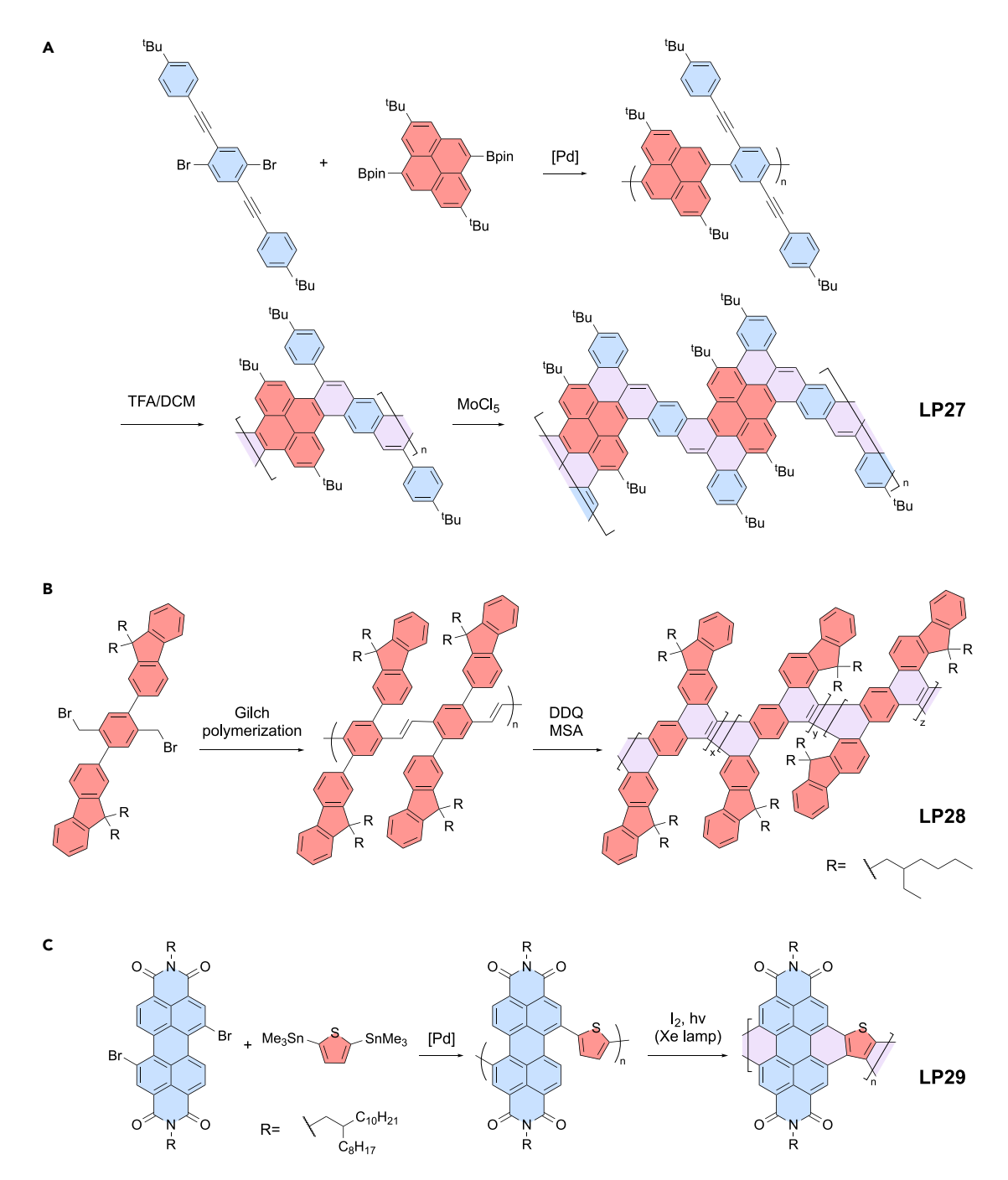
Scheme 13. Synthesis of LP24 through Scholl oxidation for post-polymerization cyclization





Scheme 14. Syntheses of LP25 and LP26 through Scholl oxidation for post-polymerization cyclization Asterisk(\*) indicates the carbon atom with <sup>13</sup>C-enriched isotope.

The DDQ-promoted C–C coupling took place between the 1- and 3-position of the fluorene units and the vinylene groups to afford a six-membered aromatic ring. A similar dehydrogenation process can also be mediated by light. Yuan and coworkers reported the synthesis of LP29 (Scheme 15C) from the precursor polymer composed



Scheme 15. Syntheses of CLPs involving Scholl oxidation for post-polymerization cyclization (A) LP27. (B) LP28. (C) LP29.

of perylene diimide and thiophene.<sup>80</sup> Despite the electron-deficient nature of the perylene diimide unit, photochemical C–C coupling at the bay position of perylene diimide with the 3-position of thiophene can be facilitated by catalytic iodine and light.

GNRs can be regarded as a distinct subcategory of carbon-rich, non-heteroatom CLPs. Oxidative coupling reaction is also widely employed as the key cyclization



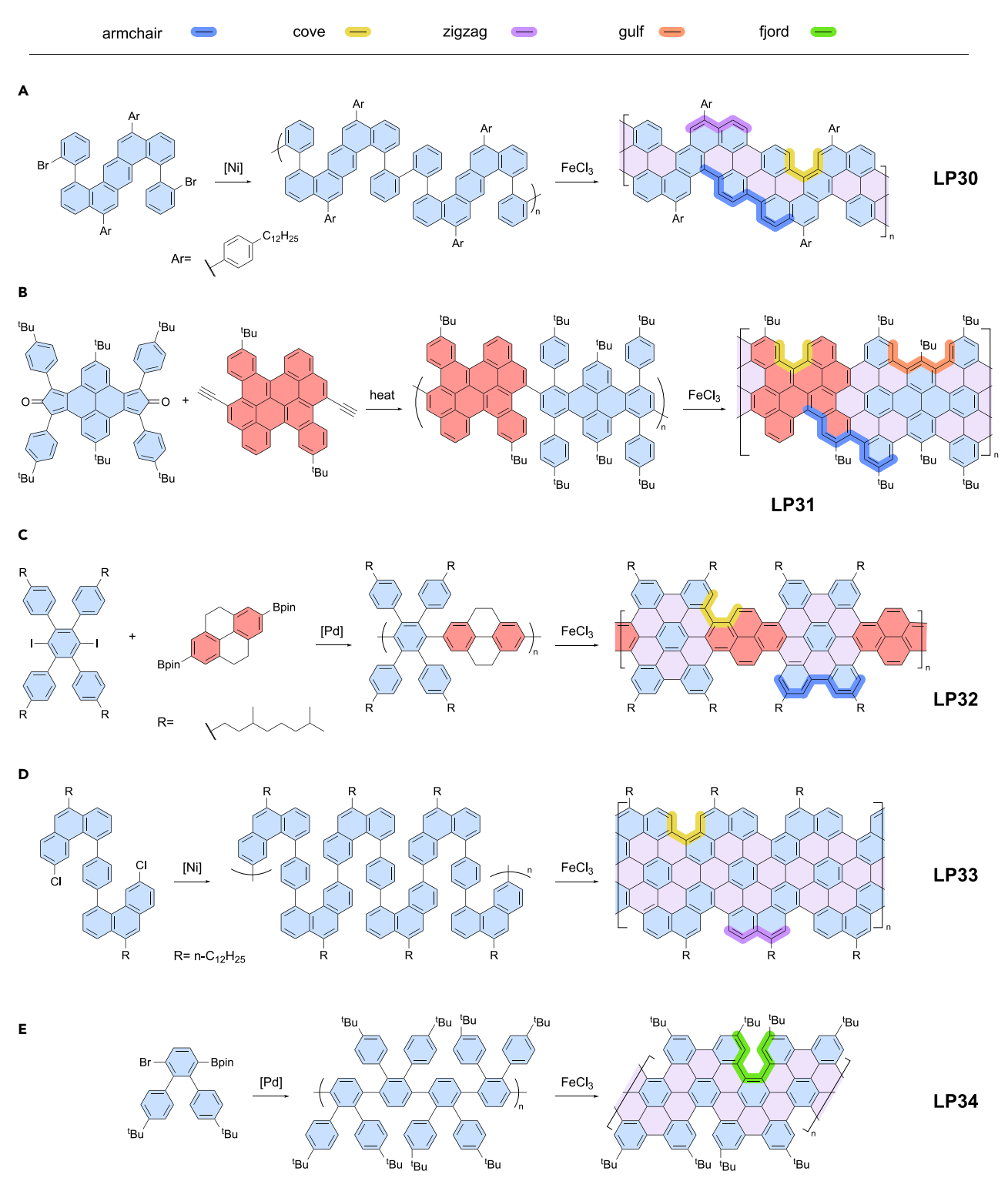


step in the solution-phase, bottom-up synthesis of GNRs. The precursor polymers are generally synthesized through cross-coupling polymerization or Diels-Alder polymerization. Subsequent post-polymerization cyclization yields quasi-one-dimensional, ribbon-like GNRs that often feature a low electronic band gap, which varies depending on the edge structure. Unlike top-down fabrication methods for GNRs, bottom-up synthesis offers structural control with potentially atomic precision. Moreover, solution-phase synthesis enables the possibility of large-scale production, a demand that presents challenges for both top-down approaches <sup>81,82</sup> and on-surface synthesis methods. <sup>10–14</sup> Here, several representative examples of recently reported GNRs are summarized. More details about the bottom-up and solution-phase synthesis of GNRs can be found in several published review articles. <sup>83–86</sup>

The molecular topologies and edge constitution play a crucial role in determining the electronic structures of GNRs, which in turn influence their photophysical and optoelectronic properties.<sup>87</sup> These structural characteristics can be precisely tailored through the design of the monomer's structure in a bottom-up synthesis approach. For example, Liu, Mai, and coworkers demonstrated the synthesis of GNR LP30 (Scheme 16A) with a combination of armchair, cove, and zigzag edge structures.<sup>88</sup> GNR LP31 (Scheme 16B), 89 LP32 (Scheme 16C), 90 and LP33 (Scheme 16D) 91 reported by Ma, Liu, Feng, and coworkers feature controlled edge structures including armchair, cove, gulf, and zigzag, achieving a band gap as low as 0.99 eV in the case of LP33. For the pyrene-embedded LP32, it was found that the direct use of highly electron-rich pyrene as the monomer resulted in side reactions during Scholl oxidation, while the replacement of pyrene with tetrahydropyrene followed by late-stage oxidation successfully afforded the desired GNR product. Owing to the limited solubility of many GNRs, the efficacy of Scholl oxidation is often assessed using solidstate characterization techniques such as FTIR, Raman spectroscopy, or sometimes by scanning tunneling microscopy (STM). To quantitatively understand the conversion efficiency of Scholl oxidation, small-molecule models are often synthesized and studied. These models serve as proxies for indirectly estimating the defect levels in GNRs. For instance, with LP31, LP32, and LP33, the isolated yields for the smallmolecule models of LP31 and LP33 exceeded 90%, while the yield for LP32's model was only around 60%. This result suggests that LP31 and LP33 have fewer defect sites on their backbones. Additionally, Müllen, Narita, and coworkers reported the synthesis of fjord-edge GNR LP34 (Scheme 16E). 92 The out-of-plane deformation brought about by the embedded [5]helicenes within the polymer backbone provides further opportunities for tuning its optical and electronic properties. Nonetheless, the isolated yield of the small-molecule model was only 54%, which is indicative of incomplete Scholl oxidation or side reactions during the GNR synthesis. Mai, Ma, Feng, and coworkers reported the synthesis of nanopore-embedded GNR LP35 (Scheme 17), which exhibits an enlarged band gap and greater solution processability, compared with its non-porous analog. 93 The high conversion of Scholl oxidation for GNR LP35 was supported by the high isolated yield of a small-molecule model.

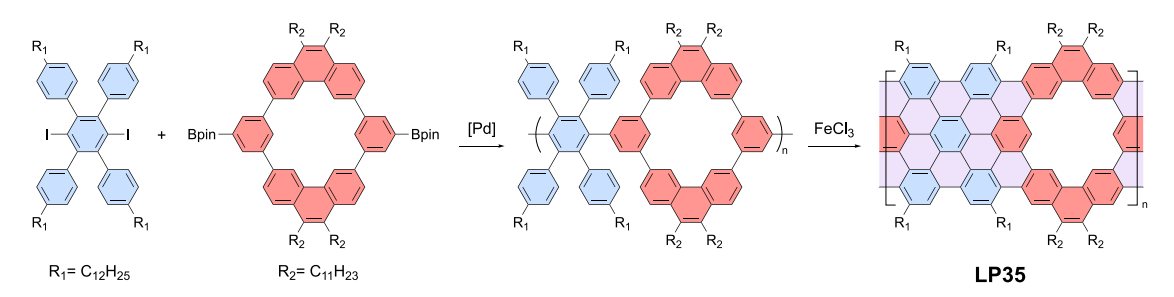
Zhu, Dong, and coworkers reported the syntheses of GNRs LP36, LP37, and LP38 featuring unsymmetrical edges (Scheme 18A). <sup>94</sup> In the case of LP36, despite the free-rotating nature of aryl-aryl C–C bonds within the backbone of the precursor polymer, the pendent phenyl rings all pointed to the same side during the regiose-lective Scholl oxidation to afford the regioregular, unsymmetrical product LP36. The desired structures of these GNRs were supported by the syntheses of small-molecule models in high yields. These unique unsymmetrical structures contribute to polarized electron distribution within the GNRs and enhanced Lewis basicity of





Scheme 16. Syntheses of GNRs through Scholl oxidation for post-polymerization cyclization (A) LP30. (B) LP31. (C) LP32. (D) LP33. (E) LP34.





Scheme 17. Synthesis of LP35 through Scholl oxidation for post-polymerization cyclization

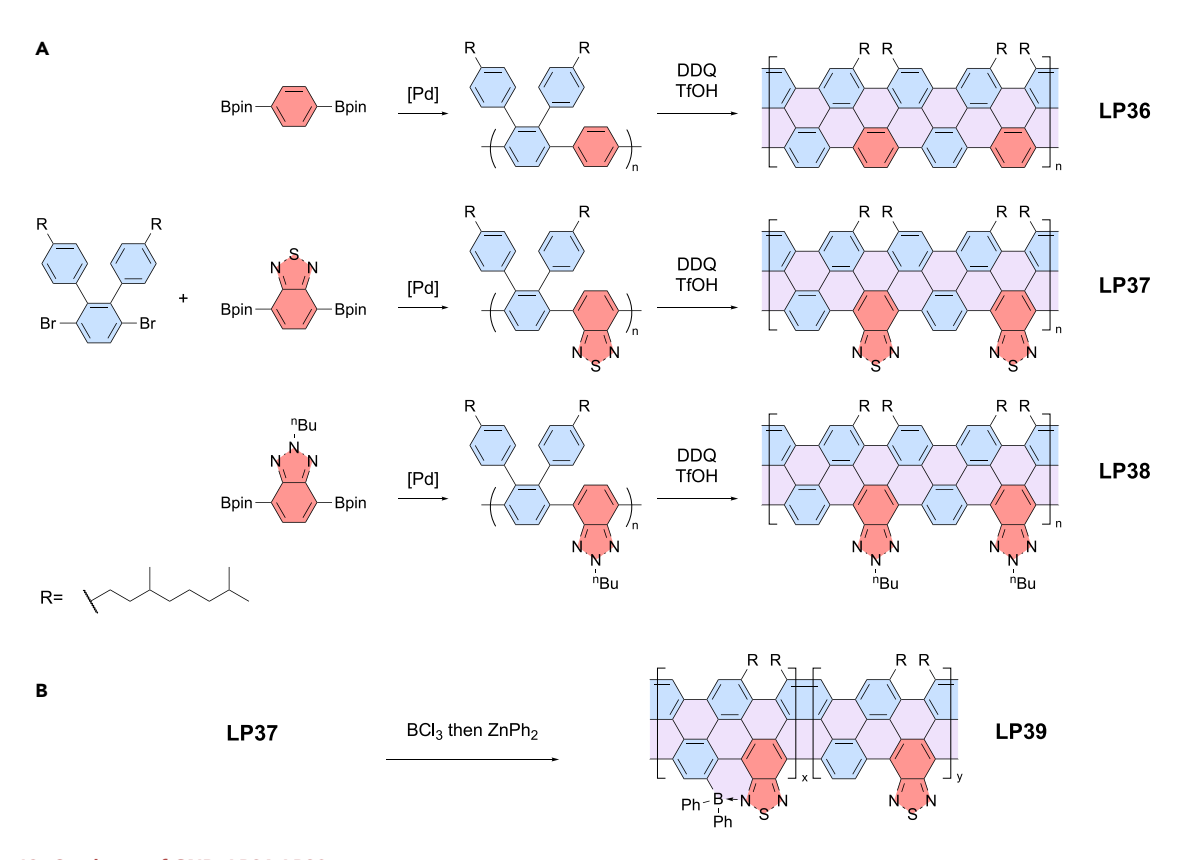
the heteroarenes for further manipulation of the band gaps. For instance, treating LP37 with  $BCl_3$  followed by  $ZnPh_2$  afforded the partially C–H borylated and N–B coordinated product LP39 (Scheme 18B), resulting in a reduction of electrochemical band gap from 1.25 to 0.80 eV.

Chen, Bogani, Anderson, and coworkers reported metal-porphyrin-embedded GNR LP40 (Scheme 19) through Ni-catalyzed cross-coupling followed by DDQ-promoted oxidative cyclization. 95 LP40 possesses an ultra-low band gap with near-infrared absorption up to 1,600 nm, and its single-molecule electronics were demonstrated. Müllen, Palma, and coworkers reported the synthesis of ABA-type triblock copolymer LP41 (Scheme 20) via Diels-Alder polymerization followed by Scholl oxidation. 96 The access to LP41, consisting of segments with different widths, provides an opportunity to achieve nanoscale diode circuitry. Fischer and coworkers reported the synthesis of aldehyde-decorated GNR LP42 (Scheme 21) via a similar strategy. 97 GNR LP42 was further transformed into a covalent organic framework (COF) by interfacial imine condensation with benzidine as the cross-linker. The phase separation of reactants (GNR LP42 and benzidine) in the organic phase and the catalyst (Sc(OTf)<sub>3</sub>) in the aqueous phase ensures the formation of a COF only at the liquid-liquid interface. Müllen, Narita, and coworkers reported the synthesis of GNRs LP43a-LP43c (Scheme 22) via post-polymerization Suzuki coupling. 98 The difference in side groups on these GNRs contributes to their unique self-assembled structures. In particular, a supramolecular rectangular network larger than 100 nm was observed for LP43a when drop-cast on graphite from its trichlorobenzene dispersion. GNR LP44 (Scheme 23) with anthracene-maleimide adduct side chains was reported by Cerullo, Mai, and coworkers. 99 This sterically bulky side chain renders LP44 highly soluble in common organic solvents.

### Electrophilic aromatic substitution

 $S_E$ Ar reactions, often mediated by acids, have been widely used for CLP synthesis from  $\pi$ -electron-rich precursors. A classic example is the synthesis of ladder-type poly(p-phenylene) (LPPP) (Scheme 24) reported by Scherf and Müllen in the early 1990s.  $^{100}$  In this case, a poly(p-phenylene) precursor functionalized with tertiary hydroxyl groups was first synthesized. A second strand of bonds was subsequently formed through intramolecular  $S_E$ Ar of the phenylene unit and a neighboring benzylic carbon center in the presence of a Lewis acid such as  $BF_3$ . Scherf and coworkers further refined this strategy to synthesize methyl-substituted LPPP (MeLPPP) (Scheme 24).  $^{101}$  The additional methyl groups in MeLPPP introduce a steric effect that prevents undesired intermolecular  $S_E$ Ar reactions during ladderization. The reaction concentration for  $S_E$ Ar cyclization must be carefully considered and optimized to avoid undesired intermolecular reactions that can lead to defect formation. Since then, a broad array of structurally diverse CLP derivatives synthesized using similar methods have been reported and studied. These examples have been summarized in several published review articles.  $^{5,8,102}$ 

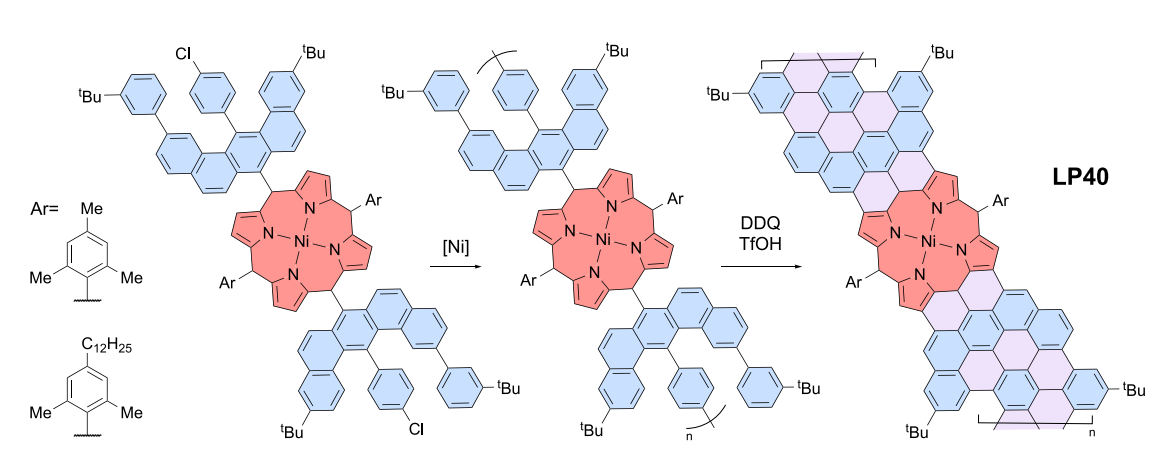




### Scheme 18. Syntheses of GNRs LP36-LP39

(A) Syntheses of LP36, LP37, and LP38 through Scholl oxidation for post-polymerization cyclization. (B) Syntheses of LP39 through partial C–H borylation and B–N bond formation.

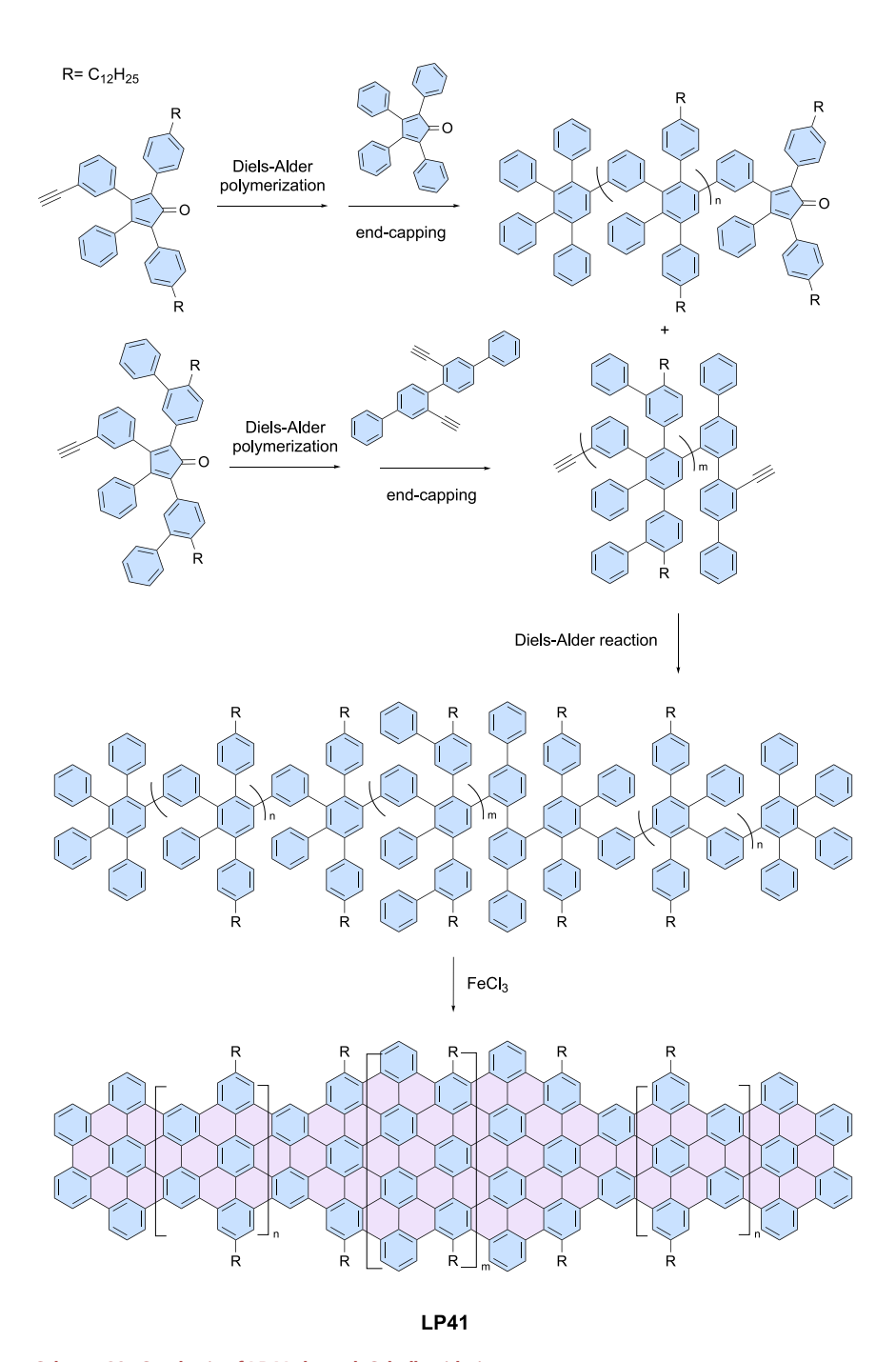
Recently, several intriguing examples of CLP synthesis, using the  $S_E$ Ar approach, have been reported. Köhler and coworkers employed this strategy to synthesize pyrene-derived CLP LP45 (Scheme 25A), in which the second strands of bonds are formed by  $S_E$ Ar of the 1,6- or 1,8-position of pyrene. <sup>103</sup> Zhang and coworkers reported the synthesis of LP46 (Scheme 25B) through a similar strategy, with the second strands of bonds formed by  $S_E$ Ar of thienothiophene. <sup>104</sup> Forster, Scherf, and coworkers reported the synthesis of LP47a (Scheme 25C) by  $S_E$ Ar of a naphthalene-derived precursor. <sup>105</sup> LP47a can be partially oxidized in the air and fully



Scheme 19. Synthesis of LP40 through Scholl oxidation for post-polymerization cyclization



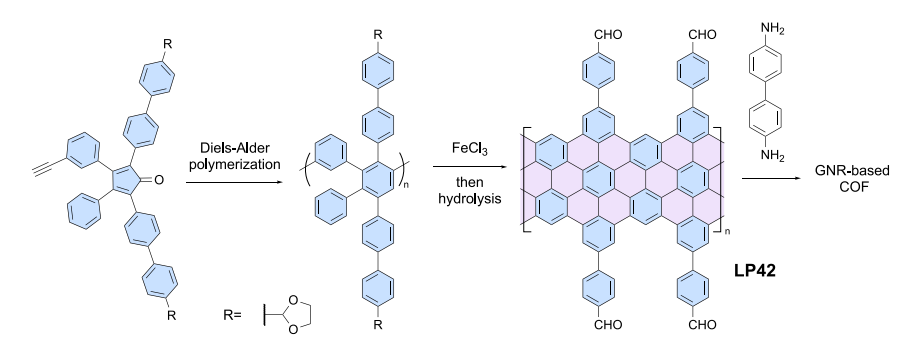




Scheme 20. Synthesis of LP41 through Scholl oxidation

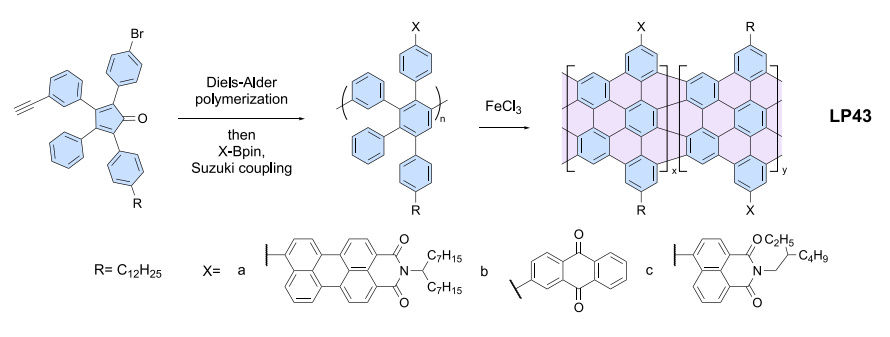
oxidized to its quinoidal form LP47b (Scheme 25C) with DDQ oxidant, although carbonyl defects were also observed due to over-oxidation. Cooper and coworkers demonstrated the synthesis of LP48 (Scheme 25D) by  $S_{E}Ar$  of phenylene and sulfoxide, followed by dealkylation and oxidation.  $^{106}$  It is noteworthy that the reaction is self-deactivated when sulfonium intermediates are formed, which likely affects the conversion rate of the cyclization step, potentially leading to uncyclized defects on the backbone.  $^{107}$ 





Scheme 21. Synthesis of LP42 through Scholl oxidation and the further interfacial synthesis of a COF from LP42

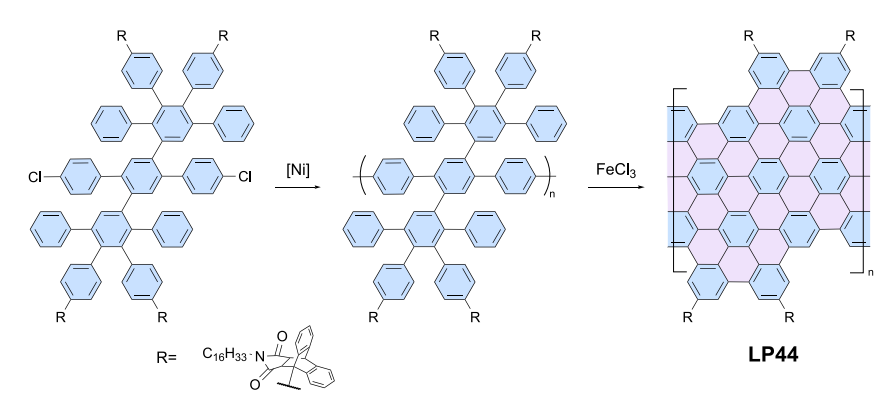
Fang and coworkers synthesized LP49a (Scheme 26A) via S<sub>E</sub>Ar from fluorene-derived precursor polymers. 108 The strong interchain complimentary hydrogen bonds of LP49a render its general insolubility in most organic solvents. Once the hydrogen bond donors are masked by protecting groups (Boc), the resulting LP49b (Scheme 26A) is soluble, and the solution-processed film shows good solvent resistance after thermal cleavage of Boc groups. More recently, CLPs LP50 (Scheme 26B) reported by Zou, Fang, and coworkers<sup>109</sup> and LP51 (Scheme 26C) reported by Xu, Ng, Fang, and coworkers<sup>110</sup> were synthesized to emulate polyaniline, which possesses redox switchability and electrical conductivity. For LP50, the fully oxidized pernigraniline state was achieved by the addition of m-CPBA as an oxidant, while the fully reduced leucoemeraldine state was obtained by treating it with hydrazine as a reductant. As for LP51, the fully oxidized pernigraniline state was accomplished by Ag<sub>2</sub>O oxidant. Treating the fully oxidized, neutral pernigraniline base of LP50 and LP51 with strong acids (such as MSA and HCl) further afforded the corresponding pernigraniline salt, both exhibiting good stability, open-shell diradical character, and electrical conductivity in the solid state.



Scheme 22. Synthesis of LP43a-c through Scholl oxidation



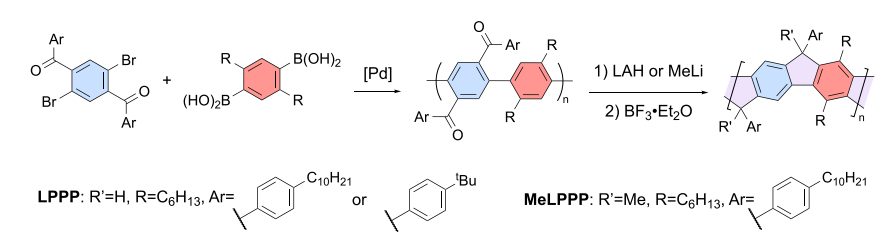




Scheme 23. Synthesis of LP44 through Scholl oxidation

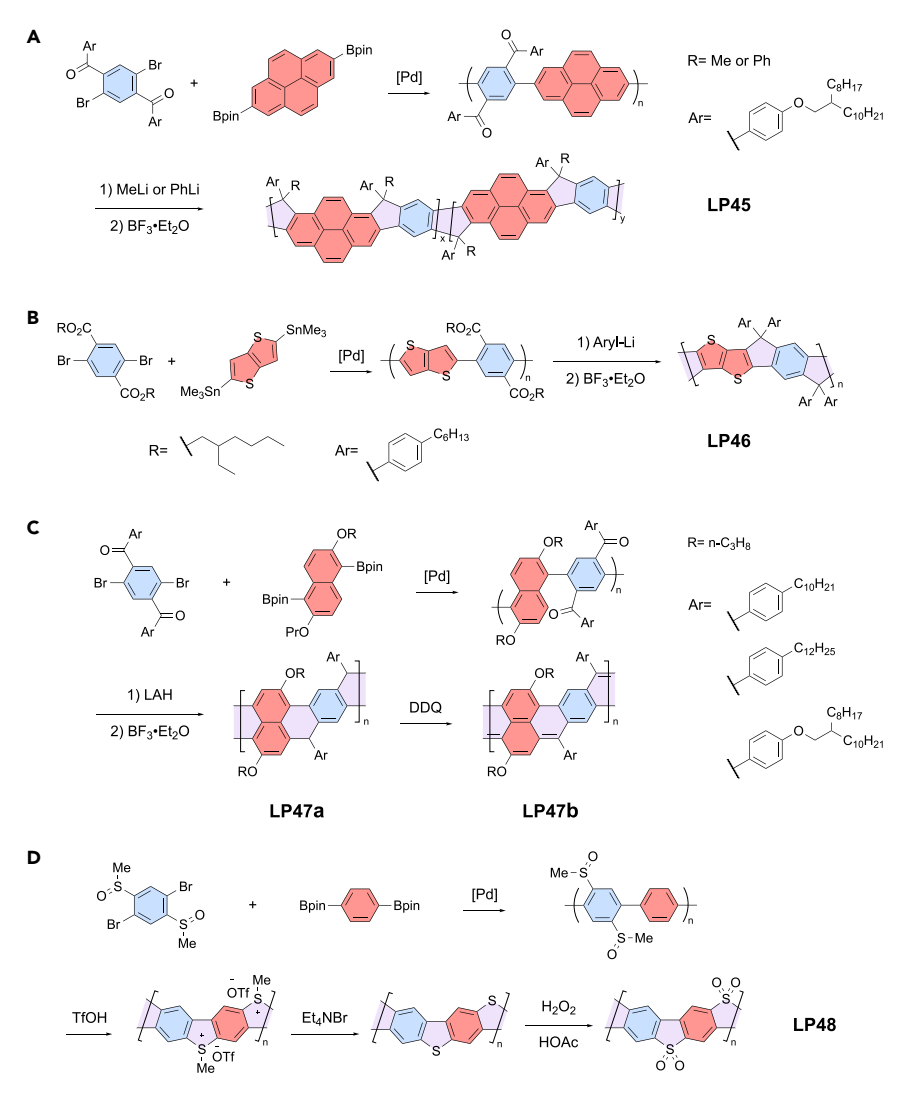
of backbone electron density as the reaction proceeded. <sup>112</sup> Thus, subsequent treatment of the polymer with a stronger Brønsted acid (triflic acid) at a lower temperature was required to drive the reaction further while avoiding side reactions, as supported by the small-molecule model reaction. More recently, Swager and coworkers reported the synthesis of oxepine-based LP54 and LP55 (Scheme 27C) through alkyne benzannulation. <sup>113</sup> The seven-member rings within the backbones were found to exhibit  $8\pi$ -electron excited-state aromatization according to Baird's rule. This feature resulted in backbone planarization upon photoexcitation, as demonstrated by the large Stokes shift virtually independent of solvent polarity.

One of the side reactions observed during alkyne benzannulation is hydride-shift rearrangement, which results in the formation of defect sites on the CLP backbone. Ikai, Yashima, and coworkers reported a strategy to address this issue. They reported the synthesis of helical CLP LP56 (Scheme 28A) with low level of defects through alkyne benzannulation, and the enantiomerically enriched polymer was successfully isolated by using preparative chiral HPLC. 114 A side reaction associated with hydride-shift rearrangement during benzannulation was identified when an unsubstituted phenyl-alkyne was used. 115,116 Interestingly, when additional 2- and 6-methyl groups were introduced onto the phenyl groups, hydride-shift rearrangement was no longer observed, as supported by the <sup>1</sup>H NMR spectra of small-molecule models. Eliminating these side reactions provides an alternative method for synthesizing low-defect ladder polymers. The same research team further synthesized helical CLP LP57 (Scheme 28B) through this modified benzannulation method. 117 By tuning the binaphthyl dihedral angles and thus the polymer helicity through varied tether lengths, the circularly polarized luminescence of these CLPs was investigated. It is noteworthy that earlier examples of alkyne benzannulation and its use for the synthesis of nanographene molecules have been discussed in a review article by Chalifoux and Senese. 118



Scheme 24. Syntheses of LPPP and MeLPPP through SEAr for post-polymerization cyclization



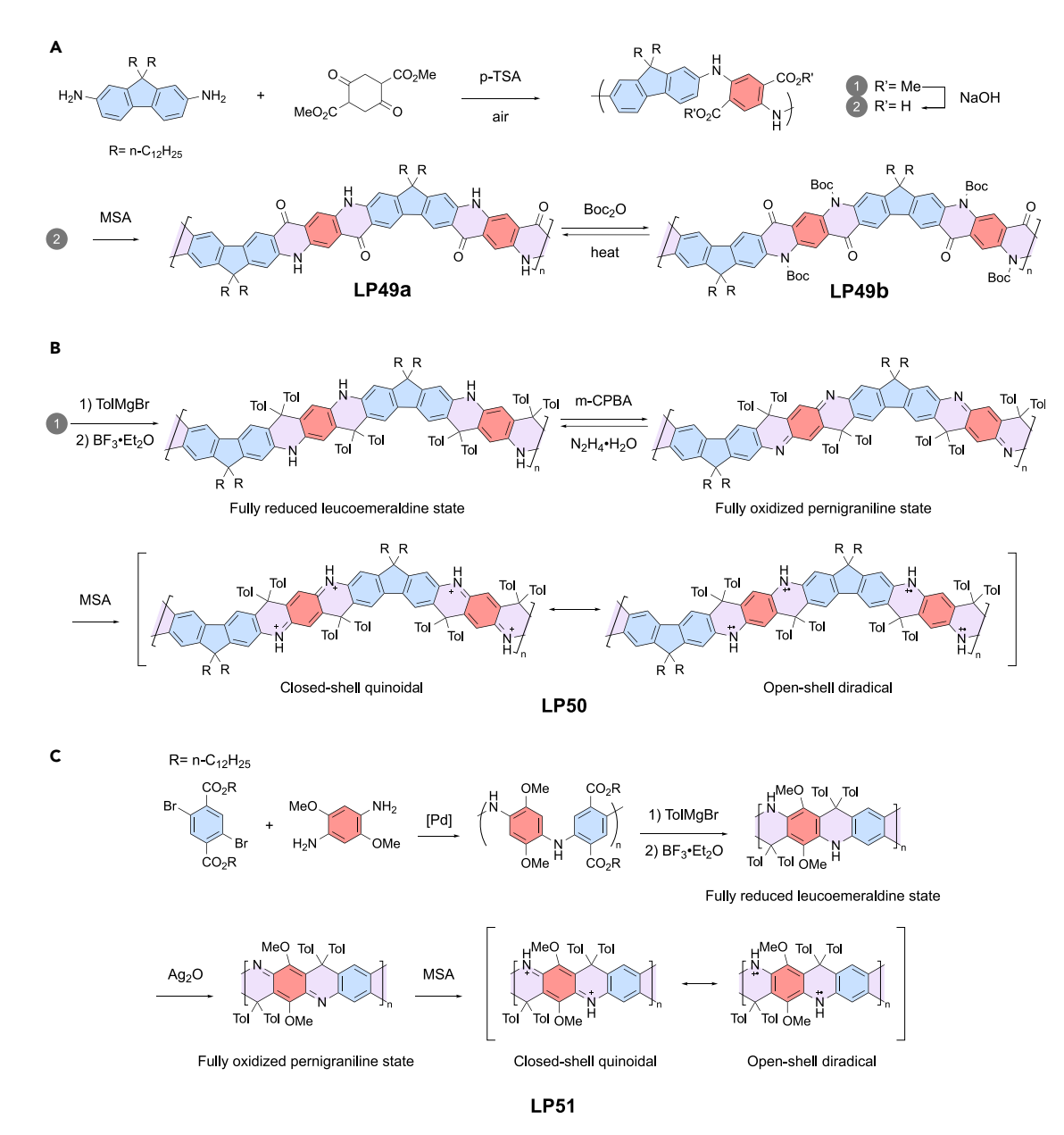


Scheme 25. Syntheses of CLPs through  $S_EAr$  post-polymerization cyclization (A) LP45. (B) LP46. (C) LP47a and LP47b. (D) LP48.

#### Photochemical cyclization

Photochemistry allows chemical reactions to proceed through excited-state pathways that are usually inaccessible via the thermal pathways, and it has been employed as an important strategy for CLP ladderization. Morin and coworkers reported light-mediated cyclodehydrochlorination (CDHC) as an efficient approach to synthesize low-defect CLPs.  $^{119-123}$  The CDHC mechanism is believed to proceed through a photochemical conrotatory (4n + 2)  $\pi$  electrocyclization, followed by the elimination of HCl molecules. The fact that almost no side product was found during CDHC precludes a radical mechanism involving photolysis of C–Cl bond.  $^{124}$  During the CDHC process, the cyclized product is usually obtained with high conversion, likely attributed to the entropic benefit of releasing HCl molecules. However, employing a chlorine substituent for cyclization introduces a challenge owing to potential undesired cross-coupling reactions involving the C–Cl bond. In this scenario, conducting the cross-coupling polymerization of precursor polymers starting from aryl iodides may be preferable to starting from aryl bromides. The selectivity among various aryl halides for cross-coupling must be



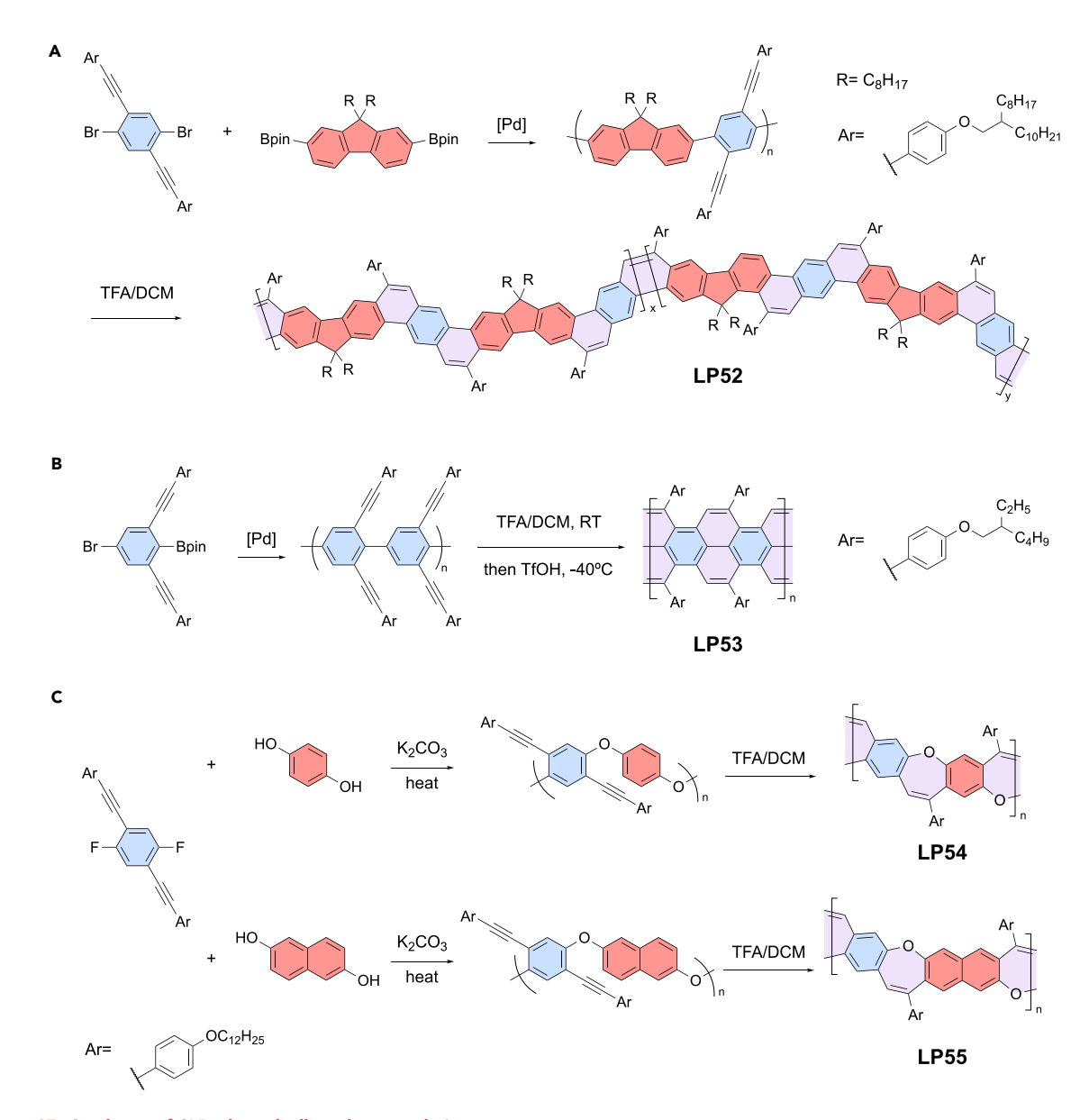


Scheme 26. Syntheses of CLPs through S<sub>E</sub>Ar post-polymerization cyclization. LP50 and LP51 are ladder-type analogs of polyaniline featuring robust redox switchability and solid-state electrical conductivity
(A) LP49a and LP49b. (B) LP50. (C) LP51.

thoroughly evaluated to ensure the preservation of chlorine atoms for subsequent CDHC.

CDHC was employed to successfully synthesize linear and helical CLPs LP58, LP59, LP60, LP61 (Scheme 29), 119,120 and LP62 (Scheme 30), 121,122 as well as pyrrole-embedded CLPs LP63 and LP64 (Scheme 31). 123 Compared with those for small-molecule models, the reaction conditions for ladder polymer synthesis required higher temperatures, and the reaction kinetics were still slower. For LP58, it is possible that as CDHC proceeds, the decreased band gap of polymers results in the lower quantum efficiency of photochemical reaction. Therefore, a two-step reaction with different energy light sources was used to promote the formation of the





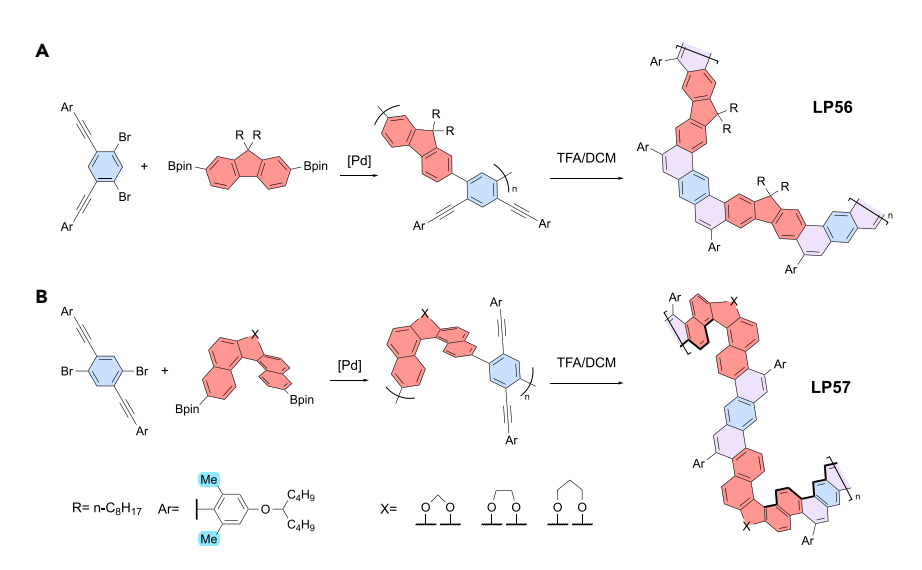
Scheme 27. Syntheses of CLPs through alkyne benzannulation (A) LP52. (B) LP53. (C) LP54 and LP55.

desired CLPs with high conversion. The optimal energy of light sources for CDHC also depends on the intrinsic electronic properties of the polymers, ranging from 254 to 365 nm depending on the structure. CDHC method is generally used for synthesizing CLPs with electron-rich units such as benzene, thiophene, and pyrrole. For electron-deficient  $\pi$ -systems such as pyridine, a significant decrease of cyclization conversion was observed,  $^{124}$  posing challenges to the synthesis of electron-deficient CLPs using this method.

#### B-O and B-N bond formation

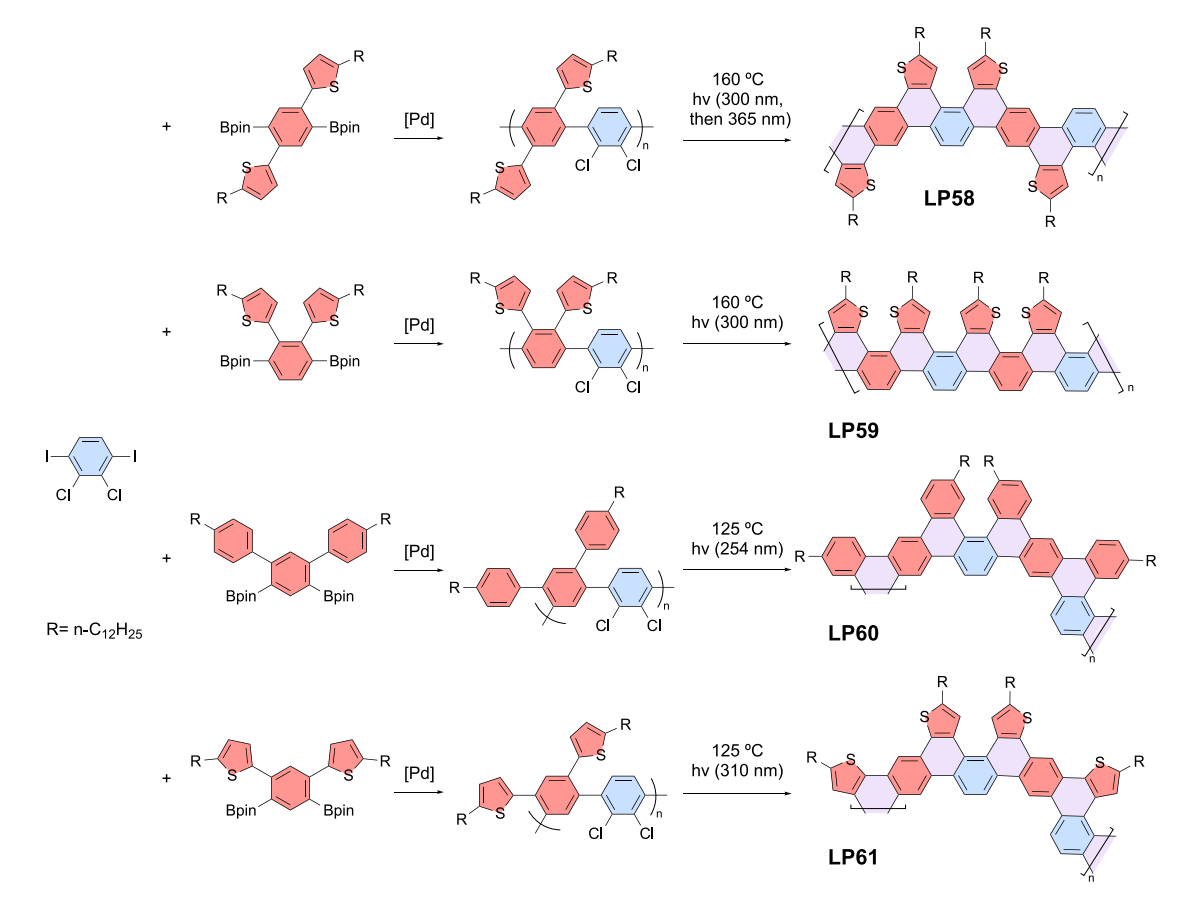
Boron-containing conjugated polymers have gained interest in recent years because of their low-lying lowest unoccupied molecular orbitals (LUMOs) and the resulting n-type electronic properties.  $^{125-127}$  These characteristics can be incorporated into CLPs by introducing boron centers into the conjugated fused  $\pi\text{-system}$  of CLPs. In





Scheme 28. Synthesis of CLPs through low-defect alkyne benzannulation from a methylprotected precursor (A) LP56. (B) LP57.

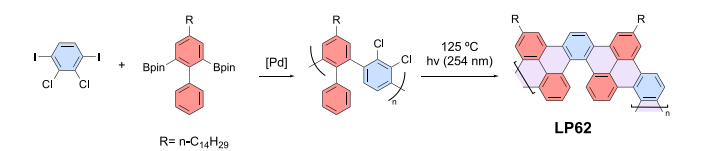
general, the formation of B–O and B–N bonds is thermodynamic favorable; however, defects can possibly arise from B–C bond formation if such transformation is incomplete or non-regioselective. Liu, Wu, and coworkers reported the syntheses of LP65



Scheme 29. Syntheses of LP58, LP59, LP60, and LP61 through photochemical post-polymerization cyclization







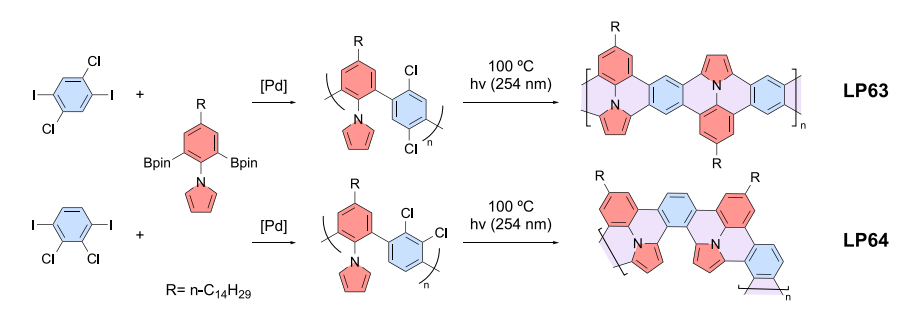
Scheme 30. Synthesis of LP62 through photochemical post-polymerization cyclization

and LP66 (Scheme 32A) by treating a hydroxyl-group functionalized, carbazolederived polymer with phenylboron dichloride. 128 Borylation of the carbazole and B-O bond formation formed the additional strand to afford a full ladder-type structure. Nitrogen centers can also be used to pair up with boron in the construction of ladder polymers. For example, Zhang, Wu, Li, and coworkers synthesized LP67 (Scheme 32B) by treating carbazole-diaminophenylene-derived precursor polymer with phenylboron dichloride, resulting in the formation of N-B bonds as the second strand of bonds for the CLP constitution. 129 This strategy was also employed for thienothiophene- and benzodithiophene-derived polymers to afford boron-containing CLPs LP68 and LP69 (Scheme 32C), as reported by Xue, Zhang, and coworkers. 130 Strong N-B bonds can also be formed between a Lewis basic nitrogen center and a Lewis acidic tri-coordinated boron center to give a tetracoordinate boron center. 131 For example, von Hauff, Pammer, and coworkers demonstrated the synthesis of LP70 (Scheme 32D) by the hydroboration of alkene groups of a pyridine-based precursor polymer. 132 In this case, the high degree of head-to-tail regionegularity of poly(pyridine) precursor was crucial for effectively constructing fully ladderized backbone by N-B bonds. The optical and electrochemical properties of these polymers were easily tailored by adjusting the hydroboration agents with varied substituents.

### Thermodynamic-driven cyclization

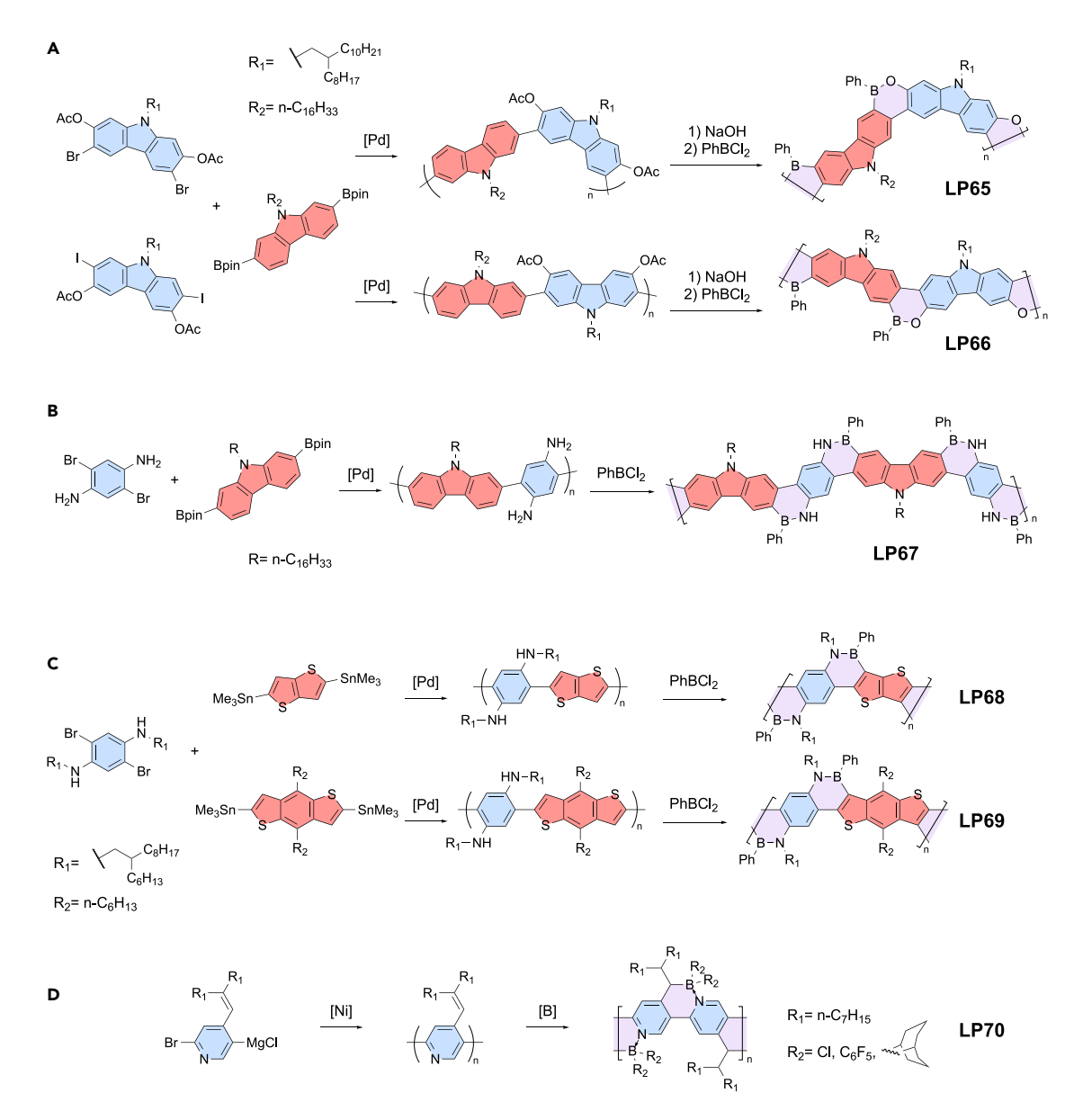
The ladderization of CLPs via thermodynamically driven cyclization offers several key advantages compared with those via kinetically controlled cyclization. For kinetically controlled cyclization methods, although high conversion rates are often observed for model small molecules, CLPs produced by these methods may still contain defects due to undesired, kinetically trapped side reactions. This problem can be mitigated if the cyclization reaction is reversible and thermodynamically driven, while the desired CLP is the most stable thermodynamic product. In such cases, the possibility of undesired, kinetically trapped side reactions is eliminated, and high cyclization conversion is expected to direct the reaction toward the desired defect-free CLP as the thermodynamic product.

Fang and coworkers reported the synthesis of CLP LP71 (Scheme 33A) via ringclosing olefin metathesis (RCM) in refluxing toluene using Grubbs II catalyst.<sup>133</sup>



Scheme 31. Syntheses of LP63 and LP64 through photochemical post-polymerization cyclization

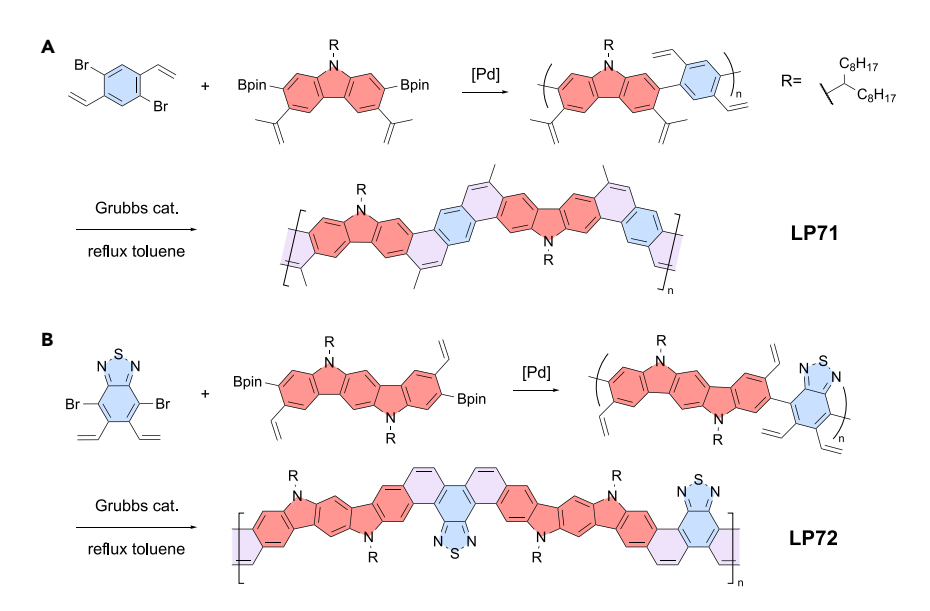




Scheme 32. Syntheses of CLPs through B–O and B–N bond formation for post-polymerization cyclization (A) LP65 and LP66. (B) LP67. (C) LP68 and LP69. (D) LP70.

The quantitative formation of the ladder-type backbone is attributed not only to enthalpy-favored aromatization and entropy-favored ethylene release but also to the thermodynamically controlled nature of olefin metathesis under these conditions. In this process, any transient side products formed through undesired cross-metathesis were further converted into the desired CLP. The same team further demonstrated that this method is applicable to the synthesis of a donor-acceptor CLP LP72 (Scheme 33B) incorporating an electron-deficient benzothia-diazole unit in the conjugated backbone, a synthetic target that is often challenging for other cyclization techniques that rely on the reactivity of electron-rich moieties. However, despite the promising characteristics, synthesis of CLPs, through this strategy and its large-scale applications, is still limited because of the high reactivity of alkenyl groups in the precursor polymer, necessitating careful





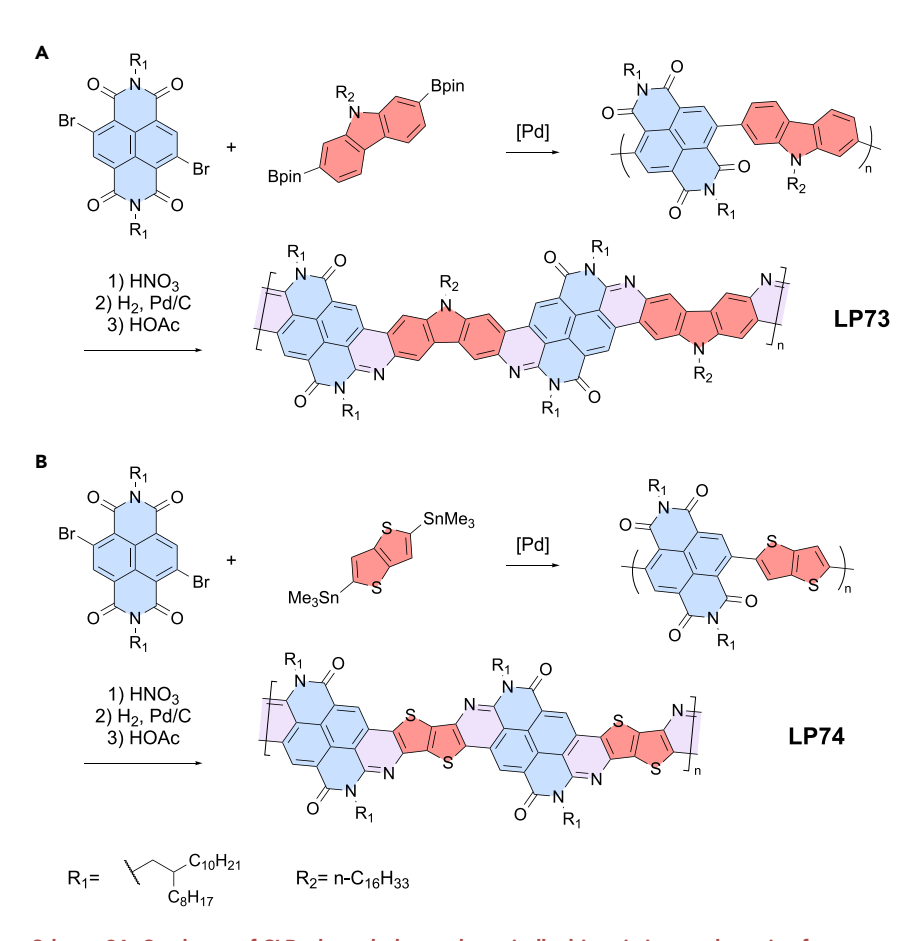
Scheme 33. Syntheses of CLPs through thermodynamically driven ring-closing metathesis (A) LP71. (B) LP72.

handling and the use of radical inhibitors for stabilization during reactions or storage.

The employment of imine condensation as the post-polymerization cyclization method represents another example of a thermodynamically driven reaction for CLP synthesis. Wu, Ba, and coworkers reported the syntheses of LP73 and LP74 (Schemes 34A and 34B) by post-polymerization nitration and reduction, followed by imine condensation. <sup>135</sup> High conversion was attainable for the serial interconversion of these functional groups, especially the last thermodynamically controlled imine condensation step. However, it is worth noting that as more synthetic steps are introduced as post-polymerization functionalization, a small percentage of incomplete conversion in each step might still result in structural defects in the final CLP.

#### Other post-polymerization cyclization methods

In principle, any cyclization reaction with high conversion and minimized side reactions can be used for the CLP ladderization with low-defect levels. Scherf and Chmil reported the synthesis of LP75 (Scheme 35) through reductive carbonyl olefination, representing one of the earliest examples of soluble GNR synthesis. 136,137 Recently, a number of new unconventional methods have been reported for the synthesis of CLPs through post-polymerization cyclization. For example, Scherf, Bahmann, Seixas de Melo, Lupton, and coworkers reported the use of an intramolecular aldol-type condensation reaction between benzylic carbanions and their neighboring ketone groups to achieve the synthesis of polyacene-derived LP76 (Scheme 36A). 138 A good conversion was achieved as supported by the nearly complete disappearance of C=O stretching in FTIR spectra. Lin and coworkers reported the synthesis of LP77 (Scheme 36B) through a phenoxazine cyclization between aryl C-H and benzophenone. 139 The proposed mechanism first involved a keto-enol tautomerization, followed by the cyclization between aryl C-H and enol group in the presence of benzoyl chloride. The successful transformation was supported by the diminishing N-H stretching in FTIR spectra and a high isolated yield (>90%) of the small-molecule model, which could be indicative of the low-defect level of the

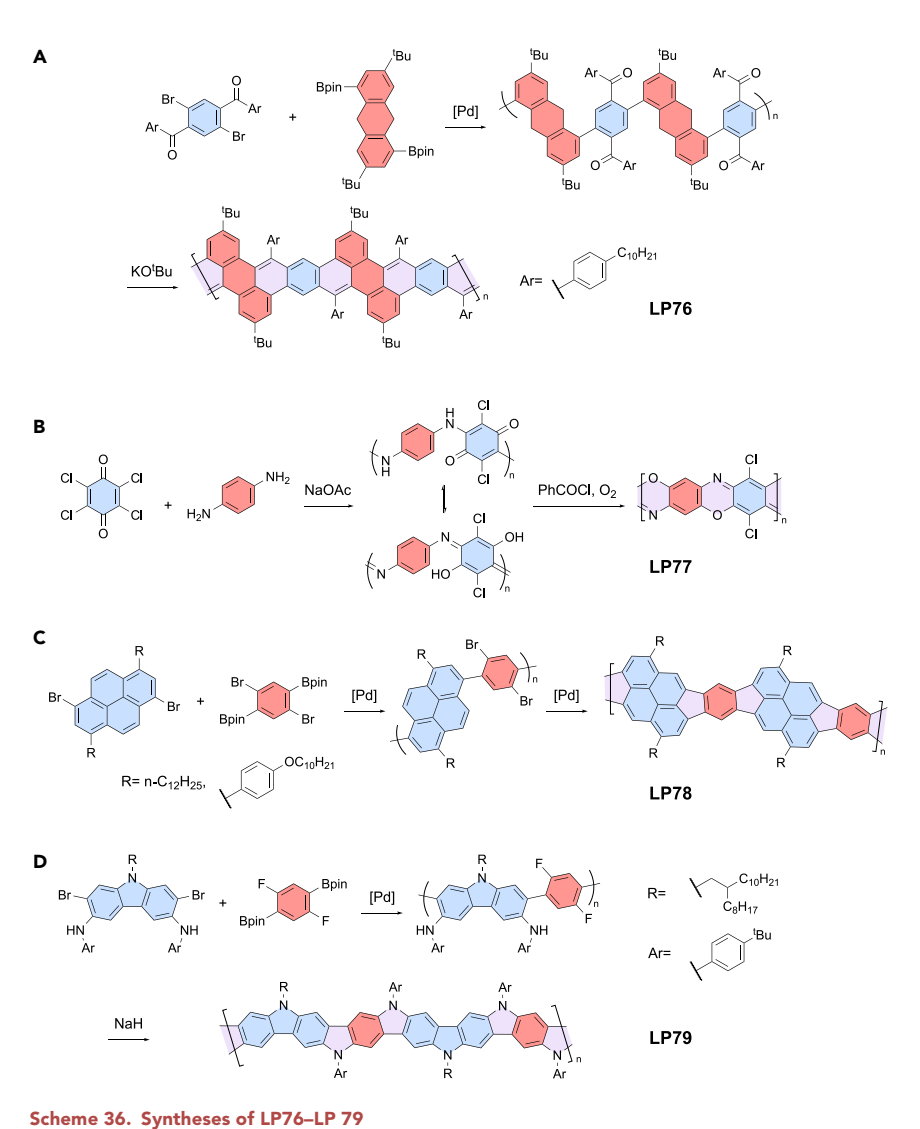


Scheme 34. Syntheses of CLPs through thermodynamically driven imine condensation for post-polymerization cyclization
(A) LP73. (B) LP74.

polymer. LP78 (Scheme 36C) reported by Plunkett and coworkers was synthesized through Suzuki polymerization followed by Heck coupling cyclization. 140 This strategy successfully afforded the product polymer that could not be obtained via Scholl oxidation. According to the small-molecule model reactions, Scholl oxidation cannot cyclize the electron-rich dimethoxy phenylene and the K region of pyrene. Replacing the dimethoxy phenylene with dibromophenylene allowed for successful Heck coupling reaction to cyclize and hence fuse the repeating units in a good conversion. For the polymer synthesis, however, it is challenging to keep all the bromine atoms on phenylene units intact during the first step of Suzuki polymerization. Ideally, the two different sets of functional groups for polymerization and post-polymerization cyclization should have orthogonal reactivities. Zhao, Wu, and coworkers demonstrated the synthesis of LP79 (Scheme 36D) by intramolecular nucleophilic

Scheme 35. Synthesis of LP75 through reductive carbonyl olefination





(A) LP76 through aldol-type condensation. (B) LP77 through C–H functionalization. (C) LP78 through Heck coupling.(D) LP79 through S<sub>N</sub>Ar for post-polymerization cyclization.

aromatic substitution ( $S_NAr$ ) cyclization of pendent secondary aniline and aryl fluoride. <sup>141</sup> The aryl fluoride groups are highly robust under the conditions for cross-coupling polymerization but effectively underwent the  $S_NAr$  cyclization in good conversion. Although the structure of LP79 resembles ladder-type polyaniline, its acid-doped property and conductivity that conventional polyaniline possesses were not reported. In addition, Uemura and coworkers reported the synthesis of LP80 (Scheme 37) from acrylonitrile in an aluminum-based MOF (DUT-5). <sup>72,142</sup> The synthesized polyacrylonitrile embedded in MOF was further cyclized to give a linear ladder-type structure in high conversion. With the MOF confinement effect, this method affords the ladder product with significantly fewer aliphatic defects than that obtained from conventional methods.

In certain cases, the synthesis of a small-molecule model may not be necessary if the ladder-type constitution of polymers can be unambiguously characterized. Lupton, Höger, and coworkers demonstrated the synthesis of LP81 (Scheme 38A) via Glaser alkyne homo-coupling polymerization of one strand of bonds, followed by the

Please cite this article in press as: Yang and Fang, Conjugated ladder polymers: Advances from syntheses to applications, Chem (2024), https://doi.org/10.1016/j.chempr.2024.04.002





Scheme 37. Synthesis of LP80 within MOF channels

formation of the second strand of bonds through Glaser coupling of another set of alkyne functions after the deprotection of pendent silyl-protected alkynes. <sup>143</sup> Clear visualization of the ladder structures was achieved by STM (Scheme 38B).

#### **CLP** synthesis via living polymerization

Most of the previously mentioned CLPs were synthesized via step-growth polymerization, which typically leads to broad chain length dispersity and difficulty in controlling the molar mass of the resulting CLP products. Although it is possible to fractionate these polymers using preparative recycling size exclusion chromatography to obtain low-dispersity samples, such fractionation can be tedious and limit the product scale. In this context, it is highly desirable to synthesize CLPs through living chain-growth polymerization, which enables the preparation of CLPs with controlled molar mass, low dispersity, precise end-group functionalization, and accurate block copolymer constitution. Low dispersity of the precursor polymers (D = 1.2–1.5) was found in the following examples, but that of the resulting CLPs did not seem to represent the true dispersity presumably due to solubility issues. The following CLPs were ladderized through oxidative dehydrogenation, whose pros and cons have been discussed in section "oxidative dehydrogenation."

Fischer and coworkers reported the synthesis of chevron GNR LP82 (Scheme 39) by a living ring-opening alkyne metathesis (ROAMP) polymerization, followed by Scholl oxidation, marking a pioneering synthesis of GNRs with controlled molar mass. 144 They further demonstrated controlled chain-growth synthesis of LP83 by employing a catalyst-transfer condensation polymerization (CTCP) strategy followed by postpolymerization cyclization. 145 Nonetheless, the solution-phase Scholl oxidation turned out to be challenging, and the final product (Scheme 40) could only be accessed through on-surface synthesis. Choi and coworkers demonstrated another synthesis of GNR LP84 (Scheme 41) with the precursor polymer synthesized by CTCP. 146 The living fidelity of CTCP was supported by the successful sequential copolymerization of two different monomers into a block copolymer. After CTCP, the first step of post-polymerization cyclization successfully proceeded through acid-catalyzed alkyne benzannulation, and the second step of cyclodehydrogenation was achieved through Scholl oxidation with DDQ in triflic acid. To access GNRs with heterostructure through living copolymerization, Ma, Feng, and coworkers demonstrated the synthesis of GNR LP85 (Scheme 42A) with two blocks possessing different edge structures through CTCP followed by Scholl oxidation. 147 The heterostructure was unambiguously characterized by STM (Scheme 42B).

# PHYSICAL PROPERTIES AND DEVICE PERFORMANCE OF CLPs

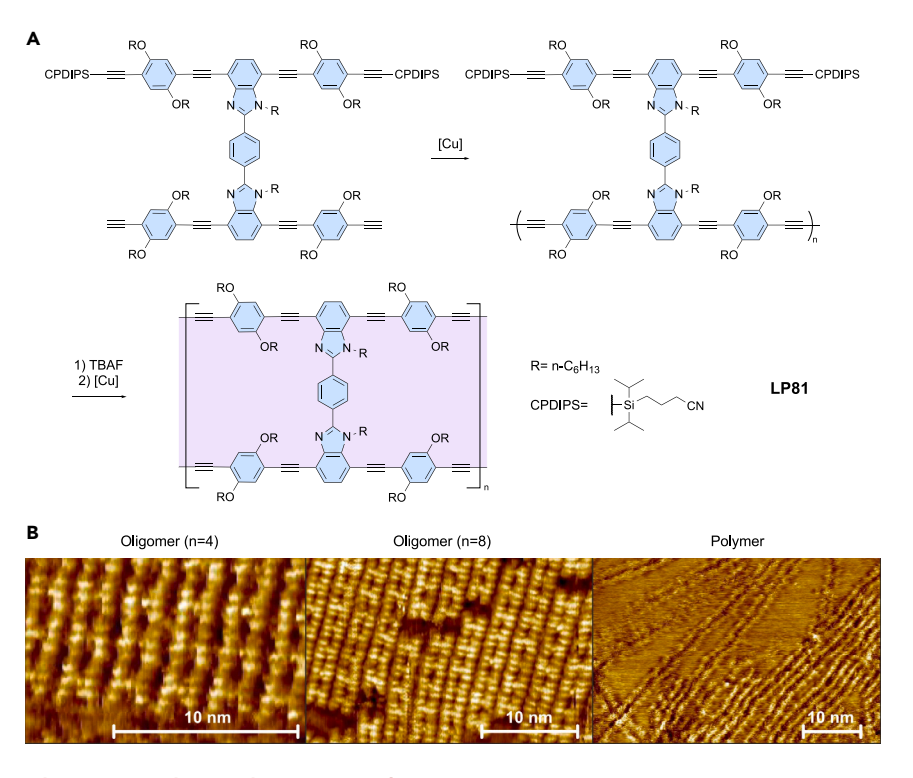
#### Photophysical and electronic properties

CLPs' special multi-stranded constitution distinguishes them from conventional conjugated polymers in many ways. The additional strand of covalent bonds limits the free torsional motion of the repeating units, thus rigidifying the local conformation of the backbone. If the conjugated backbone is coplanar in its ground state, we can anticipate a larger overlap integral between adjacent p orbitals in such a locally rigid  $\pi$ -system and consequently a greater extent of intramolecular  $\pi$ -electron delocalization and a longer effective conjugation length. <sup>148,149</sup> The local rigidity renders not only a lower reorganization energy during charge transport or photoexcitation

# Chem

# **CellPress**

# Review



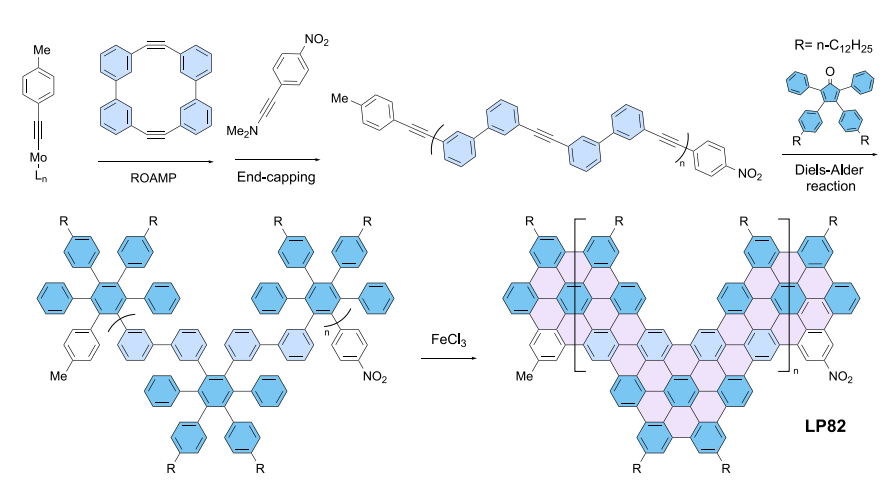
### Scheme 38. Synthesis and STM images of LP81

(A) Synthesis of LP81 through Glaser alkyne homo-coupling.

(B) STM images of LP81 oligomers and polymers (scale bar:  $10\,\mathrm{nm}$ ). Adapted from Meißner et al.  $^{143}$  and licensed under CC BY 4.0.

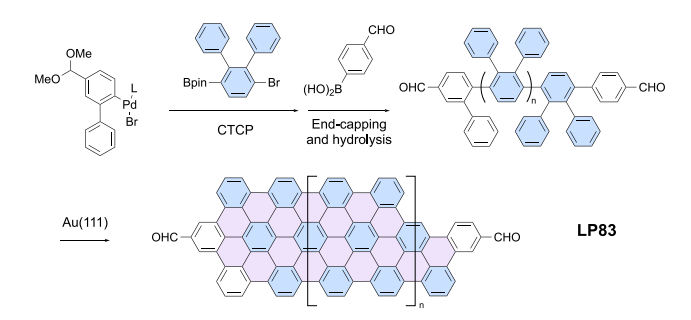
processes, <sup>33,150,151</sup> but it also contributes to the longer lifetime of excitons, polarons, and bipolarons, <sup>106,152–155</sup> as well as the formation of charge transfer complexes. <sup>156</sup> These characteristics dominate many important optical and electronic properties of CLPs.

The successful synthesis of CLPs from their single-stranded precursor polymers typically results in a bathochromic shift in their ultraviolet-visible (UV-vis) absorption and photoluminescence spectra. This shift is primarily attributed to the adoption of a



Scheme 39. Synthesis of LP82 through living ROAMP followed by Scholl oxidation

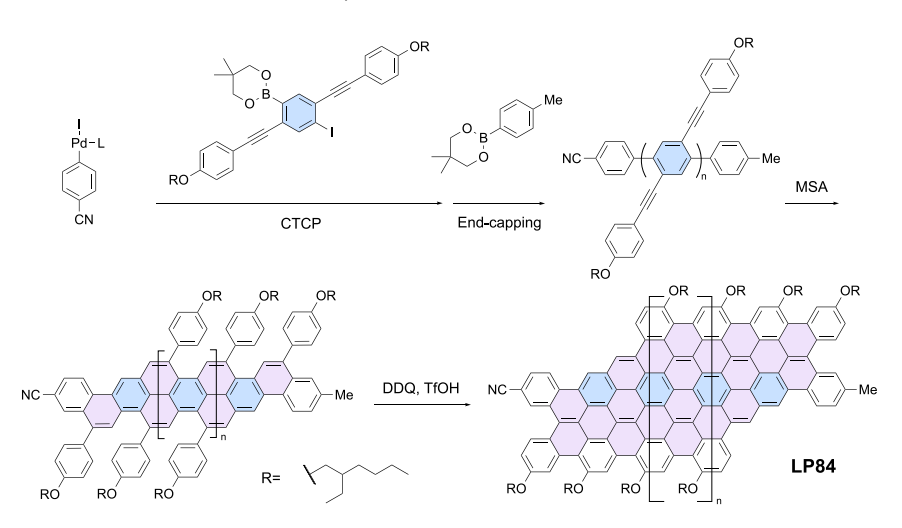




Scheme 40. Synthesis of LP83 through CTCP followed by post-polymerization on-surface cyclization

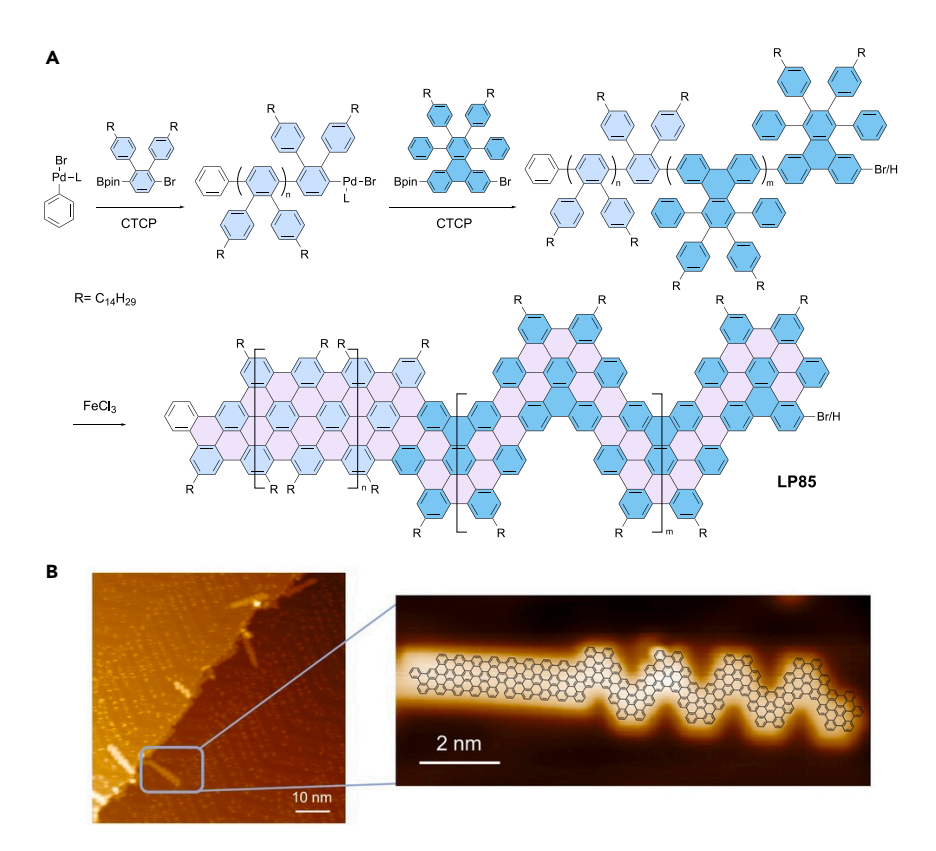
rigid and coplanar conformation of the  $\pi$ -conjugated backbone. Such optical changes have been observed not only for linear CLPs such as LPPP (Scheme 24), LP52 (Scheme 27A), and LP71 (Scheme 33A) but also for helical CLPs such as LP56 (Scheme 28A) and LP64 (Scheme 31), to name but a few here. Additionally, the increase in conjugation length should also be considered as a contributing factor to the bathochromic shift. Köhler and coworkers demonstrated that LP45 (Scheme 25A) linked by 2,7-substituted pyrene repeating units showed a bathochromic shift in its UV-vis absorption and emission spectra compared with its non-ladder precursor, indicating enhanced intrachain conjugation arising from backbone coplanarity. 103 This observation is intriguing because the 2,7-linkage pyrene unit possesses nodal planes across its frontier molecular orbitals, theoretically lacking effective electronic coupling across the polymer backbone, as observed in other non-ladder 2,7-linked oligo(pyrene)s experimentally and 2,7-diphenylpyrene computationally. 157,158 This result indicates that local backbone coplanarity can enhance effective conjugation along CLP backbone even when the conjugation pathway is apparently broken.

For many CLPs without intramolecular charge transfer, their diagnostic spectroscopic features are clear vibronic progression and small Stokes shifts, in contrast to the typically broad, featureless absorption and emission bands observed for non-ladder conjugated polymers. Clear vibronic progression is caused by the low Huang-Rhys factor of a rigid  $\pi$ -system, or weaker electron-phonon coupling, such that the electronic transitions upon excitation or radiative decay are less affected



Scheme 41. Synthesis of LP84 through CTCP followed by benzannulation and Scholl oxidation





Scheme 42. Synthesis and STM images of LP85

(A) Synthesis of diblock CLP LP85 through CTCP followed by Scholl oxidation. (B) STM images of LP85 (scale bar: 10 nm for the left and 2 nm for the right). Adapted from Zhang et al.  $^{147}$  and licensed under *CC BY 4.0*.

by vibrational motions. Small Stokes shifts are a result of subtle reorganization between the electronic ground and excited states, so that the 0–0 peak is dominant for both absorption and emission spectra according to Franck-Condon principle (see examples in Figures 5A and 5B).

In addition, the inherent backbone rigidity of CLPs diminishes inhomogeneous broadening in their optical spectra. This broadening is commonly seen in the spectra of non-ladder conjugated polymers, which exhibit the ensemble signal of various conformations stemming from the variable torsional angles between repeating units. With these distinct features in optical spectra, CLPs serve as ideal models for understanding excited-state photophysics of  $\pi$ -conjugated polymers, <sup>138</sup> such as how excitons migrate and evolve in these systems. 103 For LPPP, because it barely shows interchain electronic coupling, its ensemble emission spectra in solution-phase and solid-state are nearly identical, making it an excellent candidate for fundamental photophysical studies. Lupton and coworkers applied photon correlation spectroscopy to nanoparticles of LPPP. 159 These nanoparticles, with various sizes, serve as appropriate models for investigating the change of exciton diffusion and annihilation behaviors in a CLP from the molecular level to bulk material. The effect of the size of LPPP nanoparticles on its exciton dynamic was successfully resolved without interference from the formation of H-type aggregation. It was found that from single polymer chains to small aggregates and then to large aggregates, both singlet-singlet and singlet-triplet annihilation rates become slower (from about  $10^{11}$  to  $10^9$  s<sup>-1</sup>), which are ascribed to the more significant interchain exciton diffusion in larger aggregates.



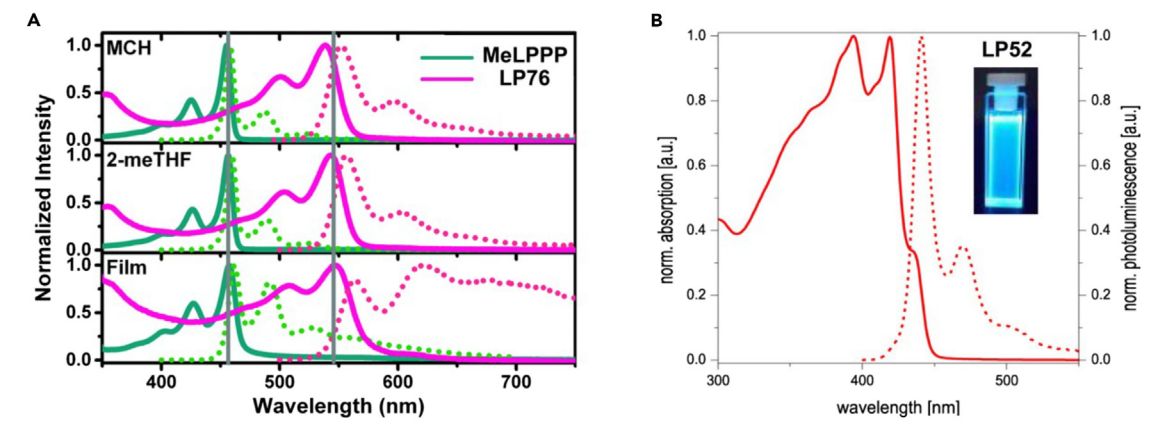


Figure 5. Photoabsorption (solid lines) and emission (dashed lines) spectra of LP52 and LP76

(A) Symmetrical patterns were observed for the absorption and emission spectra of MeLPPP and LP76 in solution and in solid state. Adapted from Unruh et al. 138 and licensed under CC BY 3.0.

(B) Unsymmetrical pattern was observed for the absorption and emission spectra of LP52 in solution due to the forbidden HOMO-LUMO transition, although the Stokes shift is still small if the weak HOMO-LUMO transition is counted. Adapted from Trilling et al. 111 with permission from Copyright © 2019, American Chemical Society.

As mentioned before, the optical spectra of most CLPs show a strong relative intensity of the 0–0 absorption or emission compared with the vibrational sidebands. This is ascribed to the backbone rigidity, according to the Franck-Condon principle, and strong intrachain electronic coupling between head-to-tail chromophores along the rigid π-conjugated backbone as a feature of J-type excitonic coupling. <sup>138,160–162</sup> Consequently, for many CLPs such as LPPP (Scheme 24), LP24 (Scheme 13), and LP76 (Scheme 36A), a mirrored image of absorption and emission spectra with the 0–0 peaks as maxima is observed with a small Stokes shift (Figure 5A). Nonetheless, this pattern is not seen for some CLPs such as LP45 (Scheme 25A), LP52 (Scheme 27A), LP56 (Scheme 28A), and LP71 (Scheme 33A), where the highest occupied molecular orbital (HOMO)-LUMO transition is likely forbidden, leading to a large difference of the apparent absorption and emission maxima, but still with a small Stokes shift if the weak forbidden HOMO-LUMO transition is counted (Figure 5B).

Despite the reported advances mentioned above, investigating the intrinsic photophysical properties of many CLPs in solution remains challenging, due to the oftenobserved strong aggregation and the resulting intermolecular  $\pi$ - $\pi$  electronic coupling. This challenge is particularly pronounced for wider CLPs, such as those referred to as GNRs. The strong aggregation in these materials means that the properties of truly solvated polymer chains cannot be probed. To overcome such aggregation, LP44 (Scheme 23) was synthesized such that it remains mainly non-aggregated in solution with a concentration up to 0.1 g/L. 99 This modification provides an opportunity to investigate the solution-phase excited-state dynamics of GNRs. The absorption of LP44 was mainly below 750 nm, in agreement with its own emission spectrum and computational simulation. By contrast, for previously reported GNRs, featureless absorption spectra with extension to near-infrared were often observed due to the scattering effect of the aggregates. The quantum yield (9.1%) and long exciton lifetime (8.7 ns) of LP44 were also successfully measured. With these values, it was further estimated that the excitons were delocalized over no more than four repeating units on the GNR, approximately corresponding to a length of 5 nm. More recently, Xu and Cerullo applied two-dimensional electronic



spectroscopy on LP44 and revealed its unique feature as a non-aggregated GNR. <sup>163</sup> With the single dissolved GNR chains in solution, the significant impacts of vibronic coupling on the optical properties of LP44 and the presence of photoexcited bright and dark state of LP44 were identified. The excited-state dynamics of LP44 also resembles more that of a large, solvated macromolecule instead of a quantum-confined solid.

For many imine-containing CLPs, such as BBL, LP3 (Scheme 2), LP50, and LP51 (Schemes 26B and 26C), a low-energy absorption band is observed because of the protonation-enhanced intramolecular charge transfer. 35,40,109,110 In addition, extensive studies on the electronic structures of BBL from both experimental and computational approaches have been reported, revealing its polaronic nature after n-type electrochemical and chemical doping. 164-166 BBL exhibits multiple redox states upon doping, and for each given redox state, there are also multiple spin multiplicity states accessible by thermal energy, rendering the experimental FTIR and UV-vis-NIR spectra hard to resolve. Recently, Zozoulenko and coworkers performed density functional theory (DFT) simulation for cis-BBL oligomer with different reduction levels from neutral to 2.00 electrons per repeating unit (eru). 164 Starting from the neutral state to 1.00 eru, each added electron localized at different naphthalenic units and remained unpaired, resulting in the increase of total spin density. It was found that the first two added electrons actually formed a triplet polaron pair, instead of a commonly assumed spinless bipolaron. Further injection of electrons from 1.00 to 2.00 eru resulted in the pairing of new added electrons to the existing ones, leading to the coexistence of polarons and bipolarons and ultimately to entirely spinless bipolarons. This progression was supported by the experimental data reported previously. 167 Fazzi and Negri demonstrated that the electronic structures of cis- and trans-BBL are actually different. 165 For cis-BBL with 1.00 eru, the most stable spin configuration among all is the one with all electrons remaining unpaired, leading to high spin species similar to what Zozoulenko and coworkers reported. For trans-BBL, by contrast, the same spin configuration is less stable. Nonetheless, for both cis- and trans-isomers, most of the spin configurations reside within an energy difference accessible by thermal energy. Upon reduction of BBL from its neutral state to 1.00 eru, four distinct reduced states were observed (0.25, 0.50, 0.85, and 1.00 eru), with the first and third ones being conductive and the second and fourth being insulating. By comparing the simulated FTIR spectra to the experimental ones for different redox states, these authors were able to resolve the electronic structure, charge distribution, and spin multiplicity in each conducting or insulating state.

### Solution-phase conformation and chain rigidity

The understanding of CLP's inherent chain conformation and rigidity in solution is particularly relevant to their intrinsic electronic and optical properties in solution and solution processability. <sup>168</sup> Additionally, polymer chain conformation affects the extent of chain entanglement, solution viscosity, solvent-polymer interactions, and hydrodynamic radius. These fundamentally intriguing topics in polymer physics have been well established for non-ladder conjugated polymers but are underexplored for CLPs. It is important to note that the "local rigidity" observed from spectroscopic characterization, as discussed in the previous section, does not necessarily translate to rigidity of the overall chain conformation at a large length scale. The former is more pertinent to the effective conjugation length on less than a few nanometer scale, whereas the latter represents the comprehensive features of the entire macromolecule, which can range from several nanometers to hundreds of nanometers.





Considering the multistranded nature of CLPs, it may be straightforward to envision these polymers adopting a rod-like conformation in solutions. In 1978, Berry reported the rod-like nature of BBL in MSA according to light scattering analysis, showing a persistence length over 150 nm. 169 However, the observed rigidity might not represent a typically neutral CLP solvated in a common solvent. BBL was dissolved in a strong acid, MSA, and was likely protonated into a polyelectrolyte formation, so that electrostatic repulsion could dominate the chain conformation. Indeed, through DFT simulation, Jenekhe and coworkers demonstrated the enhanced backbone rigidity of LP3 (Scheme 2) as the degree of protonation increased. 40 LP3 showed decent rigidity when dissolved in MSA because of the partial protonation. When dissolved in a more acidic solvent, triflic acid, an enhancement of backbone rigidity was observed. Such variation in backbone rigidity was also determined by variable-temperature UV-vis absorption spectra, where a larger hypsochromic shift at a higher temperature implied decreased backbone coplanarity and shortened effective conjugation length. The backbone of LP3-Me (Scheme 2) was found to be more flexible than that of unmethylated LP3. In contrast to LP3 and LP3-Me, the UV-vis absorption spectra of BBL in MSA does not show any significant change at high temperature, since BBL has been fully protonated in MSA and thus behaved as rigid rod.

For CLPs dissolved in common organic solvents, Ballauff and coworkers reported the solution-phase conformation of LPPP by using small-angle X-ray scattering and small-angle X-ray neutron scattering (SAXS and SANS) in 1997, revealing a much shorter persistence length of 6.5 nm compared with that of BBL. 170 The reported persistence length, comparable to or even smaller than many non-ladder conjugated polymers, <sup>171</sup> did not signify a rigid rod-like backbone conformation. Nonetheless, it was unclear if the flexibility of LPPP arises from the intrinsic twisting and bending of the backbone or from free torsional motion at possible uncyclized defects. In a recent study, Scherf, Bahmann, Seixas de Melo, Lupton, and coworkers demonstrated the backbone flexibility of LP76 (Scheme 36A) when the scale is approximately over 2 nm. 138 Single-molecule spectroscopy revealed a slower rate of intramolecular exciton annihilation for LP76, attributed to both conformational and energetic backbone heterogeneity. Despite the possibility of the slower annihilation rate being linked to uncyclized single-stranded defects, DFT simulations clearly indicated backbone flexibility over roughly seven aromatic rings with twisting and out-of-plane distortion. Meanwhile, clear vibronic progression in both absorption and emission spectra was still observed to support the local rigidity at the scale of effective conjugation length. It is also reported that distorting a single benzene does not lead to a significant loss of aromaticity, <sup>172</sup> and such slight destabilization in the case of conjugated polymers can be further compensated by the gain of entropy. Recently, a newly developed ribbon-like chain model was reported by Michaels, Qin, and coworkers for describing the turning, undulating, and twisting motions in CLPs and other conjugated polymers. 173

CLPs also show unconventional solution-phase aggregation behaviors compared with non-ladder conjugated polymers. Tabor, Fang, Gu, and coworkers reported that LP71 (Scheme 33A) exhibits a robust dynamic solution aggregation even when the concentration is down to 0.05 g/L in chlorobenzene and temperature up to 200°C. <sup>174</sup> Aggregates in solution (with a size of 100–200 nm) were observed by dynamic light scattering and SANS, although size exclusion chromatography only showed the peak for non-aggregated polymer with reasonable retention time and molar mass. These observations suggest a dynamic equilibrium between the aggregated and non-aggregated states in solution. The formation of such aggregates,





which are highly robust at high temperatures, can be attributed to the low entropy penalty of the aggregation process. This low entropy change is considered in light of the original low entropy of the CLP backbone, which lacks torsional motion.

Overall, the solution-phase polymer physics of CLPs is an area that remains largely unexplored. Studies on this topic will not only shed light on the physical characteristics of CLPs themselves but also contribute to a more complete comprehension of the broader polymer science, encompassing both single- and double-stranded polymers.

#### Stability and durability

Undesired degradation of conjugated polymers is a common challenge faced in a wide variety of applications, especially when the polymer is exposed to oxygen, UV light, heat, and/or with the input of electric current and voltage. It is widely recognized that the fused-ring constitution of CLPs markedly enhances stability in comparison with non-ladder conjugated polymers. The significantly higher structural integrity of CLPs may be attributed to both thermodynamic and kinetic factors. Thermodynamically, the graphitoid backbone of a CLP is inherently more favorable than its non-ladder counterpart. Kinetically, the backbone of a CLP is more persistent against potential scission due to a higher barrier to break multiple strands of bonds. For example, LP11 (Scheme 5) was found to be stable against 6 M HCl<sub>(aq)</sub>, 6 M NaOH<sub>(ag)</sub>, and boiling water, despite the fact that both two strands of bonds of LP11 contain imine linkages that are typically susceptible toward acid-catalyzed hydrolysis.<sup>47</sup> In this context, the superior stability of CLPs shows promise for their broad application in various devices, including electrochromic devices, <sup>109</sup> alkali-ion batteries, 41,45 supercapacitors, 45,54,110,175 solar cells, 80,132,176 organic field-effect transistors (OFETs), 73,104 OECTs, 177-187 and OTEs. 35,38,39,152,177,188-191

Stability of conductive polymer has been a long-term issue. Conventional polyaniline is a widely used redox-active conductive polymer, but the imine bonds in its oxidized state are susceptible to hydrolysis, especially when the materials are acid doped into emeraldine salt or pernigraniline salt forms. By introducing the second strand of bonds to create ladder-type polyaniline analogs LP50 and LP51 (Schemes 26B and 26C), the stability is greatly enhanced. With the ladder constitution, LP50 and LP51 can be converted into the oxidized, fully protonated form of pernigraniline salt without observable degradation, which has not been demonstrated on conventional polyaniline. As reported by Xu, Ng, Fang, and coworkers, LP51 remains intact even when dissolved in MSA for 16 days, whereas in sharp contrast, the commercial benchmark redox-active conductive polymers poly(3,4-ethylenedioxythiophene)poly(styrenesulfonate) (PEDOT:PSS) and polyaniline degrade under similar conditions in just a few days. 110 When mixed with p-toluenesulfonic acid (p-TSA) in the solid state, the absorption profile of the polymer film made by LP51 remains nearly unchanged after exposure to UV light (254 and 365 nm, 10 mW/cm) for 8 h, whereas the one made by PEDOT:PSS degrades significantly due to oxidation (Figure 6A). A robust actuator made by LP49a (Scheme 26A) reported by Liu, Zhou, Fang, and coworkers also shows outstanding thermal stability and durability against strong organic solvents and concentrated sulfuric acid, whereas those made by non-ladder polymers decompose and/or lose the actuating functions after such treatments. 192

The stability of CLPs toward light presents an opportunity to develop photocatalysts based on these polymers. For photocatalytic water oxidation, silver(I) serves as a common electron scavenger. However, the formation of silver(0) on the surfaces of photocatalysts tends to diminish the catalytic performance over time, while removal



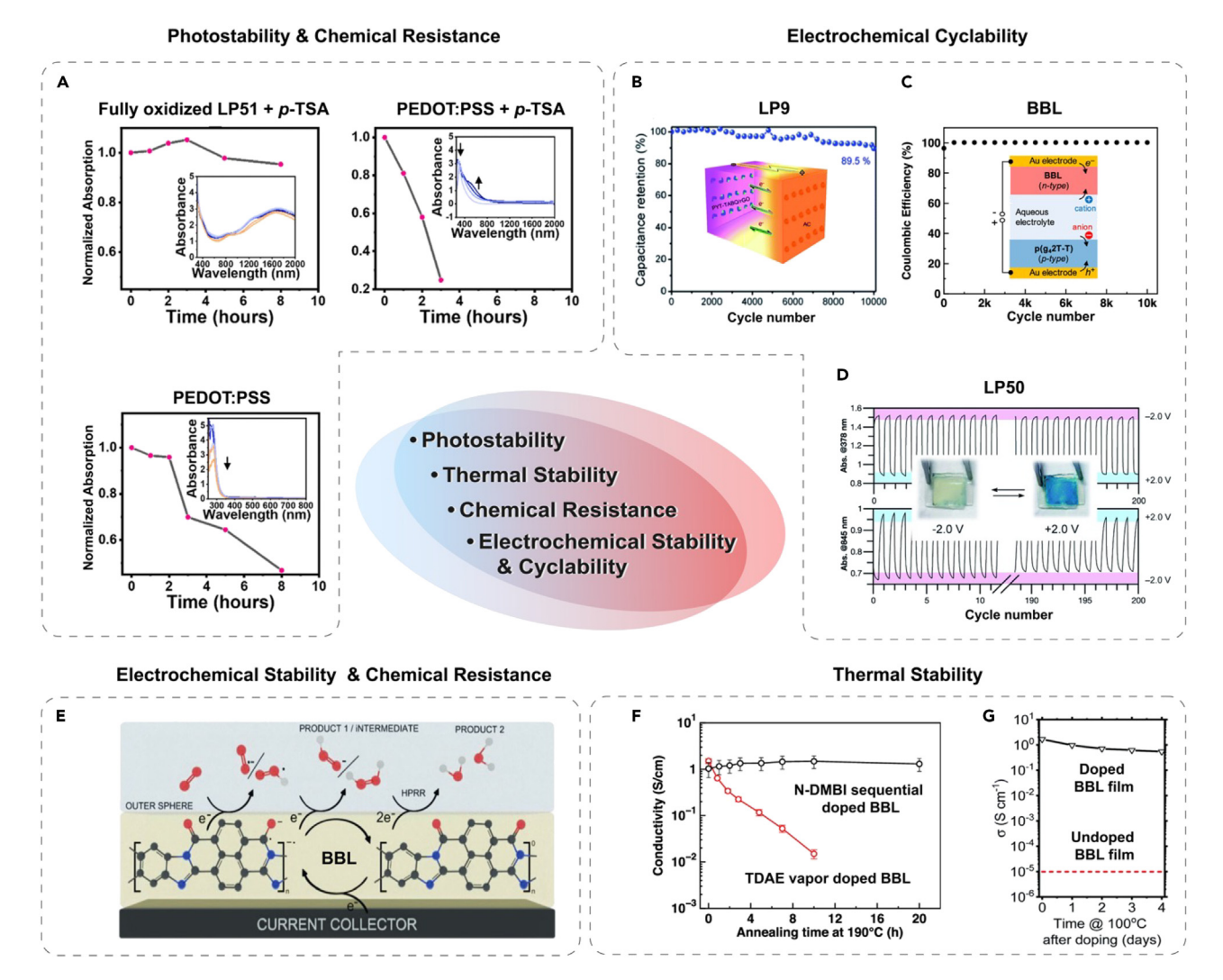


Figure 6. Stability of CLPs in various application scenarios

(A) Fully oxidized/acid-doped LP51 shows high photostability against UV light irradiation (254 and 365 nm, 10 mW/cm) for 8 h. By contrast, the pristine and acid-doped PEDOT: PSS films degrade rapidly under the same condition. Adapted from Leng et al. 110 with permission from © The Royal Society of Chemistry 2023

- (B) The supercapacitor made with LP9/reduce graphene oxide electrode and active carbon electrode shows a high capacitance retention after 10,000 cycles. Adapted from Chen et al. 45 with permission from © The Royal Society of Chemistry 2019.
- (C) The supercapacitor with BBL electrode demonstrates a superior capacitance retention after 10,000 cycles. Adapted from Volkov et al. 175 with permission from Copyright © 2019, American Chemical Society.
- (D) The electrochromic device made by **LP50** demonstrates good electrochemical cyclability for 200 cycles, with consistent color switching. Adapted from Ji et al. <sup>109</sup> and licensed under *CC BY 3.0*.
- (E) BBL electrode tolerates a broad pH range, and thus the reduction of molecular oxygen to hydrogen peroxide or water can be achieved. Adapted from Vaqin et al.  $^{193}$  and licensed under *CC BY 4.0*.
- (F) The sequentially doped BBL film (black line) shows good thermal stability with nearly unchanged conductivity after being kept at 190°C for 20 h under an inert atmosphere. Adapted from Wang et al. <sup>194</sup> and licensed under *CC BY 4.0*.
- (G) Doped and undoped BBL films show good thermal stability with high retention of their conductivities after being kept at 100°C for 4 days under an inert atmosphere. Adapted from Tam et al. 189 with permission from © The Royal Society of Chemistry 2021.

of silver(0) often requires harsh treatment that can damage the photocatalyst. To address this challenge, Wang, Wu, Xu, and coworkers reported the use of **LP6** and **LP7** (Scheme 3C) as photocatalysts for water oxidation in the presence of silver. <sup>43</sup> The silver particles deposited on these polymers can be easily removed by nitric acid treatment. Remarkably, this treatment does not significantly impact the



catalytic performance upon regeneration, thanks to the high robustness of these CLPs against strong acids.

Recently, a tremendous number of organic-based electrochromic devices, batteries, and supercapacitors have been developed. 195,196 However, many of these organic functional materials suffer from relatively fast degradation under applied current and voltage. With their excellent robustness, CLPs have found promising applications in this field, exhibiting outstanding cyclability and electrochemical durability. For example, Lutkenhaus and coworkers reported a polymer-air battery with good cyclability with a capacity retention of 98.8% after 500 cycles at 20 A/g, using BBL as the anode material. 197 Wang, Wang, Wang, Hu, and coworkers demonstrated that a composite electrode fabricated with LP9 (Scheme 3E) and rGO possesses 98% capacitance retention after 1,400 cycles for Na-ion batteries. 45 As a supercapacitor, the composite electrode also exhibits 94% capacitance retention after 10,000 cycles at 10 A/g. Without rGO, however, the capacitance retention of the LP9 electrode starts dropping after 4,000 cycles under the same condition. Nonetheless, this cyclability still remarkably outperforms many conjugated-polymer-based electrodes used for supercapacitors, which often degrade under less than a thousand cycles. 198 Moreover, the hybrid supercapacitor with the composite material and active carbon as two opposite electrodes shows a capacitance retention of 89.5% after 10,000 cycles (Figure 6B). As a cathode material in potassium cells, LP4 (Scheme 3A) shows no fade in capacity after 4,000 cycles operated at a current density of 5 A/q, as reported by Kapaev and coworkers. 41 Another composite fabricated with LP17 (Scheme 8B), carbon fiber, and carbon nanotube reported by Lu and coworkers shows 94% capacitance retention after 25,000 cycles at 100 mV/s as an electrode material.<sup>54</sup> Fabiano, Crispin, and coworkers demonstrated the use of n-type BBL and p-type polythiophene for an asymmetric aqueous supercapacitor with 99% capacitance retention after 10,000 cycles (Figure 6C). <sup>175</sup> Zou, Fang, and coworkers reported the use of LP50 (Scheme 26B) as the active material in an electrochromic device. 109 The device undergoes 200 cycles between -2.0 and +2.0 volts during operation without observable degradation (Figure 6D), demonstrating the significantly higher electrochemical robustness of LP50 than benchmark polyaniline and PEDOT:PSS. The cyclability of a supercapacitor made by LP51 (Scheme 26C) reported by Xu, Ng, Fang, and coworkers also shows no decrease in capacitance over 2,400 cycles of operation. 110 Furthermore, the good electrochemical stability of CLPs renders them suitable for durable electrocatalysts or electrode materials. For instance, during oxygen reduction reaction, the active catalyst must not be easily oxidized and should remain stable within the electrochemical potential window of the process. Vagin, Crispin, and coworkers demonstrated the use of n-doped BBL as a stable electrocatalyst. 193 Because BBL is active and stable in a wide pH range, the electrocatalytic reduction of molecular oxygen can be altered to produce either H<sub>2</sub>O<sub>2</sub> or even H<sub>2</sub>O by varying pH value (Figure 6E). The complete reduction of molecular oxygen to water with BBL electrode is worth emphasizing because this has not been demonstrated with PEDOT nor with other conducting polymers.

CLPs can also serve as suitable candidates for electronic devices requiring good stability under ambient conditions or at high temperature. <sup>33,177,189,194,199</sup> Kim, Jenekhe, and coworkers reported that the OFET made by BBL exhibits nearly unchanged electron mobility and a similar threshold voltage after being stored in ambient conditions for 200 days. <sup>33</sup> The sequentially doped BBL thin film reported by Fabiano and coworkers maintains high conductivity retention after annealing at 190°C for 20 h under an inert atmosphere (Figure 6F). <sup>194</sup> Similarly, Tam, Xu, and coworkers demonstrated that the conductivity of a sequentially doped BBL thin film





remains at the same order of magnitude after being kept at 100°C for 4 days under an inert atmosphere (Figure 6G). <sup>189</sup> The polymer blend of BBL and polyethyleneimine (PEI) nanoparticles reported by Fabiano and coworkers shows no decrease in conductivity after annealing at 200°C for 24 h under an inert atmosphere. <sup>177</sup> These examples highlight the promising prospect of BBL and potentially other CLPs as durable materials for many organic electronic applications.

### **Applications for electronic devices**

The excellent stability of CLPs enables their broad applications in electronic devices. Additionally, good carrier mobility has been observed for some CLPs due to their backbone coplanarity for efficient charge transport. An early study by Siebbeles and coworkers demonstrated that the intrachain hole mobility of LPPP is close to  $600~\text{cm}^2/\text{Vs.}^{200}$  As for BBL, Jenekhe and coworkers investigated the effect of molar mass on its field-effect electron mobility.  $^{201}$  It was found that the field-effect electron mobility increases up to  $2.74\times10^{-2}~\text{cm}^2/\text{Vs}$  as the molar masses of BBL increase (up to a degree of polymerization of 250) without saturation. This is not only attributed to BBL's rigid rod-like conformation in solid state but also to its side-chain-free feature. By contrast, the electron mobility of other n-type non-ladder conjugated polymers reaches the upper limit around a degree of polymerization of 40–60 due to their semi-flexible chain conformation and the presence of alkyl side chains.

OECTs are promising devices for next-generation bioelectronics and neuromorphic computing applications. <sup>202–204</sup> For a long time, research in the development of p-type OECTs has been well established; however, progress in n-type OECTs was hampered by the lack of suitable yet robust n-type polymers with high electron mobility comparable to their p-type counterparts. Additionally, electrochemical reversibility and stability in both air and aqueous media are critical criteria for selecting candidate materials for n-type OECTs. These requirements have prompted researchers to use n-type CLPs, such as BBL with demonstrated high stability, as the active material for OECTs.

In 2018, Fabiano and coworkers presented the use of BBL as the active channel in an n-type OECT with a record-high transconductance (up to 9.7 mS) at that time (Figures 7A–7C). This n-type OECT also demonstrates good cycling stability without current degradation and with remarkable ambient stability. The effect of molar mass of BBL on the performance of OECTs was further investigated for optimization. It was found that the device composed of high-molar-mass BBL exhibits better transconductance, a larger value of mobility  $\times$  volumetric capacitance, faster response time, and a lower threshold voltage than the low-molar-mass one. This enhancement for high-molar-mass BBL is attributed to more efficient intermolecular charge transport resulting from stronger intermolecular  $\pi$ - $\pi$  interactions and higher crystallinity.

The same group also achieved an n-type OECT with fast response time and high transconductance by using a blend of BBL and multi-walled carbon nanotubes as the electroactive material. These good performances are attributed to the synergistic effect of the large capacitance of BBL and the high electron conductivity of multi-walled carbon nanotubes, enabling an efficient charge percolation path within the BBL channels. An n-type depletion-mode OECT was also achieved by using the blend of BBL and PEI nanoparticles as the active material. The More recently, an aqueous-processable OECT made by a polymer blend of BBL and polythiophene polyelectrolyte was developed. With the ground-state electron transfer occurring between the two polymers and thus the mutual electrical doping, this polymer blend





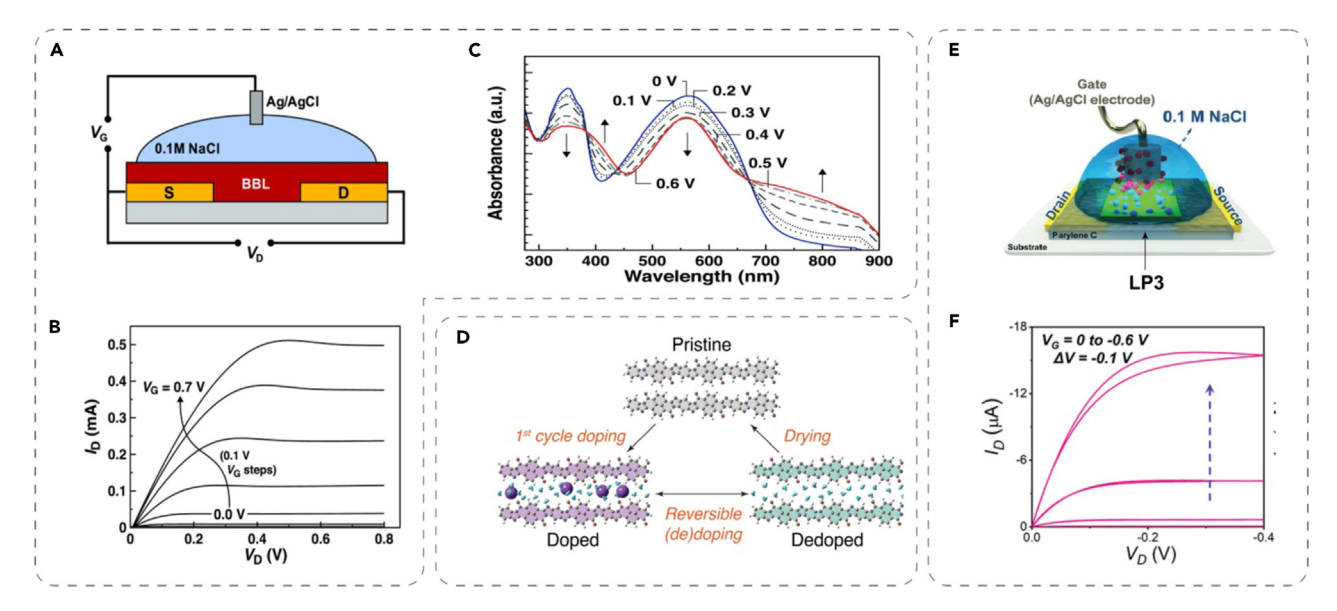


Figure 7. OECTs utilizing side-chain-free CLPs as the electroactive materials

- (A) Schematic illustration of an n-type OECT composed of BBL.
- (B) Drain current-voltage curves of BBL OECT under different gate voltage biases.
- (C) Spectroelectrochemistry measurements of BBL films under different gate voltage biases for electrochemical doping. (A)–(C) are adapted from Sun et al.  $^{178}$  and licensed under CC BY 4.0.
- (D) Changes of BBL morphology from pristine to swollen form during OECT operation and the formation of channels for cations and water transport. Reproduced from Guo et al. 184 with permission from Copyright © 2023, American Chemical Society.
- (E) Schematic illustration of a p-type OECT composed of LP3.
- (F) Drain current-voltage curves of LP3 OECT under different gate voltage biases. (E) and (F) are adapted from Wu et al. 185 with permission from © 2022 Wiley-VCH GmbH.

shows a 10,000-fold increase in electrical conductivity (from  $10^{-5}$  to  $10^{-1}$  S/cm) than the individuals. Besides, an electrochemical neuron was fabricated from two BBL-based OECTs, one modulated by Na<sup>+</sup> and another by K<sup>+</sup>. This electrochemical neuron was integrated with the vagus nerve of a mouse, and a 4.5% reduction in heart rate was observed upon the increase of Na<sup>+</sup> ion concentration.

The response time for switching on and off the drain current in OECTs strongly depends on the diffusion of ion injection into the bulk polymers for doping or ion depletion from the bulk polymers for de-doping. It is believed that incorporating hydrophilic side chains to polymers promotes the rate of ion transport within the film, but meanwhile, the presence of aliphatic side chains sacrifices the overall electronic mobility, a common problem seen in most organic electronics. Interestingly, without any hydrophilic side chains, BBL remains one of the best polymers for n-type OECTs to date. To shed light on the mechanism of the ion transport process, Inal and coworkers compared the n-type OECTs made by BBL and a conventional non-ladder polymer with hydrophilic side chains. <sup>183</sup> In the absence of side chains, BBL not only shows higher electron mobility but also greater volumetric capacitance because the majority of space is taken up by conjugated backbones. Upon doping, both polymer films are swollen by water molecules and cations, but the crystallinity of BBL remains mostly unchanged due to its ladder-type feature. By contrast, the crystalline morphology of the non-ladder polymer is disrupted upon swelling, detrimental to charge mobility and device performance.

Ginger and coworkers also studied the morphological change of the BBL film during the redox cycles in the operation of OECTs (Figure 7D). <sup>184</sup> Starting from the pristine





film, the first doping enables an irreversible uptake of water that expands the lamellar packing of BBL and thus swells the film. This irreversible swelling then creates additional hydrophilic channels for the fast transport of hydrated cations and water molecules into the bulk. After the first doping, the ion and water uptake in the subsequent redox cycles are found to be reversible, resulting in the reversible structural expansion and contraction of the BBL film, clearly observed by *in operando* grazing incidence wide-angle X-ray scattering (GIWAX). Even with the inclusion of water molecules and ions, BBL does not show a significant decrease in crystallinity due to its ladder-type feature, in agreement with the conclusion in Inal's work. <sup>183</sup>

Given the superior performances of side-chain-free BBL in n-type OECTs over other non-ladder polymers, researchers were prompted to explore other side-chain-free p-type CLPs potentially useful for p-type OECTs. Recently, Tam, Leong, and coworkers reported the use of side-chain-free LP3 (Scheme 2) for p-type OECTs with good ionic and electronic conducting properties (Figures 7E and 7F). 185 As expected from the extraordinary durability of CLPs, the LP3-based p-type OECT shows approximately 85% drain current retention after 5,000 redox cycles. Leong and coworkers further demonstrated that a more durable p-type OECT could be achieved by using the annealed LP3, leading to no drain current degradation after 4,500 redox cycles. 186 Nonetheless, the device with annealed LP3 also shows lower transconductance and higher threshold voltage, as compared with the unannealed counterpart, since a larger driving voltage is required for ions to penetrate into the annealed film. In 2023, Fabiano and coworkers reported that the p-type OECT made by LP3-Me (Scheme 2) exhibited a 25-fold increased mobility and 36-fold increased mobility × volumetric capacitance compared with the unmethylated LP3. 187 This is attributed to the enhanced crystallinity, longer coherence length, and preferential edge-on orientation of LP3-Me, as supported by GIWAX. Nonetheless, a 4-fold increase in response time was also observed, presumably due to the slightly greater hydrophobicity of LP3-Me.

The successful development of n-type OECTs, in parallel with the well-established p-type OECTs, allows the fabrication of polymer-based complementary inverters. These inverters serve as basic elements in circuits, functioning as logic gates and amplifiers. The combination of BBL-based n-type OECTs and p-type OECTs made with polythiophene with hydrophilic side chains affords complementary inverters with high gain values, large worst-case noise margins, and low power consumption. The voltage gain of an "all-CLP" BBL- and LP3-Me-based complementary inverter was reported to be higher than 190 V/V. The Another complementary inverter made by BBL and the aforementioned annealed LP3 shows long-term durability, with negligible drain current degradation for both p- and n-channels after 5,000 cycles. The voltage amplifier fabricated by this complementary inverter is able to capture signals generated by neuromuscular activities and to amplify those as output. This module was further demonstrated for the control of robotic hand motions by the neuromuscular activities from human arm gestures (Figures 8A–8C).

While individual p- and n-type OECTs have been successfully employed in complimentary inverters, the complex patterning of both channels with different polymers in manufacturing poses a disadvantage. One solution to this problem is the use of ambipolar polymers or a polymer blend of p- and n-type polymers, akin to the concept of bulk heterojunctions in organic photovoltaics. This strategy ensures low-cost fabrication of p- and n-type channels on the same polymer film using



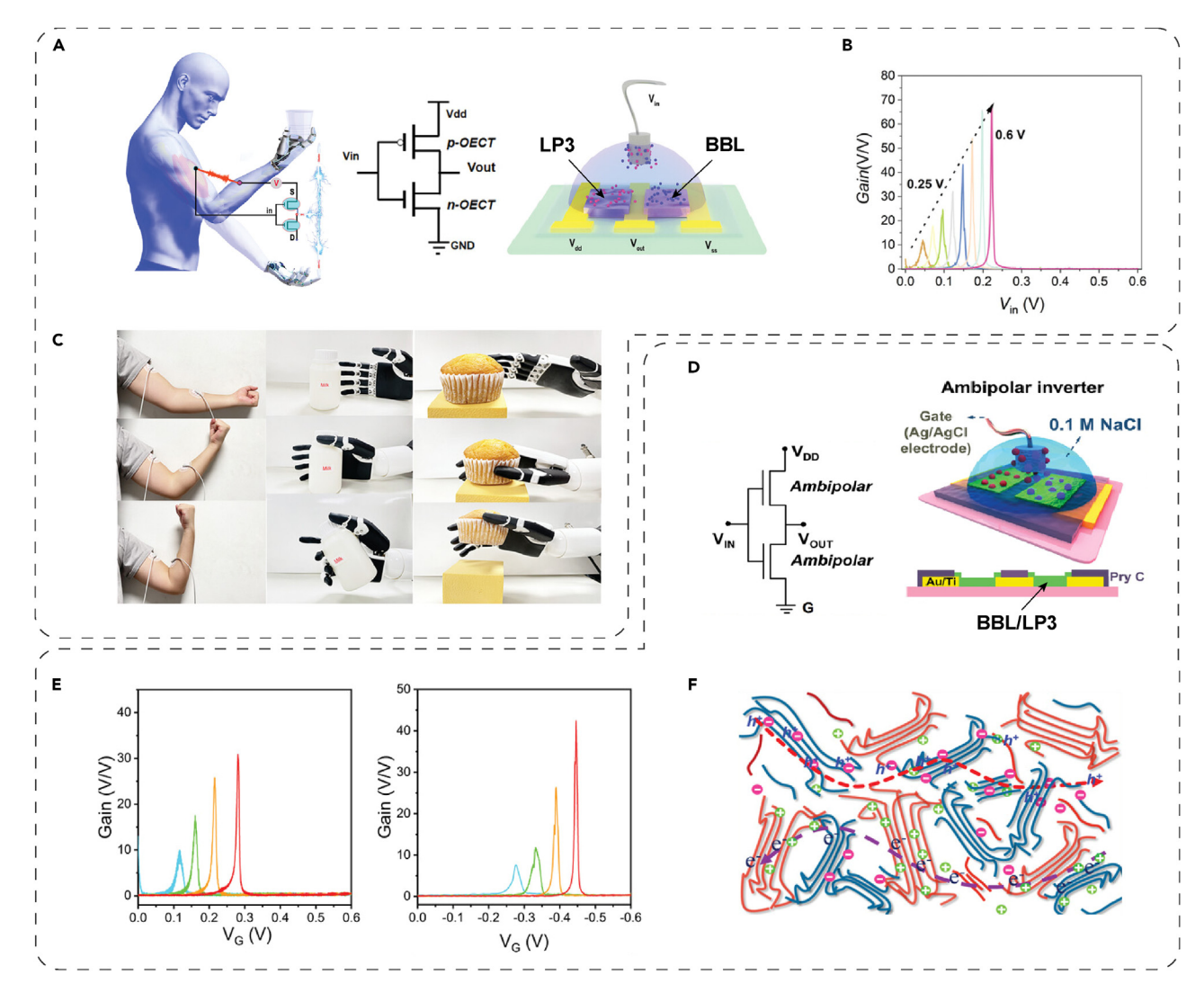


Figure 8. Inverters utilizing side-chain-free CLPs as the electroactive materials

- (A) Schematic illustration of the complementary inverter composed of n-type BBL and p-type LP3 with an application in controlling robotic hand motions by human gestures.
- (B) Voltage gain of the BBL/LP3 inverter as a function of input voltage and  $V_{\rm dd}$ .
- (C) Photos of robotic hand motions in response to human gestures mediated by the BBL/LP3 inverter. (A)–(C) are adapted from Zhou et al. 186 with permission from © 2023 Wiley-VCH GmbH.
- (D) Schematic illustration of the complementary inverter composed of ambipolar BBL/LP3 polymer blend.
- (E) Voltage gain of the ambipolar BBL/LP3 inverter under positive (left) and negative (right) V<sub>dd</sub>.
- (F) Schematic illustration of the microstructure of ambipolar BBL(orange)/LP3(blue) blend and the corresponding charges and ions transport. (D)–(F) are adapted from Wu et al. 185 with permission from © 2022 Wiley-VCH GmbH.

specific doping techniques for controlled and selective areas. Tam, Leong, and coworkers reported an all-CLP bulk heterojunction film made with n-type BBL and p-type LP3 (Figures 8D and 8E). 185 In the blended BBL:LP3 film, both BBL and LP3 are uniformly distributed, and their individual nano-size crystalline domains do not interfere with the crystallinity of each other. This is beneficial for the efficient transport of both electrons and holes in the bulk heterojunction structure (Figure 8F). The blended film also exhibits a porous fibrillar microstructure, believed to facilitate fast ion penetration and transport. This bulk heterojunction OECT maintains 90% and 100% drain current retention of p- and n-channels, respectively, after 5,000 redox



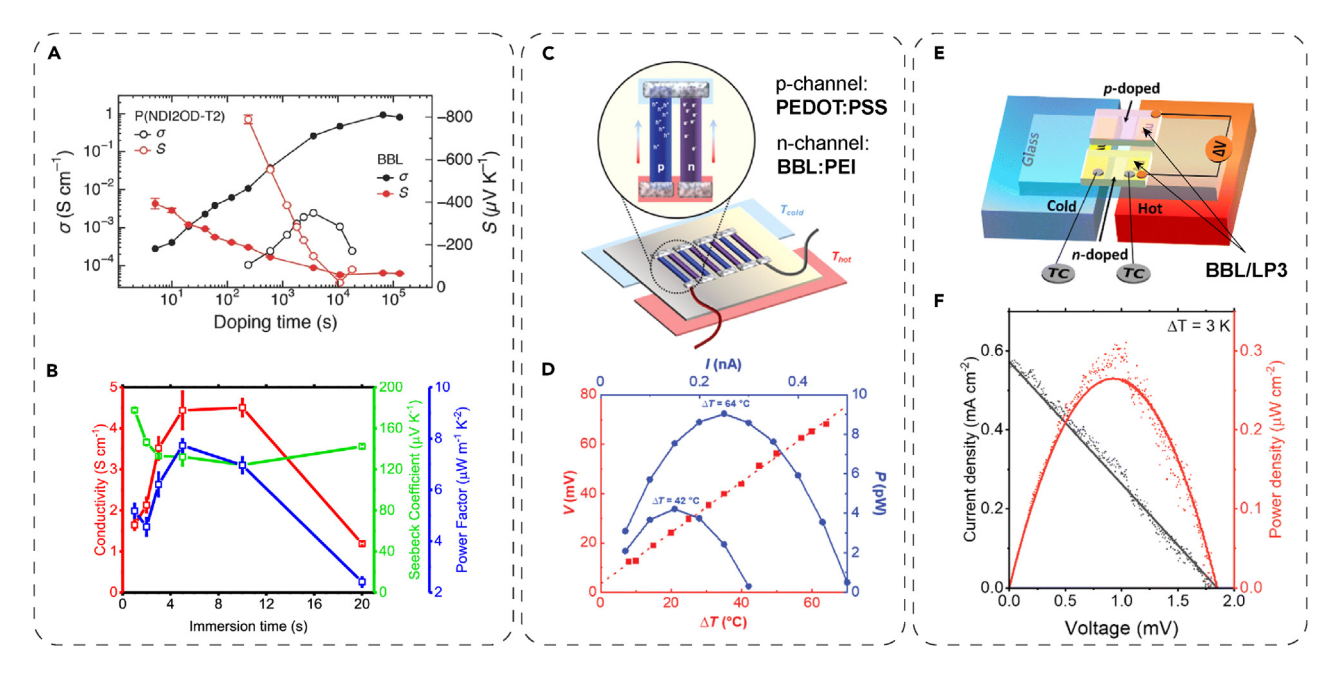


Figure 9. Thermoelectric properties of side-chain-free CLPs and the corresponding OTE devices

(A) Conductivity and Seebeck coefficient of BBL film (solid dots) as a function of doping time with tetrakis(dimethylamino)ethylene (TDAE). Adapted from Wang et al. 152 with permission from © 2016 WILEY-VCH Verlag GmbH & Co. KGaA, Weinheim.

- (B) Conductivity, Seebeck coefficient, and power factor of LP3 film as a function of doping time with FeCl<sub>3</sub>. Adapted from Tam et al.  $^{35}$  with permission from Copyright © 2022, American Chemical Society.
- (C) Schematic illustration of the OTE made with BBL and polyethyleneimine (PEI).
- (D) Open-circuit voltage (V) as a function of temperature gradients ( $\Delta T$ ) and output power (P) as a function of load current (I) for the BBL:PEI OTE. (C) and (D) are adapted from Darabi et al.<sup>190</sup> and licensed under *CC BY 4.0*.
- (E) Schematic illustration of all-CLP OTE made with ambipolar BBL/LP3.

(F) Current density (J) over voltage (V) plot and the power density as a function of voltage for the ambipolar BBL/LP3 OTE. (E) and (F) are adapted from He et al. <sup>191</sup> with permission from © The Royal Society of Chemistry 2023.

cycles of operation. With its excellent OECT performance and cyclability, it was tested for complimentary logic circuits and complimentary inverters as voltage amplifiers, showing promising applications in bioelectronics.

OTEs based on CLPs such as n-type BBL and p-type LP3 (Figures 9A and 9B) are also garnering significant research interest owing to their excellent durability in converting thermal energy to electric current or vice versa. <sup>35,38,39,152,177,188–191</sup> The thermoelectric properties of BBL doped with various n-dopants have been extensively investigated. <sup>188</sup> Good electrical conductivity was achieved due to the formation of stable polarons in BBL backbone as opposed to those in non-ladder conjugated polymers. <sup>152</sup> The OTE made by BBL also exhibits outstanding thermal and ambient stability and solvent resistance property, again owing to its double-stranded constitution. <sup>177,189</sup> As reported by Müller and coworkers, a n-type thermoelectric yarn composed of regenerated cellulose spray-coated with BBL and PEI blended nanoparticles exhibits good electrical conductivity, Seebeck coefficient, and output power (Figures 9C and 9D). <sup>190</sup> The use of BBL in thermoelectric yarn is desirable because of its robust mechanical properties, with good conductivity retention toward 1,000 cycles of bending deformation, making this material promising for wearable thermoelectric devices.

Side-chain engineering of CLPs also offers opportunities for optimizing the performance of OTEs. Tam, Meng, Huang, Xu, and coworkers demonstrated that the



p-type LP3-Ph (Scheme 2) exhibits a mixed edge-on and face-on film morphology, while LP3-Me shows an exclusive edge-on orientation. <sup>39</sup> This morphological difference induced by side chains results in a 38-times higher electrical conductivity and a 13-times greater power factor for LP3-Me with FeCl<sub>3</sub> doping. The same group further investigated the effect of substituents on the thermoelectric property of n-type LP2 (Scheme 1C). <sup>38</sup> The film morphology of tetrachlorinated LP2 was found to be face-on, while that of dichlorinated LP2 exhibited edge-on orientation, contributing to roughly a 3-times greater electrical conductivity and power factor for the latter after being doped with benzyl viologen radical cation.

As mentioned earlier, a bulk heterojunction ambipolar polymer film is beneficial for the practical fabrication of micro-devices. Additionally, the use of both p- and n-type channels in a device results in greater thermoelectric performance due to the larger differences in thermal voltage and thermal resistance. Tam, Meng, Huang, Xu, and coworkers fabricated an all-CLP-based bulk heterojunction OTE by using a p-doped LP3/n-doped BBL blend film with a good output power density (Figures 9E and 9F). 191 It was found that the n-doped blend film has conductivity similar to that of the individual n-doped BBL film, while the p-doped blend film shows significantly lower conductivity than the individual p-doped LP3 film. This variation is attributed to the disruption of the crystalline microstructure of LP3 by the highly crystalline BBL in the blend film.

#### **CONCLUSIONS AND OUTLOOKS**

CLPs have garnered significant research interest on account of their unique structures and properties that bridge the gap between conventional single-stranded polymers and 2D materials. As described in this review, the past decade has witnessed remarkable strides in CLP research, encompassing synthesis, characterization, and applications. Despite these advancements, the field is still in its infancy when compared with the much more developed research fields of conventional single-stranded polymers. It is noteworthy that BBL, as one of the earliest reported CLPs, still offers arguably the best electronic performance and has the broadest range of demonstrated applications. The potential for further research advances and discoveries in the realm of CLPs is vast, with plentiful opportunities in developing highly efficient synthetic methods, accessing innovative ladder-type structures, uncovering novel properties and functions, and pursuing transformative applications. To fully exploit these opportunities, several scientific and engineering challenges should be overcome, which are summarized below.

In terms of fundamental synthetic methods for CLPs, there are a number of important challenges and opportunities to consider. First, it is crucial to address potential defects in the CLP backbones, during both synthesis and characterization. To achieve a low level of structural defects in CLPs, highly efficient reactions should be employed for the ladderization step. These reactions may either be kinetically controlled with high conversion or thermodynamically controlled that strongly favors the desired ladder-type structure. Special attention is sometimes required to characterize the minor defects in CLPs, using methods such as STM and isotope-labeled NMR spectroscopy. Second, many CLPs, including BBL, are regio-irregular. The structural irregularity of these CLPs could lead to less well-defined properties, disorder in aggregated states, and difficulty in expanding such structures into two dimensions. Third, new developments of highly efficient cyclization methods in traditional organic synthesis could offer significant opportunities for advancing CLP synthesis. Overcoming the challenges of adapting these new methods to ladder polymer





precursors could lead to highly efficient synthesis of novel, low-defect CLPs. Fourth, the synthesis of CLPs through living polymerization represents an exciting emerging field. By overcoming the challenges of applying living polymerization techniques, such as ring-opening metathesis polymerization and catalyst-transfer polymerization, to special functional monomers for CLP synthesis, next-generation CLPs with controlled molar masses and low polydispersity can be synthesized. Specifically, the development of living polymerization of CLPs in a one-pot annulation manner is highly desirable. Last but not least, for the full potential of these synthetic methods to be realized, optimizing them to be both feasible and scalable remains a critical goal for the practical applicability of CLPs in various fields.

In terms of designing the structure, synthesis, and processing techniques for the applications of CLPs, there are several important challenges to address. First, there is the dilemma of balancing the ratio between solubilizing side chains and the backbone. CLPs without side chains, such as BBL, exhibit excellent electronic performance but are difficult to handle and process owing to poor solubility and processability. By contrast, if a large number of solubilizing side chains are introduced, the CLPs may exhibit poor electronic properties due to the insulating nature of such side chains. One potential strategy is to solution process the precursor polymers followed by ladderization in the solid state. The non-ladder precursors usually have better solubility, thereby reducing the need for large-volume side chains. Synthesizing CLPs with cleavable side chains is an alternative strategy that maintains processability while enhancing interchain charge transport.

Many critical properties of CLPs, both in solution and in the solid state, remain largely unexplored. For instance, in solution, it is still unclear whether the chains of CLPs are intrinsically as rigid as rods or as flexible as ribbons. Moreover, the effective length scale of backbone rigidity is yet to be determined. To address these questions, unconventional models are necessary to describe the polymer physics and thermodynamics. The insights gained will illuminate the fundamental polymer physics of ladder polymers and two-dimensional polymers. It is noteworthy, however, that the pronounced aggregation tendency of many coplanar CLPs presents an additional challenge for their solution-phase characterization. In the solid state, the packing modes and morphologies of CLPs are unpredictable, partly due to their poor processability. Many CLPs are either amorphous or exhibit low crystallinity in the solid state, and they are often minimally affected by extensive annealing, a consequence of the inherently low chain mobility associated with a rigid backbone and strong intermolecular interactions. These solid-state properties differ markedly from those of well-characterized non-ladder conjugated polymers, necessitating the development of a new paradigm for describing, predicting, and characterizing the solid-state structures and dynamics of CLPs.

### **ACKNOWLEDGMENTS**

We thank the U.S. National Science Foundation (award #: 2003733 and 2304968) for financial support of this work.

#### **AUTHOR CONTRIBUTIONS**

L.F. conceived the topic and outline of the review. J.S.-J.Y. and L.F. wrote and revised the manuscript.

### **DECLARATION OF INTERESTS**

The authors declare no competing interests.





# DECLARATION OF GENERATIVE AI AND AI-ASSISTED TECHNOLOGIES IN THE WRITING PROCESS

During the preparation of this work, the authors used ChatGPT4.0 in order to improve language and readability. After using this tool/service, the authors reviewed and edited the content as needed, and the authors take full responsibility for the content of the publication.

#### **REFERENCES**

- International Union of Pure and Applied Chemistry (IUPAC) (2019). Ladder Macromolecule. https://doi.org/10.1351/ goldbook.L03441.
- Staudinger, H., and Bruson, H.A. (1926). Hochpolymere Verbindungen. 8. Mitteilung. Über die polymerisation des Cyclopentadiens. Justus Liebigs Ann. Chem. 447, 110–122. https://doi.org/10.1002/jlac. 19264470111.
- Diels, O., and Alder, K. (1928). Synthesen in der hydroaromatischen Reihe. Justus Liebigs Ann. Chem. 460, 98–122. https://doi.org/10. 1002/jlac.19284600106.
- Van Deusen, R.L. (1966). Benzimidazobenzophenanthroline polymers. J. Polym. Sci. B: Polym. Lett. 4, 211–214. https://doi.org/10. 1002/pol.1966.110040310.
- Lee, J., Kalin, A.J., Yuan, T., Al-Hashimi, M., and Fang, L. (2017). Fully conjugated ladder polymers. Chem. Sci. 8, 2503–2521. https:// doi.org/10.1039/C7SC00154A.
- Lee, J. (2023). Recent progress in synthesis of conjugated ladder polymers. Asian J. Org. Chem. 12, e202300104. https://doi.org/10. 1002/ajoc.202300104.
- Yu, L., Chen, M., and Dalton, L.R. (1990). Ladder polymers: recent developments in syntheses, characterization, and potential applications as electronic and optical materials. Chem. Mater. 2, 649–659. https:// doi.org/10.1021/cm00012a013.
- Scherf, U., and Müllen, K. (1995). The synthesis of ladder polymers. In Synthesis and Photosynthesis (Springer), pp. 1–40. https:// doi.org/10.1007/3-540-58908-2\_1.
- Teo, Y.C., Lai, H.W.H., and Xia, Y. (2017). Synthesis of ladder polymers: developments, challenges, and opportunities. Chemistry 23, 14101–14112. https://doi.org/10.1002/chem. 201702219.
- Clair, S., and de Oteyza, D.G. (2019). Controlling a chemical coupling reaction on a surface: tools and strategies for on-surface synthesis. Chem. Rev. 119, 4717–4776. https:// doi.org/10.1021/acs.chemrev.8b00601.
- Sun, K., Fang, Y., and Chi, L. (2021). Onsurface synthesis on nonmetallic substrates. ACS Mater. Lett. 3, 56–63. https://doi.org/10. 1021/acsmaterialslett.0c00452.
- Song, S., Su, J., Telychko, M., Li, J., Li, G., Li, Y., Su, C., Wu, J., and Lu, J. (2021). On-surface synthesis of graphene nanostructures with π-magnetism. Chem. Soc. Rev. 50, 3238– 3262. https://doi.org/10.1039/DDCS01060J.

- Gu, Y., Qiu, Z., and Müllen, K. (2023). Graphene nanoribbons as ladder polymers – synthetic challenges and components of future electronics. In Ladder Polymers: Synthesis, Properties, Applications, and Perspectives, Y. Xia, M. Yamaguchi, and T.-Y. Luh, eds. (Wiley-VCH Verlag GmbH), pp. 59–96. https://doi.org/10.1002/ 9783527833306.ch3.
- Kitao, T., Zhang, X., and Uemura, T. (2022). Nanoconfined synthesis of conjugated ladder polymers. Polym. Chem. 13, 5003–5018. https://doi.org/10.1039/D2PY00809B.
- Che, S., and Fang, L. (2020). Porous ladder polymer networks. Chem 6, 2558–2590. https://doi.org/10.1016/j.chempr.2020. 08.002
- Wang, Y., Ghanem, B.S., Ali, Z., Hazazi, K., Han, Y., and Pinnau, I. (2021). Recent progress on polymers of intrinsic microporosity and thermally modified analogue materials for membrane-based fluid separations. Small Struct. 2, 2100049. https://doi.org/10.1002/ sstr.202100049
- Carta, M. (2023). Ladder polymers of intrinsic microporosity (PIMs). In Ladder Polymers: Synthesis, Properties, Applications, and Perspectives, Y. Xia, M. Yamaguchi, and T.-Y. Luh, eds. (Wiley-VCH Verlag GmbH), pp. 179–218. https://doi.org/10.1002/ 9783527833306.ch6.
- Attar, S., Yang, R., Chen, Z., Ji, X., Comí, M., Banerjee, S., Fang, L., Liu, Y., and Al-Hashimi, M. (2022). Thiazole fused S,N-heteroacene step-ladder polymeric semiconductors for organic transistors. Chem. Sci. 13, 12034– 12044. https://doi.org/10.1039/D2SC04661J.
- Korshak, V.V., Rusanov, A.L., Iremashvili, T.G., Plieva, L.K., and Lekae, T.V. (1975). A general method of the synthesis of "step-ladder" polymers. Makromol. Chem. 176, 1233–1271. https://doi.org/10.1002/macp.1975. 021760504.
- Du, Y., Yuan, D., Awais, M.A., and Yu, L. (2022). New semi-ladder polymers for ambipolar organic light-emitting transistors. Chem. Commun. 58, 11347–11353. https://doi.org/ 10.1039/D2CC04087E.
- Zhu, C., Mu, A.U., Wang, C., Ji, X., and Fang, L. (2018). Synthesis and solution processing of a rigid polymer enabled by active manipulation of intramolecular hydrogen bonds. ACS Macro Lett. 7, 801–806. https:// doi.org/10.1021/acsmacrolett.8b00388.
- Chen, J., Cong, S., Wang, L., Wang, Y., Lan, L., Chen, C., Zhou, Y., Li, Z., McCulloch, I., and Yue, W. (2023). Backbone coplanarity manipulation via hydrogen bonding to boost

- the n-type performance of polymeric mixed conductors operating in aqueous electrolyte. Mater. Horiz. 10, 607–618. https://doi.org/10.1039/D2MH01100J.
- Lu, Y., Yu, Z.-D., Zhang, R.-Z., Yao, Z.-F., You, H.-Y., Jiang, L., Un, H.-I., Dong, B.-W., Xiong, M., Wang, J.-Y., and Pei, J. (2019). Rigid coplanar polymers for stable n-type polymer thermoelectrics. Angew. Chem. Int. Ed. 58, 11390–11394. https://doi.org/10.1002/anie. 201905835.
- Zhang, Q., Kelly, M.A., Bauer, N., and You, W. (2017). The curious case of fluorination of conjugated polymers for solar cells. Acc. Chem. Res. 50, 2401–2409. https://doi.org/10.1021/acs.accounts.7b00326.
- Liu, B., Wang, Y., Sun, H., Gámez-Valenzuela, S., Yan, Z., Feng, K., Uddin, M.A., Koh, C., Zhou, X., López Navarrete, J.T., et al. (2022). Backbone configuration and electronic property tuning of imide-functionalized ladder-type heteroarenes-based polymer acceptors for efficient all-polymer solar cells. Adv. Funct. Mater. 32, 2200065. https://doi. org/10.1002/adfm.202200065.
- Zhang, L., Wu, J., Li, D., Li, W., Meng, Q., and Bo, Z. (2019). Ladder-like conjugated polymers used as hole-transporting materials for high-efficiency perovskite solar cells.
   J. Mater. Chem. A 7, 14473–14477. https:// doi.org/10.1039/C9TA04043A.
- Huang, Y.-W., Lin, Y.-C., Li, J.-S., Chen, W.-C., and Chueh, C.-C. (2021). Investigating the backbone conformation and configuration effects for donor–acceptor conjugated polymers with ladder-type structures synthesized through aldol polycondensation.
   J. Mater. Chem. C 9, 9473–9483. https://doi. org/10.1039/D1TC02116H.
- Chawanpunyawat, T., Funchien, P., Wongkaew, P., Henjongchom, N., Ariyarit, A., Ittisanronnachai, S., Namuangruk, S., Cheacharoen, R., Sudyoadsuk, T., Goubard, F., et al. (2020). A ladder-like dopant-free hole-transporting polymer for hysteresis-less high-efficiency perovskite solar cells with high ambient stability. ChemSusChem 13, 5058– 5066. https://doi.org/10.1002/cssc. 202001350.
- Leng, M., and Fang, L. (2023). Processing of conjugated ladder polymers. In Ladder Polymers: Synthesis, Properties, Applications, and Perspectives, Y. Xia, M. Yamaguchi, and T.-Y. Luh, eds. (Wiley-VCH Verlag GmbH), pp. 97–120. https://doi.org/10.1002/ 9783527833306.ch4.
- Ikeda, S., and Shintani, R. (2019). Rhodiumcatalyzed stitching polymerization of 1,5hexadiynes and related oligoalkynes. Angew.



- Chem. Int. Ed. Engl. 58, 5734–5738. https://doi.org/10.1002/anie.201901148.
- Ikeda, S., Hanamura, Y., Tada, H., and Shintani, R. (2021). Rhodium-catalyzed stitching polymerization of alkynylsilylacetylenes. J. Am. Chem. Soc. 143, 19559–19566. https://doi.org/10.1021/jacs. 109827.
- Togawa, S., and Shintani, R. (2022). Synthesis of poly(arylenevinylene)s by rhodium-catalyzed stitching polymerization/alkene isomerization. J. Am. Chem. Soc. 144, 18545–18551. https://doi.org/10.1021/jacs.2c07835.
- Kim, F.S., Park, C.H., Na, Y., and Jenekhe, S.A. (2019). Effects of ladder structure on the electronic properties and field-effect transistor performance of poly(benzobisimidazobenzophenanthroline). Org. Electron. 69, 301–307. https://doi.org/10.1016/j.orgel.2019.03.049.
- Belaish, I., Rettori, C., Davidov, D., McLean, M.R., Dalton, L., and Nalwa, H. (1988). Electric properties of ladder type polymers BBB and BBL. MRS Proc. 134, 689–695. https://doi.org/ 10.1557/PROC-134-689.
- Tam, T.L.D., Lin, M., Chien, S.W., and Xu, J. (2022). Facile synthesis of solubilizing a group-free, solution-processable p-type ladder conjugated polymer and its thermoelectric properties. ACS Macro Lett. 11, 110–115. https://doi.org/10.1021/acsmacrolett. 1c00696.
- West, S.M., Tran, D.K., Guo, J., Chen, S.E., Ginger, D.S., and Jenekhe, S.A. (2023). Phenazine-substituted poly (benzimidazobenzophenanthrolinedione): electronic structure, thin film morphology, electron transport, and mechanical properties of an n-type semiconducting ladder polymer. Macromolecules 56, 2081–2091. https://doi. org/10.1021/acs.macromol.2c01999.
- He, Q., Dexter Tam, T.L., Lin, T., Chien, S.W., Lin, M., Meng, H., Huang, W., and Xu, J. (2022). π-Extended poly (benzimidazoanthradiisoquinolinedione) ladder-type conjugated polymer. ACS Macro Lett. 11, 1136–1141. https://doi.org/10.1021/ acsmacrolett.2c00438.
- He, Q., Zhang, X., Tam, T.L.D., Wang, J., Chen, H., Chien, S.W., Tham, N.N., Koh, X.Q., Lee, J.J.C., Lin, M., et al. (2023). Balancing solubility and thermoelectric performance in π-extended poly (benzimidazoanthradiisoquinolinedione) ladder-type conjugated polymer. ACS Appl. Electron. Mater. https://doi.org/10.1021/ acsaelm.3c00294.
- He, Q., Wang, J., Dexter Tam, T.L., Zhang, X., Jiang, Z., Chien, S.W., Tham, N.N., Koh, X.Q., Soh, P.X., Meng, H., et al. (2023). Thermoelectric performance enhancement of p-type pyrrolo[3,2-b:4,5-b']bis[1,4] benzothiazine conjugated ladder polymer by pendant group engineering. ACS Mater. Lett. 5, 2829–2835. https://doi.org/10.1021/ acsmaterialslett.3c00758.
- West, S.M., Tran, D.K., Guo, J., Chen, S.E., Ginger, D.S., and Jenekhe, S.A. (2023). p-type semiconducting ladder poly(pyrrolobenzothiazine)s: effects of *N*-alkyl side chains on the chain conformation,

- electronic structure, and charge transport properties. Macromolecules 56, 10222– 10235. https://doi.org/10.1021/acs. macromol.3c01561.
- Kapaev, R.R., Shestakov, A.F., Vasil'ev, S.G., and Stevenson, K.J. (2021). Conjugated ladder-type polymer with hexaazatriphenylene units as a cathode material for lithium, sodium, and potassium batteries. ACS Appl. Energy Mater. 4, 10423– 10427. https://doi.org/10.1021/acsaem. 101970.
- Xie, J., Rui, X., Gu, P., Wu, J., Xu, Z.J., Yan, Q., and Zhang, Q. (2016). Novel conjugated ladder-structured oligomer anode with high lithium storage and long cycling capability. ACS Appl. Mater. Interfaces 8, 16932–16938. https://doi.org/10.1021/acsami.6b04277.
- Ma, X., Wang, H., Cheng, J., Cheng, H., Wang, L., Wu, X., and Xu, H. (2021). Fully conjugated ladder polymers as metal-free photocatalysts for visible-light-driven water oxidation. Chin. J. Chem. 39, 1079–1084. https://doi.org/10.1002/cjoc.202000614.
- Zhao, Y., Wu, M., Chen, H., Zhu, J., Liu, J., Ye, Z., Zhang, Y., Zhang, H., Ma, Y., Li, C., et al. (2021). Balance cathode-active and anode-active groups in one conjugated polymer towards high-performance all-organic lithium-ion batteries. Nano Energy 86, 106055. https://doi.org/10.1016/j.nanoen. 2021.106055.
- Chen, Y., Li, H., Tang, M., Zhuo, S., Wu, Y., Wang, E., Wang, S., Wang, C., and Hu, W. (2019). Capacitive conjugated ladder polymers for fast-charge and -discharge sodium-ion batteries and hybrid supercapacitors. J. Mater. Chem. A 7, 20891– 20898. https://doi.org/10.1039/C9TA07546A.
- Xie, J., Wang, Z., Gu, P., Zhao, Y., Xu, Z.J., and Zhang, Q. (2016). A novel quinone-based polymer electrode for high performance lithium-ion batteries. Sci. China Mater. 59, 6–11. https://doi.org/10.1007/s40843-016-0112-3.
- Yang, Y., Lin, E., Wang, S., Wang, T., Wang, Z., and Zhang, Z. (2024). Single-crystal onedimensional porous ladder covalent polymers. J. Am. Chem. Soc. 146, 782–790. https://doi.org/10.1021/jacs.3c10812.
- Ren, X., Zhang, H., Song, M., Cheng, C., Zhao, H., and Wu, Y. (2019). One-step route to ladder-type C-N linked conjugated polymers. Macromol. Chem. Phys. 220, 1900044. https:// doi.org/10.1002/macp.201900044.
- Zhu, X., Liu, F., Ba, X., and Wu, Y. (2023). Tandem Suzuki polymerization/Heck cyclization reaction to form ladder-type 9,9'-bifluorenylidene-based conjugated polymer. Polymers 15, 3360. https://doi.org/ 10.3390/polym15163360.
- Brodie, B.C. (1874). IV. On the action of electricity on gases.—II. On the electric decomposition of carbonic-acid gas. Philos. Trans. R. Soc. Lond. 164, 83–103. https://doi. org/10.1098/rstl.1874.0004.
- 51. Odziomek, M., Giusto, P., Kossmann, J., Tarakina, N.V., Heske, J., Rivadeneira, S.M., Keil, W., Schmidt, C., Mazzanti, S., Savateev, O., et al. (2022). "Red carbon": A rediscovered

- covalent crystalline semiconductor. Adv. Mater. 34, e2206405. https://doi.org/10.1002/adma.202206405.
- Carofiglio, T., Pandolfo, L., and Paiaro, G. (1986). Carbon suboxide polymers. Eur. Polym. J. 22, 491–497. https://doi.org/10. 1016/0014-3057(86)90011-X.
- Kolcu, F., and Kaya, İ. (2020). A study of the chemical and the enzyme-catalyzed oxidative polymerization of aromatic diamine bearing chlor substituents, pursuant to structural, thermal and photophysical properties. Eur. Polym. J. 133, 109767. https://doi.org/10. 1016/j.eurpolymj.2020.109767.
- 54. Acerce, M., Chiovoloni, S., Hernandez, Y., Ortuno, C., Qian, J., and Lu, J. (2021). Poly(1,5diaminonaphthalene)-grafted monolithic 3D hierarchical carbon as highly capacitive and stable supercapacitor electrodes. ACS Appl. Mater. Interfaces 13, 53736–53745. https:// doi.org/10.1021/acsami.1c13746.
- Guillerm, V., Ragon, F., Dan-Hardi, M., Devic, T., Vishnuvarthan, M., Campo, B., Vimont, A., Clet, G., Yang, Q., Maurin, G., et al. (2012). A series of isoreticular, highly stable, porous zirconium oxide based metal-organic frameworks. Angew. Chem. Int. Ed. Engl. 51, 9267–9271. https://doi.org/10.1002/anie. 201204806
- Kitao, T., MacLean, M.W.A., Nakata, K., Takayanagi, M., Nagaoka, M., and Uemura, T. (2020). Scalable and precise synthesis of armchair-edge graphene nanoribbon in metal-organic framework. J. Am. Chem. Soc. 142, 5509–5514. https://doi.org/10.1021/jacs. 0c00467
- 57. Kitao, T., Miura, T., Nakayama, R., Tsutsui, Y., Chan, Y.S., Hayashi, H., Yamada, H., Seki, S., Hitosugi, T., and Uemura, T. (2023). Synthesis of polyacene by using a metal–organic framework. Nat. Synth. 2, 848–854. https:// doi.org/10.1038/s44160-023-00310-w.
- Kissel, P., Murray, D.J., Wulftange, W.J., Catalano, V.J., and King, B.T. (2014). A nanoporous two-dimensional polymer by single-crystal-to-single-crystal photopolymerization. Nat. Chem. 6, 774–778. https://doi.org/10.1038/nchem.2008.
- Lange, R.Z., Hofer, G., Weber, T., and Schlüter, A.D. (2017). A two-dimensional polymer synthesized through topochemical [2 + 2]-cycloaddition on the multigram scale. J. Am. Chem. Soc. 139, 2053–2059. https:// doi.org/10.1021/jacs.6b11857.
- Hema, K., Ravi, A., Raju, C., and Sureshan, K.M. (2021). Polymers with advanced structural and supramolecular features synthesized through topochemical polymerization. Chem. Sci. 12, 5361–5380. https://doi.org/10.1039/D0SC07066A.
- 61. Li, X., Baldini, M., Wang, T., Chen, B., Xu, E.S., Vermilyea, B., Crespi, V.H., Hoffmann, R., Molaison, J.J., Tulk, C.A., et al. (2017). Mechanochemical synthesis of carbon nanothread single crystals. J. Am. Chem. Soc. 139, 16343–16349. https://doi.org/10.1021/jacs.7b09311.
- Xu, E.S., Lammert, P.E., and Crespi, V.H. (2015). Systematic enumeration of sp<sup>3</sup> nanothreads. Nano Lett. 15, 5124–5130.



- https://doi.org/10.1021/acs.nanolett. 5b01343
- Fitzgibbons, T.C., Guthrie, M., Xu, E.S., Crespi, V.H., Davidowski, S.K., Cody, G.D., Alem, N., and Badding, J.V. (2015). Benzenederived carbon nanothreads. Nat. Mater. 14, 43–47. https://doi.org/10.1038/nmat4088.
- 64. Li, X., Wang, T., Duan, P., Baldini, M., Huang, H.T., Chen, B., Juhl, S.J., Koeplinger, D., Crespi, V.H., Schmidt-Rohr, K., et al. (2018). Carbon nitride nanothread crystals derived from pyridine. J. Am. Chem. Soc. 140, 4969– 4972. https://doi.org/10.1021/jacs.7b13247.
- Matsuura, B.S., Huss, S., Zheng, Z., Yuan, S., Wang, T., Chen, B., Badding, J.V., Trauner, D., Elacqua, E., van Duin, A.C.T., et al. (2021). Perfect and defective <sup>13</sup>C-furan-derived nanothreads from modest-pressure synthesis analyzed by <sup>13</sup>C NMR. J. Am. Chem. Soc. 143, 9529–9542. https://doi.org/10.1021/jacs. 1003671
- 66. Jordan, R.S., Wang, Y., McCurdy, R.D., Yeung, M.T., Marsh, K.L., Khan, S.I., Kaner, R.B., and Rubin, Y. (2016). Synthesis of graphene nanoribbons via the topochemical polymerization and subsequent aromatization of a diacetylene precursor. Chem 1, 78–90. https://doi.org/10.1016/j.chempr.2016.06.010.
- 67. Jordan, R.S., Li, Y.L., Lin, C.-W., McCurdy, R.D., Lin, J.B., Brosmer, J.L., Marsh, K.L., Khan, S.I., Houk, K.N., Kaner, R.B., et al. (2017). Synthesis of N = 8 armchair graphene nanoribbons from four distinct polydiacetylenes. J. Am. Chem. Soc. *139*, 15878–15890. https://doi.org/10.1021/jacs.7b08800
- Li, Y.L., Zee, C.-T., Lin, J.B., Basile, V.M., Muni, M., Flores, M.D., Munárriz, J., Kaner, R.B., Alexandrova, A.N., Houk, K.N., et al. (2020). Fjord-edge graphene nanoribbons with sitespecific nitrogen substitution. J. Am. Chem. Soc. 142, 18093–18102. https://doi.org/10. 1021/jacs.0c07657.
- 69. Zhang, P., Tang, X., Wang, Y., Wang, X., Gao, D., Li, Y., Zheng, H., Wang, Y., Wang, X., Fu, R., et al. (2020). Distance-selected topochemical dehydro-Diels-Alder reaction of 1,4-diphenylbutadiyne toward crystalline graphitic nanoribbons. J. Am. Chem. Soc. 142, 17662–17669. https://doi.org/10.1021/jacs.0c08274.
- Saha, B., and Schatz, G.C. (2012). Carbonization in polyacrylonitrile (PAN) based carbon fibers studied by ReaxFF molecular dynamics simulations. J. Phys. Chem. B 116, 4684–4692. https://doi.org/10. 1021/io300581b.
- Soulis, S., Konstantopoulos, G., Koumoulos, E.P., and Charitidis, C.A. (2020). Impact of alternative stabilization strategies for the production of PAN-based carbon fibers with high performance. Fibers 8, 33. https://doi. org/10.3390/fib8060033.
- Zhang, X., Kitao, T., Piga, D., Hongu, R., Bracco, S., Comotti, A., Sozzani, P., and Uemura, T. (2020). Carbonization of single polyacylonitrile chains in coordination nanospaces. Chem. Sci. 11, 10844–10849. https://doi.org/10.1039/DOSC02048F.

- Hirano, T., Hanamura, H., Inoue, M., Ueda, S., Watanabe, M., Tanabiki, M., and Mikami, K. (2019). Synthesis of soluble, air-stable fully conjugated ladder polymers. Polymer 177, 282–289. https://doi.org/10.1016/j.polymer. 2019.06.014.
- Grzybowski, M., Skonieczny, K., Butenschön, H., and Gryko, D.T. (2013). Comparison of oxidative aromatic coupling and the Scholl reaction. Angew. Chem. Int. Ed. Engl. 52, 9900–9930. https://doi.org/10.1002/anie. 201210238.
- Jassas, R.S., Mughal, E.U., Sadiq, A., Alsantali, R.I., Al-Rooqi, M.M., Naeem, N., Moussa, Z., and Ahmed, S.A. (2021). Scholl reaction as a powerful tool for the synthesis of nanographenes: A systematic review. RSC Adv. 11, 32158–32202. https://doi.org/10. 1039/D1RA05910F.
- Ponugoti, N., and Parthasarathy, V. (2022). Rearrangements in Scholl reaction. Chemistry 28, e202103530. https://doi.org/10.1002/ chem.202103530.
- Bheemireddy, S.R., Hautzinger, M.P., Li, T., Lee, B., and Plunkett, K.N. (2017). Conjugated ladder polymers by a cyclopentannulation polymerization. J. Am. Chem. Soc. 139, 5801– 5807. https://doi.org/10.1021/jacs.6b12916.
- Shen, X., Wu, Y., Bai, L., Zhao, H., and Ba, X. (2017). Microwave-assisted synthesis of 4,9-linked pyrene-based ladder conjugated polymers. J. Polym. Sci. Part A: Polym. Chem. 55, 1285–1288. https://doi.org/10.1002/pola. 28494.
- Takagi, K., and Yamada, Y. (2019). Ladderization of poly(p-phenylenevinylene) derivative: synthesis of polycyclic aromatic hydrocarbon polymer by intramolecular oxidative cyclization. Polymer 179, 121607. https://doi.org/10.1016/j.polymer.2019. 121607.
- Wang, L., Hu, M., Zhang, Y., Yuan, Z., Hu, Y., Zhao, X., and Chen, Y. (2019). Single-strand and ladder-type polymeric acceptors based on regioisomerically-pure perylene diimides towards all-polymer solar cells. Polymer 162, 108–115. https://doi.org/10.1016/j.polymer. 2018.12.041.
- Sahu, D., Sutar, H., Senapati, P., Murmu, R., and Roy, D. (2021). Graphene, graphenederivatives and composites: fundamentals, synthesis approaches to applications.
   J. Compos. Sci. 5, 181. https://doi.org/10. 3390/jcs5070181.
- Kumar, N., Salehiyan, R., Chauke, V., Joseph Botlhoko, O., Setshedi, K., Scriba, M., Masukume, M., and Sinha Ray, S. (2021). Topdown synthesis of graphene: A comprehensive review. FlatChem 27, 100224. https://doi.org/10.1016/j.flatc.2021.100224.
- 83. Yoon, K.-Y., and Dong, G. (2020). Liquid-phase bottom-up synthesis of graphene nanoribbons. Mater. Chem. Front. 4, 29–45. https://doi.org/10.1039/C9QM00519F.
- Niu, W., Liu, J., Mai, Y., Müllen, K., and Feng, X. (2019). Synthetic engineering of graphene nanoribbons with excellent liquid-phase processability. J. Trends Chem. 1, 549–558. https://doi.org/10.1016/j.trechm.2019. 06.008.

- Shekhirev, M., and Sinitskii, A. (2017). Solution synthesis of atomically precise graphene nanoribbons. Sci. Rev. 2, 20160108. https:// doi.org/10.1515/psr-2016-0108.
- Gu, Y., Qiu, Z., and Müllen, K. (2022). Nanographenes and graphene nanoribbons as multitalents of present and future materials science. J. Am. Chem. Soc. 144, 11499–11524. https://doi.org/10.1021/jacs.2c02491.
- Ritter, K.A., and Lyding, J.W. (2009). The influence of edge structure on the electronic properties of graphene quantum dots and nanoribbons. Nat. Mater. 8, 235–242. https:// doi.org/10.1038/nmat2378.
- Niu, W., Ma, J., Soltani, P., Zheng, W., Liu, F., Popov, A.A., Weigand, J.J., Komber, H., Poliani, E., Casiraghi, C., et al. (2020). A curved graphene nanoribbon with multi-edge structure and high intrinsic charge carrier mobility. J. Am. Chem. Soc. 142, 18293– 18298. https://doi.org/10.1021/jacs.0c07013.
- 89. Yang, L., Ma, J., Zheng, W., Osella, S., Droste, J., Komber, H., Liu, K., Böckmann, S., Beljonne, D., Hansen, M.R., et al. (2022). Solution synthesis and characterization of a long and curved graphene nanoribbon with hybrid cove-armchair-gulf edge structures. Adv. Sci. (Weinh) 9, e2200708. https://doi.org/10.1002/advs.202200708.
- Obermann, S., Zheng, W., Melidonie, J., Böckmann, S., Osella, S., Arisnabarreta, N., Guerrero-León, L.A., Hennersdorf, F., Beljonne, D., Weigand, J.J., et al. (2023). Curved graphene nanoribbons derived from tetrahydropyrene-based polyphenylenes via one-pot K-region oxidation and Scholl cyclization. Chem. Sci. 14, 8607–8614. https:// doi.org/10.1039/D3SC02824K.
- Wang, X., Ma, J., Zheng, W., Osella, S., Arisnabarreta, N., Droste, J., Serra, G., Ivasenko, O., Lucotti, A., Beljonne, D., et al. (2022). Cove-edged graphene nanoribbons with incorporation of periodic zigzag-edge segments. J. Am. Chem. Soc. 144, 228–235. https://doi.org/10.1021/jacs.1c09000.
- Yao, X., Zheng, W., Osella, S., Qiu, Z., Fu, S., Schollmeyer, D., Müller, B., Beljonne, D., Bonn, M., Wang, H.I., et al. (2021). Synthesis of nonplanar graphene nanoribbon with fjord edges. J. Am. Chem. Soc. 143, 5654–5658. https://doi.org/10.1021/jacs.1c01882.
- 93. Niu, W., Fu, Y., Serra, G., Liu, K., Droste, J., Lee, Y., Ling, Z., Xu, F., Cojal González, J.D., Lucotti, A., et al. (2023). Bottom-up solution synthesis of graphene nanoribbons with precisely engineered nanopores. Angew. Chem. Int. Ed. Engl. 62, e202305737. https://doi.org/10.1002/anie.202305737.
- Li, G., Yoon, K.-Y., Zhong, X., Wang, J., Zhang, R., Guest, J.R., Wen, J., Zhu, X.Y., and Dong, G. (2018). A modular synthetic approach for band-gap engineering of armchair graphene nanoribbons. Nat. Commun. 9, 1687. https:// doi.org/10.1038/s41467-018-03747-2.
- Chen, Q., Lodi, A., Zhang, H., Gee, A., Wang, H.I., Kong, F., Clarke, M., Edmondson, M., Hart, J., O'Shea, J.N., et al. (2024). Nat. Chem. https://doi.org/10.1038/s41557-024-01477-1.
- 96. Zhang, X., Hu, Y., Lien-Medrano, C.R., Li, J., Shi, J., Qin, X., Liao, Z., Wang, Y., Wang, Z., Li,



- J., et al. (2023). Photoresponse of solutionsynthesized graphene nanoribbon heterojunctions on diamond indicating phototunable photodiode polarity. J. Am. Chem. Soc. 145, 8757–8763. https://doi.org/ 10.1021/jacs.2c13822.
- Veber, G., Diercks, C.S., Rogers, C., Perkins, W.S., Ciston, J., Lee, K., Llinas, J.P., Liebman-Peláez, A., Zhu, C., Bokor, J., et al. (2020). Reticular growth of graphene nanoribbon 2D covalent organic frameworks. Chem 6, 1125– 1133. https://doi.org/10.1016/j.chempr.2020. 01.022.
- Keerthi, A., Radha, B., Rizzo, D., Lu, H., Diez Cabanes, V., Hou, I.C.-Y., Beljonne, D., Cornil, J., Casiraghi, C., Baumgarten, M., et al. (2017). Edge functionalization of structurally defined graphene nanoribbons for modulating the self-assembled structures. J. Am. Chem. Soc. 139, 16454–16457. https://doi.org/10.1021/ jacs.7b09031.
- Huang, Y., Xu, F., Ganzer, L., Camargo, F.V.A., Nagahara, T., Teyssandier, J., Van Gorp, H., Basse, K., Straasø, L.A., Nagyte, V., et al. (2018). Intrinsic properties of single graphene nanoribbons in solution: synthetic and spectroscopic studies. J. Am. Chem. Soc. 140, 10416–10420. https://doi.org/10.1021/jacs. 8b06028.
- Scherf, U., and Müllen, K. (1991). Polyarylenes and poly(arylenevinylenes), 7. A soluble ladder polymer via bridging of functionalized poly(p-phenylene)-precursors. Makromol. Chem. Rapid Commun. 12, 489–497. https:// doi.org/10.1002/marc.1991.030120806.
- 101. Scherf, U., Bohnen, A., and Müllen, K. (1992). Polyarylenes and poly(arylenevinylene)s, 9 The oxidized states of a (1,4-phenylene) ladder polymer. Makromol. Chem. 193, 1127–1133. https://doi.org/10.1002/macp.1992. 021930511.
- 102. Fahnenstich, U., Koch, K.-H., Pollmann, M., Scherf, U., Wagner, M., Wegener, S., and Müllen, K. (1992). Design of novel structurally defined ladder-type polymers. Makromol. Chem. Macromol. Symp. 54–55, 465–476. https://doi.org/10.1002/masy.19920540134.
- 103. Rudnick, A., Kass, K.-J., Preis, E., Scherf, U., Bässler, H., and Köhler, A. (2017). Interplay of localized pyrene chromophores and π-conjugation in novel poly(2,7-pyrene) ladder polymers. J. Chem. Phys. 146, 174903. https://doi.org/10.1063/1.4982046.
- 104. Yin, Y., Zhang, S., Chen, D., Guo, F., Yu, G., Zhao, L., and Zhang, Y. (2018). Synthesis of an indacenodithiophene-based fully conjugated ladder polymer and its optical and electronic properties. Polym. Chem. 9, 2227–2231. https://doi.org/10.1039/C8PY00351C.
- 105. Ockfen, M.C., Forster, M., and Scherf, U. (2018). Scope and limitations of the dehydrogenative generation of graphenic nanoribbons from methylene-bridged, aromatic ladder polymers. Macromol. Rapid Commun. 39, e1800569. https://doi.org/10. 1002/marc.201800569.
- 106. Vogel, A., Forster, M., Wilbraham, L., Smith, C.L., Cowan, A.J., Zwijnenburg, M.A., Sprick, R.S., and Cooper, A.I. (2019). Photocatalytically active ladder polymers.

- Faraday Discuss. 215, 84–97. https://doi.org/10.1039/C8FD00197A.
- Haryono, A., Miyatake, K., Natori, J., and Tsuchida, E. (1999). Synthesis of a novel oligo(p-phenylene) ladder by sulfide and sulfonio groups. Macromolecules 32, 3146– 3149. https://doi.org/10.1021/may817774.
- 108. Zou, Y., Ji, X., Cai, J., Yuan, T., Stanton, D.J., Lin, Y.-H., Naraghi, M., and Fang, L. (2017). Synthesis and solution processing of a hydrogen-bonded ladder polymer. Chem 2, 139–152. https://doi.org/10.1016/j.chempr. 2016.12.008.
- 109. Ji, X., Leng, M., Xie, H., Wang, C., Dunbar, K.R., Zou, Y., and Fang, L. (2020). Extraordinary electrochemical stability and extended polaron delocalization of laddertype polyaniline-analogous polymers. Chem. Sci. 11, 12737–12745. https://doi.org/10.1039/ D0SC03348K.
- 110. Leng, M., Koripally, N., Huang, J., Vriza, A., Lee, K.Y., Ji, X., Li, C., Hays, M., Tu, Q., Dunbar, K., et al. (2023). Synthesis and exceptional operational durability of polyaniline-inspired conductive ladder polymers. Mater. Horiz. 10, 4354–4364. https://doi.org/10.1039/D3MH00883E.
- 111. Trilling, F., Ausländer, M.-K., and Scherf, U. (2019). Ladder-type polymers and ladder-type polyelectrolytes with on-chain dibenz[a,h] anthracene chromophores. Macromolecules 52, 3115–3122. https://doi.org/10.1021/acs.macromol.9b00396.
- 112. Yang, W., Lucotti, A., Tommasini, M., and Chalifoux, W.A. (2016). Bottom-up synthesis of soluble and narrow graphene nanoribbons using alkyne benzannulations. J. Am. Chem. Soc. 138, 9137–9144. https://doi.org/10.1021/ iacs.6b03014.
- 113. Wu, N.M.-W., Warndorf, M.C., Alexander-Katz, A., and Swager, T.M. (2024). Oxepinebased π-conjugated ladder/step-ladder polymers with excited-state aromaticity. Macromolecules 57, 991–1000. https://doi. org/10.1021/acs.macromol.3c02036.
- 114. Ikai, T., Miyoshi, S., Oki, K., Saha, R., Hijikata, Y., and Yashima, E. (2023). Defect-free synthesis of a fully π-conjugated helical ladder polymer and resolution into a pair of enantiomeric helical ladders. Angew. Chem. Int. Ed. Engl. 62, e202301962. https://doi.org/10.1002/anie.202301962.
- 115. Zheng, W., Ikai, T., and Yashima, E. (2021). Synthesis of single-handed helical spiroconjugated ladder polymers through quantitative and chemoselective cyclizations\*. Angew. Chem. Int. Ed. Engl. 60, 11294–11299. https://doi.org/10.1002/anie. 202102885.
- 116. Zheng, W., Oki, K., Saha, R., Hijikata, Y., Yashima, E., and Ikai, T. (2023). One-handed helical tubular ladder polymers for chromatographic enantioseparation. Angew. Chem. Int. Ed. Engl. 62, e202218297. https:// doi.org/10.1002/anje.202218297.
- 117. Ikai, T., Mishima, N., Matsumoto, T., Miyoshi, S., Oki, K., and Yashima, E. (2024). 2,2'-Tethered binaphthyl-embedded onehanded helical ladder polymers: impact of the tether length on helical geometry and

- chiroptical property. Angew. Chem. Int. Ed. Engl. 63, e202318712. https://doi.org/10.1002/anie.202318712.
- Senese, A.D., and Chalifoux, W.A. (2018). Nanographene and graphene nanoribbon synthesis via alkyne benzannulations. Molecules 24, 118. https://doi.org/10.3390/ molecules24010118.
- 119. Miao, D., Daigle, M., Lucotti, A., Boismenu-Lavoie, J., Tommasini, M., and Morin, J.F. (2018). Toward thiophene-annulated graphene nanoribbons. Angew. Chem. Int. Ed. Engl. 57, 3588–3592. https://doi.org/10. 1002/anie.201710585.
- Daigle, M., and Morin, J.-F. (2017). Helical conjugated ladder polymers: tuning the conformation and properties through edge design. Macromolecules 50, 9257–9264. https://doi.org/10.1021/acs.macromol. 7b01722.
- Daigle, M., Miao, D., Lucotti, A., Tommasini, M., and Morin, J.-F. (2017). Helically coiled graphene nanoribbons. Angew. Chem. Int. Ed. Engl. 56, 6213–6217. https://doi.org/10. 1002/anie.201611834.
- Chalifoux, W.A. (2017). The synthesis of nonplanar, helically coiled graphene nanoribbons. Angew. Chem. Int. Ed. Engl. 56, 8048–8050. https://doi.org/10.1002/anie. 201702687.
- 123. Miao, D., Di Michele, V., Gagnon, F., Aumaître, C., Lucotti, A., Del Zoppo, M., Lirette, F., Tommasini, M., and Morin, J.-F. (2021). Pyrrole-embedded linear and helical graphene nanoribbons. J. Am. Chem. Soc. 143, 11302–11308. https://doi.org/10.1021/ jacs.1c05616.
- Daigle, M., Picard-Lafond, A., Soligo, E., and Morin, J.-F. (2016). Regioselective synthesis of nanographenes by photochemical cyclodehydrochlorination. Angew. Chem. Int. Ed. Engl. 55, 2042–2047. https://doi.org/10. 1002/anie.201509130.
- 125. Dou, C., Liu, J., and Wang, L. (2017). Conjugated polymers containing B ← N unit as electron acceptors for all-polymer solar cells. Sci. China Chem. 60, 450–459. https:// doi.org/10.1007/s11426-016-0503-x.
- 126. Zhao, R., Liu, J., and Wang, L. (2020). Polymer acceptors containing B ← N units for organic photovoltaics. Acc. Chem. Res. 53, 1557–1567. https://doi.org/10.1021/acs.accounts. 0c00281.
- Huang, J., and Li, Y. (2018). BN Embedded polycyclic π-conjugated systems: synthesis, optoelectronic properties, and photovoltaic applications. Front. Chem. 6, 341. https://doi. org/10.3389/fchem.2018.00341.
- 128. Chen, S., Liu, F., Wang, C., Shen, J., and Wu, Y. (2019). Simple route to synthesize fully conjugated ladder isomer copolymers with carbazole units. Polymers 11, 1619. https://doi.org/10.3390/polym11101619.
- 129. Liu, F., Zhang, H., Dong, J., Wu, Y., and Li, W. (2018). Highly efficient synthesis of a ladder-type BN-heteroacene and polyheteroacene. Asian J. Org. Chem. 7, 465–470. https://doi.org/10.1002/ajoc.201700571.



- Qiang, P., Sun, Z., Xue, B., and Zhang, F. (2021). rr-Extended ladder-type conjugated polymers via BN-annulation. Org. Mater. 03, 221–227. https://doi.org/10.1055/s-0041-1727181.
- 131. Zhu, C., Ji, X., You, D., Chen, T.L., Mu, A.U., Barker, K.P., Klivansky, L.M., Liu, Y., and Fang, L. (2018). Extraordinary redox activities in ladder-type conjugated molecules enabled by B ← N coordination-promoted delocalization and hyperconjugation. J. Am. Chem. Soc. 140, 18173–18182. https://doi. org/10.1021/jacs.8b11337.
- 132. Grandl, M., Schepper, J., Maity, S., Peukert, A., von Hauff, E., and Pammer, F. (2019). N → B ladder polymers prepared by postfunctionalization: tuning of electron affinity and evaluation as acceptors in all-polymer solar cells. Macromolecules *52*, 1013–1024. https://doi.org/10.1021/acs.macromol.8b02595.
- Lee, J., Rajeeva, B.B., Yuan, T., Guo, Z.-H., Lin, Y.-H., Al-Hashimi, M., Zheng, Y., and Fang, L. (2016). Thermodynamic synthesis of solution processable ladder polymers. Chem. Sci. 7, 881–889. https://doi.org/10.1039/ C5SC02385H.
- 134. Lee, J., Kalin, A.J., Wang, C., Early, J.T., Al-Hashimi, M., and Fang, L. (2018). Donor– acceptor conjugated ladder polymer via aromatization-driven thermodynamic annulation. Polym. Chem. 9, 1603–1609. https://doi.org/10.1039/C7PY02059G.
- 135. Liu, F., Wu, Y., Wang, C., Ma, J., Wu, F., Zhang, Y., and Ba, X. (2018). Synthesis and characterization of fully conjugated ladder naphthalene bisimide copolymers. Polymers 10, 790. https://doi.org/10.3390/polym10070790.
- Chmil, K., and Scherf, U. (1993). A simple twostep synthesis of a novel, fully aromatic ladder-type polymer. Makromol. Chem. Rapid Commun. 14, 217–222. https://doi.org/ 10.1002/marc.1993.030140401.
- Chmil, K., and Scherf, U. (1997). Conjugated all-carbon ladder polymers: improved solubility and molecular weights. Acta Polym. 48, 208–211. https://doi.org/10.1002/actp. 1997.010480506.
- 138. Unruh, M.T., Scherf, U., Bahmann, H., Rodrigues, A.C.B., Cunha, C., Seixas de Melo, J.S., Schedlbauer, J., and Lupton, J.M. (2021). Unexpectedly flexible graphene nanoribbons with a polyacene ladder skeleton. J. Mater. Chem. C 9, 16208–16216. https://doi.org/10. 1039/D1TC02302K.
- 139. Gong, X., Zhang, Y., Wen, H., Fan, Y., Han, P., Sun, Y., Zhang, X., Yang, H., and Lin, B. (2016). Phenoxazine-based conjugated ladder polymers as novel electrode materials for supercapacitors. ChemElectroChem 3, 1837– 1846. https://doi.org/10.1002/celc. 201600381.
- Uddin, A., Pandey, K., and Plunkett, K.N. (2022). Indacenodipyrene containing small molecules and ladder polymers. Tetrahedron Chem. 2, 100019. https://doi.org/10.1016/j. tchem.2022.100019.
- 141. Wang, H., Zhao, H., Chen, S., Bai, L., Su, Z., and Wu, Y. (2021). Effective synthesis of

- ladder-type oligo(p-aniline)s and poly(p-aniline)s via intramolecular  $S_NAr$  reaction. Org. Lett. 23, 2217–2221. https://doi.org/10.1021/acs.orglett.1c00363.
- 142. Senkovska, I., Hoffmann, F., Fröba, M., Getzschmann, J., Böhlmann, W., and Kaskel, S. (2009). New highly porous aluminium based metal-organic frameworks: Al(OH)(ndc) (ndc=2,6-naphthalene dicarboxylate) and Al(OH)(bpdc) (bpdc=4,4'-biphenyl dicarboxylate). Micropor. Mesopor. Mater. 122, 93–98. https://doi.org/10.1016/j. micromeso.2009.02.020.
- 143. Meißner, S.A., Eder, T., Keller, T.J., Hofmeister, D.A., Spicher, S., Jester, S.-S., Vogelsang, J., Grimme, S., Lupton, J.M., and Höger, S. (2021). Nanoscale π-conjugated ladders. Nat. Commun. 12, 6614. https://doi. org/10.1038/s41467-021-26688-9.
- 144. von Kugelgen, S., Piskun, I., Griffin, J.H., Eckdahl, C.T., Jarenwattananon, N.N., and Fischer, F.R. (2019). Templated synthesis of end-functionalized graphene nanoribbons through living ring-opening alkyne metathesis polymerization. J. Am. Chem. Soc. 141, 11050–11058. https://doi.org/10.1021/jacs. 9b01805
- Pun, S.H., Delgado, A., Dadich, C., Cronin, A., and Fischer, F.R. (2024). Controlled catalysttransfer polymerization in graphene nanoribbon synthesis. Chem 10, 675–685. https://doi.org/10.1016/j.chempr.2023. 11.002.
- 146. Lee, J., Ryu, H., Park, S., Cho, M., and Choi, T.-L. (2023). Living suzuki-miyaura catalysttransfer polymerization for precision synthesis of length-controlled armchair graphene nanoribbons and their block copolymers. J. Am. Chem. Soc. 145, 15488–15495. https:// doi.org/10.1021/jacs.3c04130.
- 147. Zhang, J.-J., Liu, K., Xiao, Y., Yu, X., Huang, L., Gao, H.-J., Ma, J., and Feng, X. (2023). Precision graphene nanoribbon heterojunctions by chain-growth polymerization. Angew. Chem. Int. Ed. Engl. 62, e202310880. https://doi.org/10.1002/anie. 202310880.
- 148. Ammenhäuser, R., Helfer, A., and Scherf, U. (2020). Reliably estimating the length of the effectively conjugated segment in ladder poly(para-phenylene)s. Org. Mater. 02, 159–164. https://doi.org/10.1055/s-0040-1710348.
- 149. Lee, J., Li, H., Kalin, A.J., Yuan, T., Wang, C., Olson, T., Li, H., and Fang, L. (2017). Extended ladder-type benzo[k]tetraphene-derived oligomers. Angew. Chem. Int. Ed. Engl. 56, 13727–13731. https://doi.org/10.1002/anie. 201707595.
- 150. Li, C., Yan, P.J., Chen, Y., Yang, R., and Sun, M. (2022). Spectral investigation on single molecular optoelectronics of ladder phenylenes. Spectrochim. Acta A Mol. Biomol. Spectrosc. 278, 121283. https://doi.org/10.1016/j.saa.2022.121283.
- 151. Khodabakhshi, E., Ramanan, C., Michels, J.J., Bonus, S., Hertel, D., Meerholz, K., Forster, M., Scherf, U., and Blom, P.W.M. (2020). Trapassisted triplet emission in ladder-polymerbased light-emitting diodes. Adv. Electron.

- Mater. 6, 2000082. https://doi.org/10.1002/aelm.202000082.
- 152. Wang, S., Sun, H., Ail, U., Vagin, M., Persson, P.O.A., Andreasen, J.W., Thiel, W., Berggren, M., Crispin, X., Fazzi, D., et al. (2016). Thermoelectric properties of solutionprocessed n-doped ladder-type conducting polymers. Adv. Mater. 28, 10764–10771. https://doi.org/10.1002/adma.201603731.
- 153. Fukuda, K., Fujiyoshi, J.-y., Matsui, H., Nagami, T., Takamuku, S., Kitagawa, Y., Champagne, B., and Nakano, M. (2017). A theoretical study on quasi-one-dimensional open-shell singlet ladder oligomers: multiradical nature, aromaticity and second hyperpolarizability. Org. Chem. Front. 4, 779–789. https://doi.org/10.1039/ C7QO00108H.
- Schedlbauer, J., Scherf, U., Vogelsang, J., and Lupton, J.M. (2020). Dynamic quenching of triplet excitons in single conjugated-polymer chains. J. Phys. Chem. Lett. 11, 5192–5198. https://doi.org/10.1021/acs.jpclett.0c01308.
- 155. Hollingsworth, W.R., Lee, J., Fang, L., and Ayzner, A.L. (2017). Exciton relaxation in highly rigid conjugated polymers: correlating radiative dynamics with structural heterogeneity and wavefunction delocalization. ACS Energy Lett. 2, 2096– 2102. https://doi.org/10.1021/acsenergylett. 7b00535.
- 156. Sosorev, A.Y. (2022). Charge-transfer complexes of linear and ladder-type conjugated polymers as promising organic narrow-gap semiconductors. J. Exp. Theor. Phys. 135, 100–106. https://doi.org/10.1134/ S106377612207007X.
- Kreyenschmidt, M., Baumgarten, M., Tyutyulkov, N., and Müllen, K. (1994).
   2,2'-Bipyrenyl and para-terpyrenyl—a new type of electronically decoupled oligoarylene. Angew. Chem. Int. Ed. Engl. 33, 1957–1959. https://doi.org/10.1002/anie.199419571.
- 158. Shirai, S., and Inagaki, S. (2020). Ab initio study on the excited states of pyrene and its derivatives using multi-reference perturbation theory methods. RSC Adv. 10, 12988–12998. https://doi.org/10.1039/C9RA10483F.
- Schedlbauer, J., Streicher, S., Forster, M., Scherf, U., Vogelsang, J., and Lupton, J.M. (2022). Tracking exciton diffusion and exciton annihilation in single nanoparticles of conjugated polymers by photon correlation spectroscopy. Adv. Opt. Mater. 10, 2200092. https://doi.org/10.1002/adom.202200092.
- Marcus, M., Milward, J.D., Köhler, A., and Barford, W. (2018). Structural information for conjugated polymers from optical modeling. J. Phys. Chem. A 122, 3621–3625. https://doi. org/10.1021/acs.jpca.8b01585.
- 161. Spano, F.C., and Silva, C. (2014). H- and J-aggregate behavior in polymeric semiconductors. Annu. Rev. Phys. Chem. 65, 477–500. https://doi.org/10.1146/annurevphyschem-040513-103639.
- 162. Hestand, N.J., and Spano, F.C. (2018). Expanded theory of H- and J-molecular aggregates: the effects of vibronic coupling and intermolecular charge transfer. Chem.



- Rev. 118, 7069–7163. https://doi.org/10.1021/acs.chemrev.7b00581.
- 163. Nagahara, T., Camargo, F.V.A., Xu, F., Ganzer, L., Russo, M., Zhang, P., Perri, A., de la Cruz Valbuena, G., Heisler, I.A., D'Andrea, C., et al. (2024). Electronic structure of isolated graphene nanoribbons in solution revealed by two-dimensional electronic spectroscopy. Nano Lett. 24, 797–804. https://doi.org/10. 1021/acs.nanolett.3c02665.
- 164. Ghosh, S., Gueskine, V., Berggren, M., and Zozoulenko, I.V. (2019). Electronic structures and optical absorption of n-type conducting polymers at different doping levels. J. Phys. Chem. C 123, 15467–15476. https://doi.org/ 10.1021/acs.jpcc.9b04634.
- 165. Fazzi, D., and Negri, F. (2021). Addressing the elusive polaronic nature of multiple redox states in a π-conjugated ladder-type polymer. Adv. Electron. Mater. 7, 2000786. https://doi. org/10.1002/aelm.20200786.
- 166. Fazzi, D., Fabiano, S., Ruoko, T.-P., Meerholz, K., and Negri, F. (2019). Polarons in π-conjugated ladder-type polymers: A broken symmetry density functional description. J. Mater. Chem. C 7, 12876– 12885. https://doi.org/10.1039/C9TC03283E.
- 167. Zheng, T., Badrun, F., Brown, I.M., Leopold, D.J., and Sandreczki, T.C. (1999). Correlation of electron spin concentration and conductivity in the ladder polymer BBL as a function of electrochemical potential. Synth. Met. 107, 39–45. https://doi.org/10.1016/ S0379-6779(99)00138-1.
- 168. Cao, Z., Leng, M., Cao, Y., Gu, X., and Fang, L. (2022). How rigid are conjugated non-ladder and ladder polymers? J. Polym. Sci. 60, 298–310. https://doi.org/10.1002/pol. 20210550.
- 169. Berry, G.C. (1978). Properties of an optically anisotropic heterocyclic ladder polymer (BBL) in dilute solution. J. Polym. Sci. Polym. Symp. 65, 143–172. https://doi.org/10.1002/polc. 5070650115.
- Hickl, P., Ballauff, M., Scherf, U., Müllen, K., and Lindner, P. (1997). Characterization of a ladder polymer by small-angle X-ray and neutron scattering. Macromolecules 30, 273–279. https://doi.org/10.1021/ma961038s.
- Kuei, B., and Gomez, E.D. (2016). Chain conformations and phase behavior of conjugated polymers. Soft Matter 13, 49–67. https://doi.org/10.1039/C6SM00979D.
- 172. Jenneskens, L.W., Havenith, R.W.A., Soncini, A., and Fowler, P.W. (2011). Aromaticity of strongly bent benzene rings: persistence of a diatropic ring current and its shielding cone in [5]paracyclophane. Phys. Chem. Chem. Phys. 13, 16861–16866. https://doi.org/10.1039/ C1CP21950B.
- 173. Michaels, W., Spakowitz, A.J., and Qin, J. (2023). Conformational statistics of ribbon-like chains. Macromolecules 56, 8359–8368. https://doi.org/10.1021/acs.macromol. 3r01430
- 174. Ma, G., Leng, M., Li, S., Cao, Z., Cao, Y., Tabor, D.P., Fang, L., and Gu, X. (2022). Robust chain aggregation of low-entropy rigid ladder polymers in solution. J. Mater. Chem. C 10,

- 13896–13904. https://doi.org/10.1039/ D2TC00761D.
- 175. Volkov, A.V., Sun, H., Kroon, R., Ruoko, T.-P., Che, C., Edberg, J., Müller, C., Fabiano, S., and Crispin, X. (2019). Asymmetric aqueous supercapacitor based on p- and n-type conducting polymers. ACS Appl. Energy Mater. 2, 5350–5355. https://doi.org/10.1021/ acsaem.9b00853.
- 176. Ueda, Y., Kurokawa, Y., Nishii, K., Kanematsu, H., Fukumoto, T., and Kato, T. (2022). Morphology control of monomer–polymer hybrid electron acceptor for bulk-heterojunction solar cell based on P3HT and Ti-alkoxide with ladder polymer. Materials (Basel) 15, 1195. https://doi.org/10.3390/ma15031195.
- 177. Yang, C.-Y., Stoeckel, M.-A., Ruoko, T.-P., Wu, H.-Y., Liu, X., Kolhe, N.B., Wu, Z., Puttisong, Y., Musumeci, C., Massetti, M., et al. (2021). A high-conductivity n-type polymeric ink for printed electronics. Nat. Commun. 12, 2354. https://doi.org/10.1038/s41467-021-22528-y.
- 178. Sun, H., Vagin, M., Wang, S., Crispin, X., Forchheimer, R., Berggren, M., and Fabiano, S. (2018). Complementary logic circuits based on high-performance n-type organic electrochemical transistors. Adv. Mater. 30, 1704916. https://doi.org/10.1002/adma. 201704916.
- 179. Wu, H.-Y., Yang, C.-Y., Li, Q., Kolhe, N.B., Strakosas, X., Stoeckel, M.-A., Wu, Z., Jin, W., Savvakis, M., Kroon, R., et al. (2022). Influence of molecular weight on the organic electrochemical transistor performance of ladder-type conjugated polymers. Adv. Mater. 34, e2106235. https://doi.org/10.1002/ adma.202106235.
- 180. Zhang, S., Massetti, M., Ruoko, T.-P., Tu, D., Yang, C.-Y., Liu, X., Wu, Z., Lee, Y., Kroon, R., Persson, P.O.Å., et al. (2022). Synergistic effect of multi-walled carbon nanotubes and laddertype conjugated polymers on the performance of n-type organic electrochemical transistors. Adv. Funct. Mater. 32, 2106447. https://doi.org/10.1002/ adfm.202106447.
- 181. Liu, T., Heimonen, J., Zhang, Q., Yang, C.-Y., Huang, J.-D., Wu, H.-Y., Stoeckel, M.-A., van der Pol, T.P.A., Li, Y., Jeong, S.Y., et al. (2023). Ground-state electron transfer in all-polymer donor:acceptor blends enables aqueous processing of water-insoluble conjugated polymers. Nat. Commun. 14, 8454. https:// doi.org/10.1038/s41467-023-44153-7.
- 182. Harikesh, P.C., Yang, C.-Y., Wu, H.-Y., Zhang, S., Donahue, M.J., Caravaca, A.S., Huang, J.-D., Olofsson, P.S., Berggren, M., Tu, D., et al. (2023). lon-tunable antiambipolarity in mixed ion–electron conducting polymers enables biorealistic organic electrochemical neurons. Nat. Mater. 22, 242–248. https://doi.org/10.1038/s41563-022-01450-8.
- 183. Surgailis, J., Savva, A., Druet, V., Paulsen, B.D., Wu, R., Hamidi-Sakr, A., Ohayon, D., Nikiforidis, G., Chen, X., McCulloch, I., et al. (2021). Mixed conduction in an n-type organic semiconductor in the absence of hydrophilic side-chains. Adv. Funct. Mater. 31, 2010165. https://doi.org/10.1002/adfm.202010165.

- 184. Guo, J., Flagg, L.O., Tran, D.K., Chen, S.E., Li, R., Kolhe, N.B., Giridharagopal, R., Jenekhe, S.A., Richter, L.J., and Ginger, D.S. (2023). Hydration of a side-chain-free n-type semiconducting ladder polymer driven by electrochemical doping. J. Am. Chem. Soc. 145, 1866–1876. https://doi.org/10.1021/jacs. 2c11468.
- 185. Wu, X., Tam, T.L.D., Chen, S., Salim, T., Zhao, X., Zhou, Z., Lin, M., Xu, J., Loo, Y.-L., and Leong, W.L. (2022). All-polymer bulk-heterojunction organic electrochemical transistors with balanced ionic and electronic transport. Adv. Mater. 34, e2206118. https://doi.org/10.1002/adma.202206118.
- 186. Zhou, Z., Wu, X., Tam, T.L.D., Tang, C.G., Chen, S., Hou, K., Li, T., He, Q., Sit, J.-J., Xu, J., et al. (2024). Highly stable ladder-type conjugated polymer based organic electrochemical transistors for low power and signal processing-free surface electromyogram triggered robotic hand control. Adv. Funct. Mater. 34, 2305780. https://doi.org/10.1002/adfm.202305780.
- 187. Wu, H.Y., Huang, J.D., Jeong, S.Y., Liu, T., Wu, Z., van der Pol, T., Wang, Q., Stoeckel, M.A., Li, Q., Fahlman, M., et al. (2023). Stable organic electrochemical neurons based on p-type and n-type ladder polymers. Mater. Horiz. 10, 4213–4223. https://doi.org/10.1039/D3MH00858D.
- 188. Tam, T.L.D., Lin, M., Handoko, A.D., and Xu, J. (2021). Thermoelectric performances of n-doped ladder-type conjugated polymers using various viologen radical cations. ACS Appl. Polym. Mater. 3, 5596–5603. https://doi.org/10.1021/acsapm.1c00920.
- 189. Tam, T.L.D., Lin, M., Handoko, A.D., Lin, T.T., and Xu, J. (2021). High-performance & thermally stable n-type polymer thermoelectrics based on a benzyl viologen radical cation-doped ladder-type conjugated polymer. J. Mater. Chem. A 9, 11787–11793. https://doi.org/10.1039/D1TA01645H.
- Darabi, S., Yang, C.-Y., Li, Z., Huang, J.-D., Hummel, M., Sixta, H., Fabiano, S., and Müller, C. (2023). Polymer-based n-type yarn for organic thermoelectric textiles. Adv. Electron. Mater. 9, 2201235. https://doi.org/10.1002/ aelm.202201235.
- 191. He, Q., Tam, T.L.D., Koh, X.Q., Tham, N.N., Meng, H., Huang, W., and Xu, J. (2022). P- and N-dopable ambipolar bulk heterojunction thermoelectrics based on ladder-type conjugated polymers. J. Mater. Chem. C 11, 204–210. https://doi.org/10.1039/ D2TC03684C.
- 192. Yu, K., Ji, X., Yuan, T., Cheng, Y., Li, J., Hu, X., Liu, Z., Zhou, X., and Fang, L. (2021). Robust jumping actuator with a shrimp-shell architecture. Adv. Mater. 33, e2104558. https://doi.org/10.1002/adma.202104558.
- 193. Vagin, M., Gueskine, V., Mitraka, E., Wang, S., Singh, A., Zozoulenko, I., Berggren, M., Fabiano, S., and Crispin, X. (2021). Negativelydoped conducting polymers for oxygen reduction reaction. Adv. Energy Mater. 11, 2002664. https://doi.org/10.1002/aenm. 202002664.
- 194. Wang, S., Ruoko, T.-P., Wang, G., Riera-Galindo, S., Hultmark, S., Puttisong, Y., Moro,



- F., Yan, H., Chen, W.M., Berggren, M., et al. (2020). Sequential doping of ladder-type conjugated polymers for thermally stable n-type organic conductors. ACS Appl. Mater. Interfaces 12, 53003–53011. https://doi.org/10.1021/acsami.0c16254.
- 195. Mauger, A., Julien, C., Paolella, A., Armand, M., and Zaghib, K. (2019). Recent progress on organic electrodes materials for rechargeable batteries and supercapacitors. Materials (Basel) 12, 1770. https://doi.org/10.3390/ ma12111770.
- 196. Gu, C., Jia, A.-B., Zhang, Y.-M., and Zhang, S.X.-A. (2022). Emerging electrochromic materials and devices for future displays. Chem. Rev. 122, 14679–14721. https://doi. org/10.1021/acs.chemrev.1c01055.
- 197. Ma, T., Yang, Y., Johnson, D., Hansen, K., Xiang, S., Thakur, R.M., Djire, A., and Lutkenhaus, J.L. (2023). Understanding the mechanism of a conjugated ladder polymer

- as a stable anode for acidic polymer-air batteries. Joule 7, 2261–2273. https://doi.org/10.1016/j.joule.2023.08.009.
- Wang, G., Zhang, L., and Zhang, J. (2012). A review of electrode materials for electrochemical supercapacitors. Chem. Soc. Rev. 41, 797–828. https://doi.org/10.1039/ C1C\$15060J.
- 199. Yura, R., Kumagai, S., Adachi, K., Hashizume, D., Okamoto, T., and Nonoguchi, Y. (2023). Crown ether salt-doped ladder-type conducting polymers for air-stable n-type thermoelectric materials. Chem. Commun. (Camb) 59, 5531–5534. https://doi.org/10. 1039/D3CC00840A.
- Prins, P., Grozema, F.C., Schins, J.M., Patil, S., Scherf, U., and Siebbeles, L.D.A. (2006). High intrachain hole mobility on molecular wires of ladder-type poly(p-phenylenes). Phys. Rev. Lett. 96, 146601. https://doi.org/10.1103/ PhysRevLett.96.146601.

- 201. Tran, D.K., West, S.M., Guo, J., Chen, S.E., Ginger, D.S., and Jenekhe, S.A. (2024). Chain length dependence of electron transport in an n-type conjugated polymer with a rigid-rod chain topology. J. Am. Chem. Soc. 146, 1435– 1446. https://doi.org/10.1021/jacs.3c10650.
- Zhao, Z., Tian, Z., and Yan, F. (2023). Flexible organic electrochemical transistors for bioelectronics. Physiol. Sci. 4, 101673. https:// doi.org/10.1016/j.xcrp.2023.101673.
- Nawaz, A., Liu, Q., Leong, W.L., Fairfull-Smith, K.E., and Sonar, P. (2021). Organic electrochemical transistors for in vivo bioelectronics. Adv. Mater. 33, e2101874. https://doi.org/10.1002/adma.202101874.
- Rashid, R.B., Ji, X., and Rivnay, J. (2021). Organic electrochemical transistors in bioelectronic circuits. Biosens. Bioelectron. 190, 113461. https://doi.org/10.1016/j.bios. 2021.113461.